THEORY OF CONTACT-LIMITED SOLAR CELLS

by

ELLIS TURNBULL ROE

A DISSERTATION

Presented to the Department of Physics
and the Graduate School of the University of Oregon
in partial fulfillment of the requirements
for the degree of
Doctor of Philosophy

September 2019

DISSERTATION APPROVAL PAGE

Student: Ellis Turnbull Roe

Title: Theory of Contact-limited Solar Cells.

This dissertation has been accepted and approved in partial fulfillment of the requirements for the Doctor of Philosophy degree in the Department of Physics by:

Benjamín J. Alemán	Chair
Mark C. Lonergan	Advisor
Richard P. Taylor	Core Member
Hailin Wang	Core Member
Shannon W. Boettcher	Institutional Representative

and

Janet Woodruff-Borden	Vice Provost and Dean of the Graduate School

Original approval signatures are on file with the University of Oregon Graduate School.

Degree awarded September 2019

DISSERTATION ABSTRACT

Ellis Turnbull Roe

Doctor of Philosophy

Department of Physics

September 2019

Title: Theory of Contact-limited Solar Cells.

The International Panel on Climate Change has made it clear that drastic action is required in order to prevent warming of global average temperatures from reaching 1.5-2.0°C above the pre-industrial average. If this is to be achieved, global power generation from photovoltaics will need to increase by more than an order of magnitude. Most of the dominant and upcoming photovoltaic technologies, including silicon and metal-halide perovskites, are limited more by their contacts than recombination in the bulk of the absorber. While we have a very good understanding of how bulk recombination limits the efficiency of a solar cell, we do not completely understand how contact processes determine the efficiency of a solar cell.

This work attempts to fill this gap in the literature by considering a solar cell model that is completely dominated by solar photon generation and contact recombination. The partial currents of electrons and holes at both contacts to an intrinsic absorber are assumed to be linearly proportional to the excess carrier density at the contacts. By linking the currents across the device with the continuity equation, assuming the quasi-Fermi levels are approximately flat, and adding the partial currents at each contact, an expression for the current-voltage behavior can be algebraically calculated. The resulting analytic expression provides useful qualitative and quantitative insights into how the four equilibrium exchange current densities, which determine the rate of electron and hole extraction at both contacts, shape the current-voltage curve. In particular, it demonstrates that the features of the curve depend on the relative rate at which a particular carrier (electron or hole) is collected at one contact vs. the other. The model provides a unified explanation for non-ideal contact related behavior seen in the literature, such as S-shaped curves and dark/light crossover (i.e. failure of superposition). The work will be insightful for researchers investigating technologies with yet-to-be optimized contacts.

This dissertation includes both previously published/unpublished co-authored material.

CURRICULUM VITAE

NAME OF AUTHOR: Ellis Turnbull Roe

GRADUATE AND UNDERGRADUATE SCHOOLS ATTENDED:
University of Oregon, Eugene, OR
Western Washington University, Bellingham, WA

DEGREES AWARDED:
Doctor of Philosophy, Physics, 2019, University of Oregon
Bachelor of Science, Physics, 2013, Western Washington University

AREAS OF SPECIAL INTEREST:
Solid State Physics
Semiconductor Device Physics
Photovoltaics

PROFESSIONAL EXPERIENCE:

Graduate Research Fellow, Department of Physics, University of Oregon, Eugene, OR, 2014-2019

Graduate Teaching Fellow, Department of Physics, University of Oregon, Eugene, OR, 2013-2014

Teaching Assistant, Department of Physics and Astronomy, Western Washington University, Bellingham, WA, 2010-2013

Undergraduate Researcher, Department of Physics and Astronomy, Western Washington University, Bellingham, WA, 2012-2013

GRANTS, AWARDS AND HONORS:

Weiser First-year Teaching Assistant Award, University of Oregon, 2014

Dept. of Phys. & Astr. Outstanding Graduate, Western Washington University, 2013

Veit Memorial Scholarship, Western Washington University, 2012

Raymond Mcleod Memorial Scholarship, Western Washington University, 2011

PUBLICATIONS:

E.T. Roe, K.E. Egelhofer, M.C. Lonergan, Exchange Current Density Model for the Contact-determined Current-voltage Behavior of Solar Cells. 2019. Under 2nd review @ J. of Appl. Phys

E.T. Roe, K.E. Egelhofer, M.C. Lonergan, Limits of Contact Selectivity/Recombination on the Open-Circuit Voltage of a Photovoltaic. Appl. Energy Mater. 2018. 1 (3), 1037-1046

C.W. Warren, *E.T. Roe*, D.W. Miller, W.N. Shafarman, M.C. Lonergan. An Improved Method for Determining Carrier Densities via Drive Level Capacitance Profiling. Appl. Phys. Lett. 2017, 110 (20), 203901

D.W. Miller, G.E. Eperon, *E.T. Roe*, C.W. Warren, H.J. Snaith, M.C. Lonergan. Defect States in Perovskite Solar Cells Associated with Hysteresis and Performance. Appl. Phys. Lett. 2016, 109 (15), 153902

C.M. Sutter-Fella, D.W. Miller, Q.P. Ngo, *E.T. Roe*, F.M. Toma, I.D. Sharp, M.C. Lonergan, A. Javey. Band Tailing and Deep Defect States in CH3NH3Pb(I1-xBrx)3 Perovskites as Revealed by Sub-Bandgap Photocurrent. ACS Energy Lett. 2017, 2 (3), 709-715

H-P. Wang, C.M. Sutter-Fella, P. L., M. Hettick, M. Zheng, D-H. Lien, D.W. Miller, C.W. Warren, *E.T. Roe*, M.C. Lonergan, H.L. Guthrey, N.M. Haegel, J.W. Ager, C. Carraro, R. Maboudian, J-H. He, A. Javey. Increased Optoelectronic Quality and Uniformity of Hydrogenated p-InP Thin Films. Chem. Mater. 2016, 28 (13), 4602-4607

ACKNOWLEDGEMENTS

I have been incredibly privileged, throughout my life, to have had the opportunities and support that allowed me to pursue a Ph.D. in physics.

My parents, Dave and Sarah, deserve credit for their patience throughout my childhood. Were it not for their encouragement, and the example set by my sister Kelsey, whom I followed to Western Washington University in Bellingham, I would have never gone to college. At WWU, I found a subject I enjoyed learning: physics. The entire department of physics at WWU deserves credit for competently teaching my classmates and I physics, and mentoring us as we became scientists. In particular, I thank my undergrad adviser and mentor, Brad Johnson, for seeing value in my work and intellect but also for grounding my expectations better to reality (particularly those about what I might study in graduate school). In Bellingham, I met my wife Mallorey, who has been a constant source of comfort, encouragement, and love ever since.

Throughout my time in grad school at UO, I have been fortunate to have worked with many people, especially those whom I've done research with. Chuck Warren, Wes Miller, and Colin Bradley (previous graduates of the Lonergan lab) deserve much thanks for teaching me much of what I've learned about solar cell characterization, device physics, and programming. I also thank current lab members Kira Egelhofer and Zack Crawford, and last but not least, my adviser Mark Lonergan. Mark, who is a professor of chemistry, was kind enough to take on and fund a graduate student who knew almost no chemistry, or solar cell device physics when stepping into the lab. I have known Mark for five years now. He has always been an exemplary role model, and has taught me much about solar cells, communication skills, and life in

general. In addition, I greatly appreciate that Mark always makes significant effort to work with all his students regardless of how busy he is, and that he is happy to talk about life outside the lab.

My work has been made possible by the Division of Chemical Sciences, Geosciences, and Biosciences, Office of Basic Energy Sciences of the U.S. Department of Energy through grant DE-SC0012363 and the Department of Energy via the Bay Area Photovoltaic Consortium award No. DE-EE004946.

TABLE OF CONTENTS

Chapter Page

Chapter Page

APPENDICES

LIST OF FIGURES

LIST OF TABLES

Table Page

CHAPTER I

INTRODUCTION

Overview

This dissertation lays out the contact-limited solar cell theory I developed, with the help of my adviser Mark Lonergan, over the last several years. The theory is entirely analytic, and I have derived every unique equation presented myself, though some initial calculations and the motivation to pursue this theoretical investigation were provided by Mark. Numerical simulations were performed in order to evaluate how various assumptions in the model hold up in more realistic devices, and those presented were performed by me (with the sole exception of Fig. 9), though some of the inspiration for a few of them was provided by Mark.

Chapter 1 introduces the essential motivation for studying solar cells (spoiler alert: climate change is real and man-made) and very briefly introduces the most essential concepts of semiconductors and solar cell current-voltage characterization. It was written entirely for this dissertation and has not been published. Chapter 2 provides the reader with a sense of the literature previously published that relates to the topic. First, it introduces some of the very basic theory relating to solar cells and their limitations as has been known for decades, then it provides an overview of recent literature pertaining to the effect contacts have on solar cell performance. It is primarily taken from the Introduction section of E.T. Roe, K.E. Egelhofer, M.C. Lonergan, "Exchange current density model for the contact-determined current-voltage behavior of solar cells." *J. Appl. Phys. 2019.* 125 (22) 225302 (Roe et al. 2019).[1] Chapter 3 details the model on which the theory I have developed is based, laying out the key assumptions and setting up the calculations that need to be performed. It combines the Model sections of E.T. Roe, K.E. Egelhofer, M.C. Lonergan, "Limits of Contact Selectivity/Recombination on the Open-Circuit Voltage of a Photovoltaic." *Appl. Energy Mater. 2018.* 1 (3), 1037-1046 (Roe et al. 2018)[2] and Roe et al. 2019.[1] It has been re-written from the ground up to ensure that the presentation is appropriate for all the results presented later on. Chapter 4 walks the reader through the gory algebraic details of the calculations used to derive the primary results of the work (those who are not mathematically curious may skip this chapter). Chapter 4 is compiled from the supplementary materials of both works. Chapter 5 discusses the nature of the most important result derived, the contact limited solar cell's current-voltage curve. Some of it has been written for the purposes of the dissertation, while the rest is taken from the Results and Discussion section of Roe et al. 2019. Chapter 6 discusses the ramifications of the contact limited current-voltage expression on the critical solar cell performance parameters and was compiled from the Results sections of both works. Chapter 7 discusses the simulations performed to evaluate the theory and was compiled from the Simulations section of the main text and the supplementary material of Roe et al. 2019. Finally, Chapter 8 is new material, written as a conclusion to the dissertation.

Throughout this dissertation, I will walk the reader through the calculations and simulations I did both by hand and with the help of a computer. I will use the pronoun 'we' colloquially when walking the reader through this, as I encourage the reader to do the calculations and thinking with me. As I have learned throughout my time in grad school, the only way to truly understand someone else's work is go through the physics, equation by equation, figure by figure, until you understand what each one means and where it came from.

Solar Cell Basics

According to the International Panel on Climate Change (IPCC), global average temperatures are at 1.0± 0.2°C above their pre-industrial levels as of 2017.[3] The IPCC predicts that the effects of allowing the global average temperature to exceed 1.5°C will be devastating. While 1.5°C may not sound like much, this is an average, and the temperature extremes on land at mid latitudes (where most human beings live) are projected to warm up to about 3°C, or over 5°F. This will cause continued rising sea levels, increased severity of droughts and desertification, increased probability of hurricanes and other extreme weather, extinction of plant and animal species and countless knock-on effects that will not be discussed here for the sake of brevity.

Needless to say, the climate change skeptic need only look to our nearest heavenly neighbor, the planet Venus, to observe the catastrophic effects of the run-away greenhouse effect, primarily caused by carbon-dioxide (CO_2).[4] The surface temperature of Venus is approximately 470°C, or ∼740 K. The atmosphere of Venus is much more dense than ours, and over 96% of it is CO_2.[5] One can easily predict what the steady-state temperature of the surface of Venus should be, if it were able to radiate energy like a planet without a such a thick atmosphere (i.e. an emissivity of ∼1), given the sun's blackbody radiation and the distance between venus and the sun (0.7 AU). At steady state, the power absorbed by Venus (P_{in}) must be equal to the power emitted (P_{out}). The power absorbed is equal to the total luminosity of the sun times the solid angle of Venus when viewed from the sun divided by 4π:

$$P_{in} = L_{\odot}\left(\frac{\pi R_v^2}{4\pi D_v^2}\right) \tag{1.1}$$

where R_v is the radius of Venus, D_v is the distance from Venus to the sun (which is very close to constant, as Venus' orbit is almost a perfect circle), and $L_\odot$ is the total luminosity of the sun, given approximately by

$$L_\odot = (4\pi R_\odot^2)\sigma T_\odot^4 \tag{1.2}$$

where σ is the Stefan-Boltzmann constant, $T_\odot$ is the surface temperature of the sun (approximately 5800 K), and $R_\odot$ is the radius of the sun. Meanwhile, the power emitted is given by

$$P_{out} = (4\pi R_v^2)\sigma T_v^4 \tag{1.3}$$

where R_v is the radius of Venus, and T_v is its temperature. Setting $P_{in} = P_{out}$ and solving for T_v readily gives the steady-state temperature of Venus:

$$T_v = T_\odot \sqrt{\frac{R_\odot}{2D_v}} \approx 330\text{K} \tag{1.4}$$

This is considerably warmer than the earth's average temperature (which is pretty well approximated by this calculation, for the time being). To give some perspective, 330 K is 134°F, which is about the hottest temperature that the earth's surface ever approaches (with the exception of volcanoes and related phenomena). However, the actual temperature of Venus is ∼870°F, which is easily hot enough to melt lead; in fact, it is around the temperature of lava crusts.[6, 7] While earth's atmosphere will never be as dense as Venus', there is absolutely no question that increased carbon concentrations are a threat to the delicate balance between the solar energy that the earth absorbs, and that which it emits.

Global average CO_2 concentrations are above 400 parts-per-million (ppm) as of 2017, while pre-industrial levels averaged around 250 ppm for the last 800,000 years.[8, 9] In the last two centuries, just as humankind began burning fossil fuels, carbon dioxide levels have skyrocketed up to levels not seen in over 10 million years.[10] The rate of increase of carbon concentration over the last two centuries is orders of magnitude larger than the largest rate of change due to natural emissions (such as volcanoes) in the last 800,000 years. There is no doubt that our burning of fossil fuels is the primary cause of rising CO_2 concentrations. While there are other greenhouse gases that also contribute to global worming, CO_2 is by far the most dominant contributor.[11] The IPCC predicts that we will reach 1.5°C of warming somewhere between 2030 and 2050 if we do not dramatically curb the amount of CO_2 we are spewing into the atmosphere.[3]

The cumulative global installed photovoltaic capacity was over 300 GW as of 2016,[12] but this was only about 2% of total global electricity demand in 2016. In total, all renewables only accounted for about 8% of total global energy demand (not including hydro-electric sources). While no single renewable energy source should be prioritized above all others, new innovations in photovoltaics will be necessary in order to reach 10+ TW of installed photovoltaic capacity by 2030.[13] In order to avoid the catastrophic effects of a 1.5-2°C increase in global temperature, we will need to (among other things) increase our photovoltaic electricity generation by well over an order of magnitude.

The two most important metrics for any given type of solar cell are its cost and its power conversion efficiency (or just efficiency). Reducing cost and increasing efficiency are both essential if we are to accelerate the growth of global installed photovoltaic capacity. Both of these metrics are related, in different ways, to the choice of materials used to build the solar cell. While no fundamental thermodynamic limit exists for the lowest possible cost of a solar cell given its materials, the efficiency of a solar cell is limited by the semiconducting material chosen to absorb the solar photons (this limit can be exceeded with tandem cells, but they have a high cost and are not a significant fraction of global installed capacity as of 2016).[14] This limit is known as the Detailed-Balance, or Shockley-Queisser (SQ) limit,[15] and it is critical when assessing the possible gains from improving a given technology or whether or not a new technology will be viable. However, this limit does not concern itself with the limits due to materials used to contact the solar cell. In fact, as we will see, our understanding of how solar cell contacts determine device performance is incomplete, at best.

Before we get into that, a basic summary of semiconductor physics is in order. A semiconductor is a material whose conductivity increases with temperature (as opposed to a metal, whose conductivity decreases with increasing temperature). In order to understand why a semiconductor's conductivity increases with temperature, some very basic quantum mechanics is necessary. In an extended solid such as a semiconductor crystal, electron states are delocalized, and there are so many states that they occupy quasi-continuous bands in energy-space (as opposed to the discrete states of the hydrogen atom). The effect of the periodic potential provided by the lattice nuclei is to create regions of energy space where there are no states (i.e. the density of states is zero). The mathematical description of the density of states is critical to the quantitative description of semiconductors, refer to Appendix A for the derivation.

There are only so many electrons in a material, and they fill up states up to an energy called the Fermi energy, E_f. At absolute zero temperature, every electronic state below the Fermi-energy is occupied with an electron, and every state above it is unoccupied. The function that describes the occupancy of states according to their energy (E) relative to the Fermi-energy as a function of temperature is the Fermi-Dirac distribution:

$$f(E) = \frac{1}{e^{\frac{E-E_f}{k_B T}} + 1} \tag{1.5}$$

where k_B is the Boltzmann constant. At absolute zero, $f(E)$ is a step function centered at E_f, and as temperature increases, the function becomes more and more smooth. In the limit $E - E_f \gg k_B T$, $f(E)$ reduces to the Boltzmann distribution:

$$f(E) \approx e^{-\frac{\left(E-E_f\right)}{k_B T}} \tag{1.6}$$

Consider Fig. 1, which shows typical band diagrams for a metal, an intrinsic semiconductor, and a doped semiconductor from left to right. The metal is distinguished by the fact that the Fermi-level intersects a band. This means that, even at a low temperatures, there are a very large number of accessible states that are unoccupied and hence available for conduction.

In contrast, an intrinsic semiconductor's Fermi-level is (roughly) halfway between the two closest bands; the density of states at the Fermi-level is zero. The closest band of states below the Fermi-level is called the valence band, while the closest band above is called the conduction band. The energy difference between the conduction and valence band edges is called the bandgap energy, E_g. Electrons in the valence band are unable to conduct electricity, because there are no unoccupied states that are next to them (the sum of momenta of electrons in a fully occupied band is zero). A very small number of electrons, however, will have enough thermal energy to jump

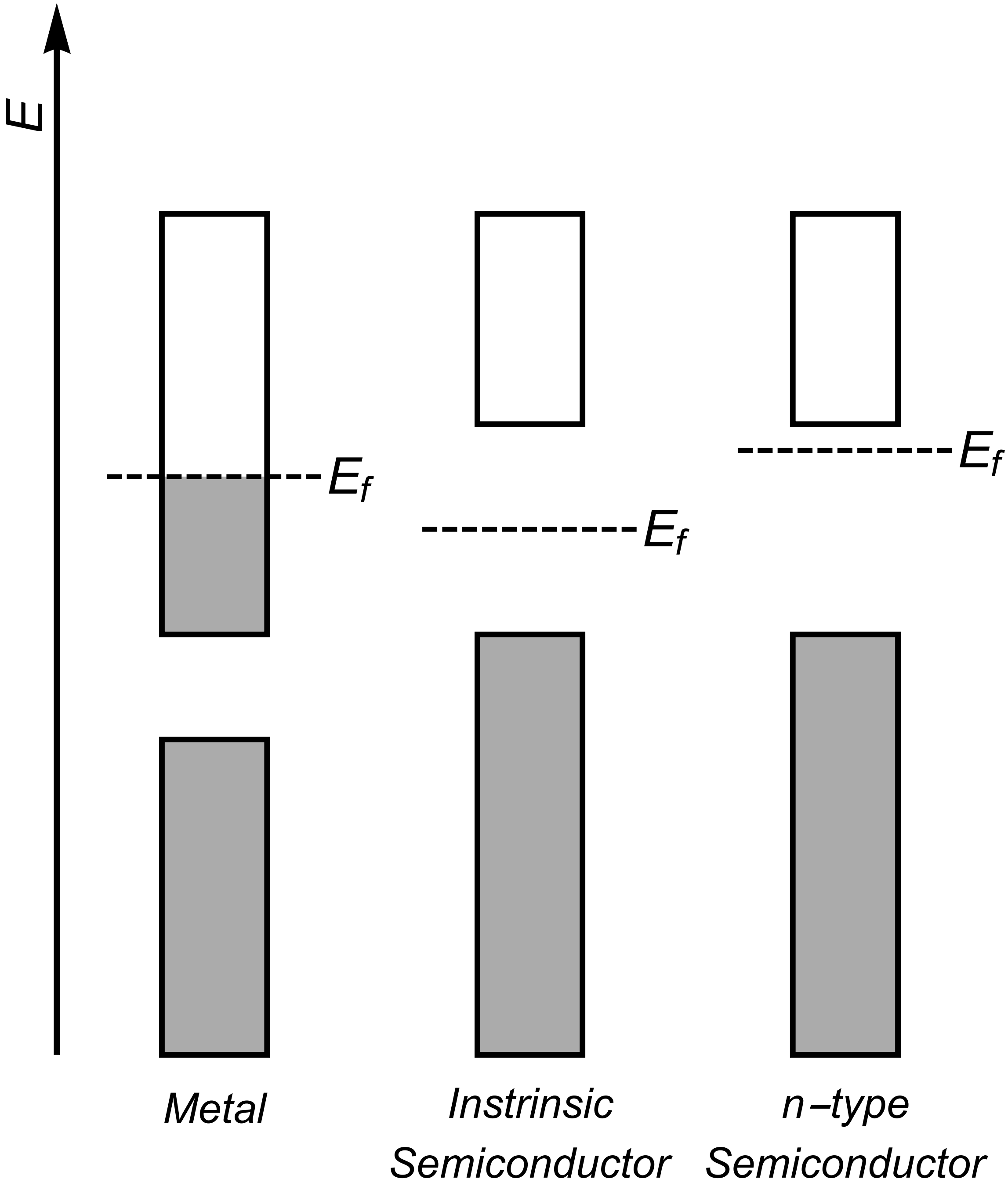

FIGURE 1. Energy band diagram for a generic metal (left), intrinsic semiconductor (center), and n-type semiconductor (right). The rectangles indicate a band with many continuous states, while the energies outside of the rectangles denote energies with no states. Fermi-levels, E_f, are indicated with dashed lines, and occupied states are filled in with gray. Note that the horizontal axis is meaningless.

the bandgap, to the conduction band, where there are plenty of available states. Those electrons that exist in the conduction band are called free-electrons as they are free to conduct electricity. Additionally, the electrons leave behind unoccupied states, which also conduct electricity. These are called holes, as they represent the absence of electrons in a sea of electrons, in the same way a bubble represents an absence of water in a sea of water. The density of both free electrons and holes in a semiconductor increases with temperature because a larger fraction will have sufficient energy to jump to the appropriate band, leading to a higher conductivity at higher temperatures.

A doped semiconductor is similar to an intrinsic semiconductor, except that the Fermi-level is much closer to one of the two bands (the right most band diagram in Fig. 1 is that of an n-type semiconductor, as it's Fermi-level is closest to the conduction band). In an n-type semiconductor, there are relatively large numbers of free electrons, and very, very few holes. Thus, in an n-type semiconductor, electrons are usually called majority carriers, and holes are called minority carriers. A balance between free electrons and holes is not necessary for conduction, however, and a doped semiconductor is orders of magnitude more conductive than an intrinsic semiconductor with the same bandgap at the same temperature. For a mathematical description of the density of electrons and holes in a semiconductor as a function of the Fermi energy, refer to Appendix B.

Semiconductors are unique in how they interact with light. Whether or not a photon interacts with a semiconductor is governed, to a reasonable approximation, by the relation between the photon energy (E_γ) and the bandgap energy. If a photon incident onto a slab of semiconductor has energy $E_\gamma > E_g$, the photon will be absorbed by the semiconductor, while those photons with $E_\gamma < E_g$ will pass straight through the semiconductor. Most of the time, when a photon is absorbed by a semiconductor, the energy of the photon is transferred to an electron in the valence band, allowing it to jump to the conduction band, leaving behind a hole. Thus, a free electron and hole are generated. With large numbers of photons hitting a semiconductor (such as a semiconductor out in the sun), many free electrons and holes are generated, creating a large excess of free carriers (if the semiconductor is highly doped, the excess may only be in the minority carrier).

To describe the densities of electrons and holes under non-equilibrium conditions (such as under illumination or applied bias), separate Fermi-levels are required for electrons and holes. These are dubbed E_{fn} and E_{fp}, respectively. The larger the difference between E_{fn} and E_{fp}, the further the semiconductor is being driven from equilibrium. Of course, nature does not like this, and there is a reverse process that drives semiconductors back towards equilibrium. This is called direct recombination (there other types of recombination, such as Auger and Shockley-Read-Hall (SRH) recombination, but direct recombination is all that is necessary for us to understand the basic operation of solar cells), in which the electron falls back to the hole in the valence band, releasing a photon with $E = E_g$ in the process. In steady state, the rates of generation and recombination match so that the population, and hence the quasi-Fermi levels, do not change with time.

The splitting of quasi-Fermi levels also represents energy that can be captured; however, this can only be done by extracting the electrons and holes to an external circuit. This is where the contacts to the semiconducting absorber come into play. Because electrons and holes have opposite charge, they must be extracted from the absorber at opposite contacts (if they are collected at the same contact, the net current is zero; this amounts to contact recombination). Thus, some asymmetry in the contact properties must exist, in order for a solar cell to function. This asymmetry can be achieved in multiple ways, some of which will be explored in Chapter 7.

The essential processes in a solar cell are the generation of electrons and holes via photon absorption, transport of carriers to contacts before they can recombine in the bulk of the absorber, and the selective extraction of electrons at one contact and holes at the other. This work will investigate the limits that the rates of equilibrium electron and hole extraction at both contacts determine the efficiency of a solar cell.

In order to understand how to think about improving the efficiency or performance of solar cells, it is essential to understand the basic parameters and performance metrics of solar cells. In the most basic sense, a photovoltaic device, or solar cell, converts photon energy into electronic energy by absorbing photons and separating the excited charge carriers to two different contacts. Like other semiconductor based electronic devices, solar cells are characterized by their current-voltage ($I(V)$) behavior. For a solar cell, it is of course important to distinguish whether a measurement was made in the dark or in the light. In the dark, the ideal solar cell has the $I(V)$ characteristics of an ideal diode. Generally, the current is normalized by the area of the solar cell and thus a current density-voltage ($J(V)$) curve is measured. The term 'current density' will regularly be shortened to 'current' throughout this work. However, the symbol I will always refer to current, while J will always refer to a current density. The $J(V)$ characteristics of the ideal diode (see Appendix C for derivation in the case of the *p*-*n* junction, and Appendix D for derivation via detailed balance) are given by

$$J(V) = J_0 \left(e^{\frac{qV}{k_B T}} - 1 \right) \tag{1.7}$$

where J is the current density, q is the electron charge, V is the applied voltage, k_B the Boltzmann constant, J_0 the saturation current or equilibrium exchange current density and T is the temperature. In the dark, the solar cell consumes power at every point on the $J(V)$ curve other than the origin. The power density used by the solar cell, like any other device obeys

$$P = JV \tag{1.8}$$

Since the dark $J(V)$ curve exists only in quadrants one and three, the $J \times V$ product is always positive. Our sign convention for power therefore indicates that a positive power value refers to the solar cell consuming energy and visa versa for a negative power.

When exposed to light, the solar cell will generate an additional current, J_L, which flows in the same direction as the reverse bias current. This is because the current due to generation of electrons and holes must oppose that due to recombination. Since recombination is the cause of the current in forward bias in the dark (which is positive in the usual convention), the light current must be negative. Ideal $J(V)$ behavior of a solar cell under illumination is given by

$$J = J_0 \left(e^{\frac{qV}{k_B T}} - 1 \right) - J_L \tag{1.9}$$

where J_L is the illumination current density. Figure 2 is a plot of a light and dark $J(V)$ curves, as well as the power density, for a sample ideal solar cell, with $J_0 = 10^{-9}\,\mathrm{mA/cm^2}$ and at $T = 298\,\mathrm{K}$. Quadrant four is known as the 'power quadrant' because the current voltage product is negative thus indicating that power is being generated, not consumed by the solar cell. We now define several important quantities used to characterize solar cells. The short-circuit current density (J_{sc}) is the current at zero bias, equal to the illumination current for an ideal solar cell with no series resistance. The open-circuit voltage (V_{oc}) is the voltage at which the current crosses zero. To determine the maximum power, one simply needs to maximize the JV product, which is equivalent to finding the largest area rectangle that fits between the origin and the $J(V)$ curve inside quadrant four (this is the gray rectangle in Fig. 2). Even for an ideal solar cell, the maximum power generated is less than $J_{sc} \times V_{oc}$, as long as $T > 0$. The maximum power point is defined by the current J_m and voltage V_m, and the fill factor (FF) is defined by

$$FF = \frac{I_m P_m}{J_{sc} V_{oc}}. \tag{1.10}$$

The power conversion efficiency (η), describes the efficiency of the solar cell in terms of these parameters

$$\eta \equiv \frac{P_{out}}{P_{in}} = \frac{FF J_{sc} V_{oc}}{P_{in}} = \frac{I_m P_m}{P_{in}} \tag{1.11}$$

where P_{in} is the total solar power incident on the device. When measuring solar cell efficiency, the AM 1.5 spectrum is typically used, which corresponds to a total incident power of $\sim$ 100mW/cm^2. Therefore, the efficiency of the ideal solar cell characterized in Fig. 2 in % is approximately equal to the maximum power. The efficiency of the device shown is $\sim 21\%$, meaning that for every Joule of solar energy incident on the device, 0.21 Joules of electric energy can be extracted as long as it is operated at its maximum power point given by V_m.

Measuring the $J(V)$ curve under 1 sun is the fundamental way to characterize a solar cell, as what we ultimately care about is how much electric power we get

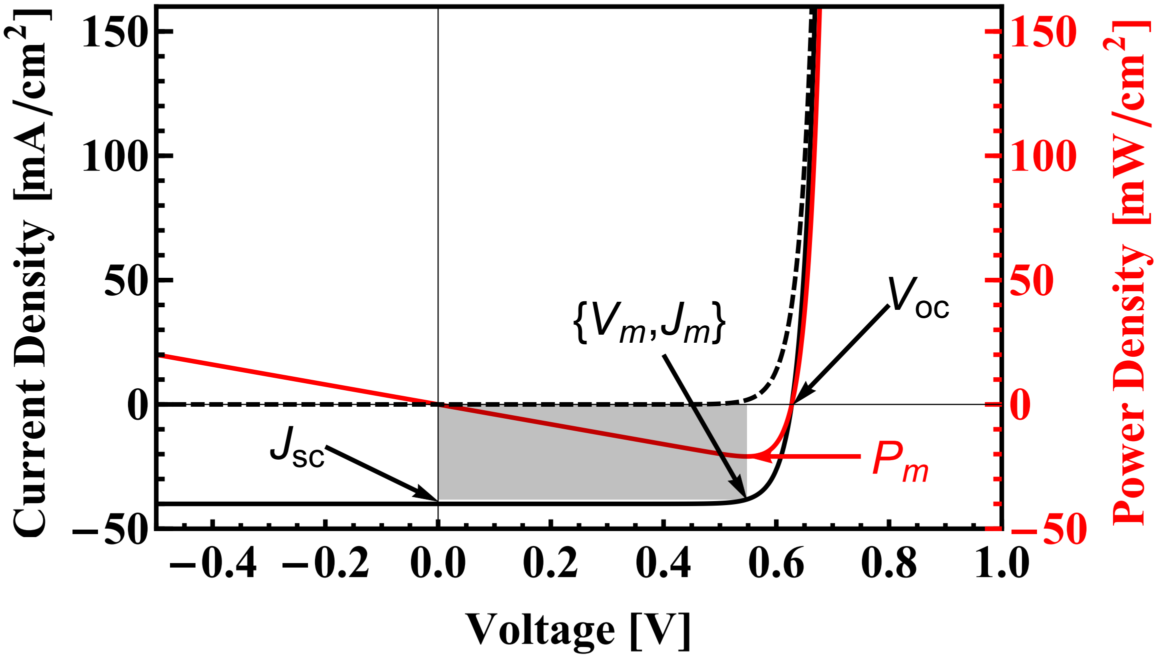

FIGURE 2. Light (solid black) and dark (dashed black) $J(V)$ curves for an ideal solar cell, dictated by eq. 1.9 with $T = 298\,\mathrm{K}$, $J_0 = 10^{-9}\,\mathrm{mA/cm^2}$, and $J_L = 0$ for dark and $J_L = 40\,\mathrm{mA/cm^2}$ for light. The power density (P) as a function of voltage is shown in red. Here, negative corresponds to power generated, and positive indicates power is being consumed.

out of it for the given spectrum of incident solar photons. Ultimately, if a researcher makes in improvement to a given solar cell technology, that improvement is either measured in reduced cost or increased efficiency (or both). However, it is generally advantageous to have an understanding of why the solar cell improved, if its efficiency increased. The goal of this work is to provide a more complete picture of how the contacts to a solar cell determine the resulting $J(V)$ curve so that researchers may more readily explain changes in $J(V)$ behavior in their devices, assuming they have reason to believe their device is contact-limited. The next chapter will delve a little bit into the history of theoretical calculations of solar cell limitations, and deeper into existing literature that relates to how contacts can affect solar cell performance to give the reader some perspective on what is currently known.

CHAPTER II

BACKGROUND

This chapter will explore the motivation for why we need a better model for how solar cell contacts determine performance. The majority of it is taken from Roe et al. 2019, however changes have been made to make it appropriate for the dissertation format, and the first several paragraphs have been modified to include a discussion of the literature of the state of most relevant solar cell technologies. Numerous relevant references have been added.

A solar cell, at its most basic level, must consist of an absorber material and two contacts on either end. The choice of absorber material places limits on the efficiency of the device. Very simply, the bandgap energy determines how much of the solar spectrum is absorbed (which determines the J_{sc} of the device), but it also places an upper limit on the energy per carrier that can be extracted (i.e. the voltage). Therefore, a compromise must be reached to optimize a solar cell's efficiency in accordance with the solar spectrum. The first rigorous calculation of this limiting efficiency was performed by Shockley and Queisser (SQ) in 1961,[15] and it has been extensively expanded upon since.[16–19] SQ assumed that the rate constant for radiative recombination was equal at thermal equilibrium and under solar illumination, and they determined it by calculating the equal and opposite rate of generation of electrons and holes in the absorber due to photons from a 300 K environment (see Appendix D for a simplified derivation). In order to determine $J(V)$, they also had to assume that the quasi-Fermi level splitting in the absorber was equal to the voltage across the device. This is not always the case, however, because the contacts to the absorber must be able to support this voltage by selectively allowing electrons to flow out one end of the device and holes out the other. Any difference between the quasi-Fermi-level splitting in the bulk of the absorber and the voltage across the device is related to the rate at which electrons and holes are able to be extracted (see Chapter 6).

Considering the limitations that contacts place on a solar cell's performance is then critical to a more comprehensive understanding of solar cells. Furthermore, it so happens that most of today's prominent photovoltaic absorber technologies are near the radiative limit described by SQ, and many are thought to be in fact limited by contact passivation or other contact related limitations. GaAs, is the most efficient single junction (i.e. single absorber) solar cell technology[20] and is also the closest technology to its radiative limit of 33% according to recent studies.[21, 22] Meanwhile, CdTe is thought to be limited by an undesirable barrier that is difficult to avoid at the back contact,[23–26] while CIGS devices are strongly affected by the properties of the CdS/CIGS interface.[27, 28] By far the most industrialized technology is silicon. It has been known for some time that the dominant issue preventing silicon solar cells from approaching the SQ limit is contact passivation.[29] This issue is still thought to be the biggest limiting factor today in the traditional bulk junction design.[30, 31] Even in the heterojunction interdigitated back contact structure, optimization of contact passivation is still producing results.[32–34] Finally, metal-halide perovskite absorbers are already near their radiative limit,[35–37] and significant recombination limitations are introduced when the absorber is contacted.[36, 38–40]

In this work, we will calculate an analytic $J(V)$ curve as determined by all *four* rates that dictate electron and hole extraction at *each* contact. Our approach provides both quantitative and intuitive understanding of how a range of contacts can determine solar cell performance. It is limited by the extent to which the layer(s) that make up the contacts can be effectively modeled by setting the boundary partial currents proportional to the product of the excess carrier density times a voltage independent constant. We call this boundary condition (see eq. 3.1) ‘ideal diode like’ in that it is a rate equation describing the net transfer of a given species that has an upper bound in one direction but not the other.

The dependence of solar cell performance on contacts has long been recognized; development of selective contacts for everything from silicon to organics and perovskites has been extensive.[26, 32–34, 38, 41–49] Theoretical understanding of the mechanisms by which contacts can limit or improve device performance is, however, incomplete. Much of the recent literature, as discussed below, has focused on either a contact’s ability to extract its intended carrier, or reject the ‘wrong’ carrier. Of course, both contacts in a device must extract their intended carrier *and* reject the wrong carrier to some extent in order for a solar cell to generate power, so a complete understanding of the contacts’ limitations on a solar cell should consider all four of these processes.

Throughout this work, I will refer to the collection of the ‘intended’ carrier at a contact as the majority process for that contact, and to the associated carrier as the majority carrier. Accordingly, the term minority is used for the ‘wrong’ process / carrier at a contact. Note that I will use the term ‘bulk majority/minority carrier’ explicitly when referring instead to the traditional definition based on the doping of the semiconductor.

The notion that a solar cell’s performance can be limited by a contact’s ability to extract its majority carrier is intuitive. Indeed, numerous studies have explored how this can limit the open-circuit voltage (V_{oc}) of a device.[50–55] Wagenpfahl et al. calculated an analytic expression for the V_{oc} of a solar cell due to an electric field associated with the build up of majority carriers at a contact that is caused by the reduction of the charge transfer velocity of majority carriers.[51] Simulated $J(V)$ also suggested that a reduced charge transfer velocity of majority carriers at a contact can be the cause of so-called S-shaped curves that can ruin the fill factor. This notion was confirmed by Sandberg et al. whose simulations also showed S-shaped curves being affected by the injection barrier, carrier mobilities, and trap densities at the interface.[52] Niemegeers and Burgelman used a back-to-back diode equivalent circuit to model the current 'rollover' effect (analogous to S-shaped curves) in CdTe solar cells.[50] The saturation current of the back diode, quantifying the collection of majority carrier holes, is limited by the work function alignment of the metal used for the back contact; this was shown to determine the current value at which the $J(V)$ curve rolls over in forward bias, thus affecting the fill factor of the device.

It is equally intuitive that the failure of a contact to reject the wrong carrier, or minority carrier, leads to unwanted surface recombination and, hence, reduced efficiency. Mora-Sero and Bisquert considered a 'sandwich' model (i.e. an absorber sandwiched by two different contacts) using one ideal contact paired with a contact whose selectivity is reduced by allowing electrons to escape depending on ρ, the resistivity to minority carrier flow at the contact.[56] They calculated a $J(V)$ curve whose V_{oc} and J_{sc} are strongly affected by ρ. Sandberg et al. also considered a sandwich-type solar cell architecture and derived analytic expressions for the V_{oc} in various regimes delineated by ohmic vs. non-ohmic contacts.[54] For a single non-ohmic contact paired with an ohmic contact, regimes dominated by diffusion-limited surface recombination and interface-kinetics-limited surface recombination were considered. They calculated an effective diffusion velocity parameter following Crowell and Sze [57] that, compared to the charge transfer velocity of minority carriers, can be used to determine whether kinetics or diffusion determines recombination rates at V_{oc}.

Brendel and Peibst defined selectivity as the ratio of the minority to majority carrier resistivity of an interface and modeled $J(V)$ behavior with a diode characterized by the minority-carrier resistivity in series with a resistor determined by the majority-carrier resistivity.[53] This allowed them to determine the optimum contact area for various types of silicon solar cells based on the selectivity (i.e. resistivity) ratio of the contact. This model hints at the potential interplay between both ‘majority’ and ‘minority’ processes at a contact determining device performance, a concept touched on by others.[51, 58] However, none of the above models consider all four processes independently.

It is instructive to take a step back from these focused studies and consider a simpler, more general model. Perhaps the simplest theoretical model of contact limited $J(V)$ behavior is a parallel combination of a diode governed by the ideal diode equation and a current source whose current value is J_L (i.e the light current). The $J(V)$ curve for such a device obeys that of the ideal solar cell in eq. 1.9:

$$J(V) = J_0(e^{V/V_T} - 1) - J_L. \tag{2.1}$$

This is effectively the same equation as that derived in the SQ limit, except as we will see, the J_0 in this case is determined entirely by the contact(s) and not by radiative recombination in the bulk. The maximum power (density) of a device obeying eq. 2.1 is determined by the balance of J_0 and J_L, given by

$$P_{max} = J(V_{max}) \times V_{max} \tag{2.2}$$

where

$$V_{max} = V_T \left(W \left[e(1 + \frac{J_L}{J_0}) \right] \right) \tag{2.3}$$

where W is the Lambert W function. As is commonly understood, the ratio of J_L to J_0 determines the efficiency, thus minimizing J_0 is critical to maximizing the device efficiency.

The origin of J_0 depends on which simple diode model we consider. In the case of the Schottky diode, the J_0 is determined by the potential barrier for bulk majority carriers at the metal-semiconductor interface via thermionic emission:

$$J_0 = A^* T^2 e^{-\frac{\phi_b}{qV_T}} \tag{2.4}$$

where ϕ_b is the barrier height (i.e. ϕ_b is the energy difference between the band of the bulk majority carrier and the Fermi level at the interface at equilibrium) and A^* is the effective Richardson constant.[59] Note that while one considers the rate of bulk majority carriers that are able to escape the potential barrier at the interface, these carriers are the minority carriers at the interface. In other words, for a typical Schottky diode based on a p-type semiconductor, the Fermi level of the isolated metal used to make the contact is generally located in the top half of the bandgap, meaning it is effectively an electron-selective contact. The J_0 in this case measures the ability of holes to travel over the potential barrier at the interface, where they are considered minority carriers in this work.

Meanwhile, for the Shockley model of a $p-n$ junction, the J_0 is calculated by considering the diffusion of minority carriers on either side of the depletion region.[60] Here,

$$J_0 = q\left(\frac{D_p p_{n0}}{L_p} + \frac{D_n n_{p0}}{L_n}\right) \tag{2.5}$$

where D_p is the diffusion constant for holes, p_{n0} is the equilibrium concentration for holes on the n-type side, and L_p is the hole diffusion length and visa versa for the other term. The origin of this J_0 is, of course, bulk recombination in the quasi-neutral regions on both sides of the depletion region. However, because typical $p-n$ junctions have good ohmic contacts on both sides, the 'interfaces' between the depletion region (in which recombination is neglected) and the quasi-neutral regions on both sides are the rate-determining interfaces. In this way, the p and n quasi-neutral regions can be thought of as the contacts to the depletion region. Thus the two terms in J_0 are determined by the recombination of minority carriers for each contact (i.e. holes on the n-side and electrons on the p-side).

The performance of the simple solar cell model of eq. 2.1 is limited in both cases by carriers escaping to the wrong contact. For the Schottky diode, only one J_0 is considered, associated with the rectifying contact. Meanwhile, with the $p-n$ junction, two J_0's are considered; one for each side of the junction resulting in the two terms of eq. 2.5. In order to reduce the escape of minority carriers in the ideal Schottky diode, one can either use a metal whose Fermi level is closer to the intended carrier's band or one can introduce a thin insulating layer that reduces the flow of both carriers.[33, 61, 62] For the $p-n$ junction, reduction of minority carrier leakage can be achieved by strongly doping the n and p layers. This has already been recognized; state-of-the-art silicon technology uses highly n and p doped regions as the electron and hole selective contacts respectively.[33, 63]

It is critical to note that in both the Shockley model of the $p-n$ junction and the Schottky diode model, one effectively assumes that the bulk quasi-Fermi-level splitting is equal to the applied voltage. For the $p-n$ junction, this is guaranteed with the assumption of low injection of majority carriers at the edges of the depletion region. With the Schottky diode, one implicitly assumes that the other contact to, for instance, our p-type material is able to perfectly extract holes. In other words, one assumes for both cases that the majority processes at each contact are very fast so that no build up of that carrier is required at the contact in order to support the current. This assumption is not generally valid, nor can one always assume perfect rejection of minority carriers at a contact; a thorough contact-determined solar cell model must consider the ability of majority carriers to escape *as well as* the ability of minority carriers to escape at *both* contacts.

As discussed above, our analysis will focus on the effect of the J_0's on the performance of the solar cell, and thus it is important to note that they are measurable quantities associated with an interface.[64–68] For a given solar cell, there are four J_0's to measure, two for each interface. The J_0's may not all be readily measurable from the solar cell itself, measuring all four may require four different devices. To measure the hole J_0 of an electron selective contact for example, one could make a device with a p-type wafer of the absorber in question with an ohmic contact at the other end of the device. Measurement of the $J(V)$ curve in the dark can then be performed to extract J_0. In principle, one can then measure the *electron* J_0 of this same contact by contacting it to an n-type wafer, as long as one can make a contact that is even more ohmic than the electron selective contact in question. If this is not possible, it may be possible to calculate the majority J_0 with additional information. For example, in the case of a Schottky contact with a known barrier height to an absorber with a known bandgap, one could calculate the approximate electron J_0 from the barrier height and the hole J_0.

In this chapter, the motivation for a more comprehensive model of how solar cell contacts determine the performance of solar cells is spelled out. It is clear that such a model needs to account for all four J_0's of a solar cell. The next chapter will spell out the model that we use in order to determine the contact-limited $J(V)$ curve as a function of the four J_0's.

CHAPTER III

MODEL

This chapter will describe the simplified physical model which was used to derive the contact-determined performance of a solar cell. The model was used in both of my first author papers.[1, 2] The model is described in both papers to some extent as the two papers used it to calculate different things; this chapter presents the model in a way that should prepare the reader for both sets of calculations (that of the $J(V)$ and the $V_{oc}/\Delta E_f$).

We assume a 'sandwich' solar cell model in that a 1-D semiconducting absorber is sandwiched by two contacts on either end to extract electrons and holes. The absorber is assumed to be intrinsic. Consider the life of an electron in the conduction band of the absorber that was generated via photon absorption. There are different ways the life of said electron could end (i.e. leave the conduction band of the absorber). It could recombine with a hole in the bulk of the absorber via some form of bulk recombination, it could recombine with a hole at one of the contacts, or if we are lucky, it could escape the device to an external circuit where it can do work. SQ neglected the second option (contact recombination) when calculating their limit; we do the opposite and neglect bulk recombination, as we seek an understanding of how contacts, rather than bulk recombination, limit device performance.

A diagram of our model is presented in Fig. 3. The 1-D absorber exists between the positions x^{α} and x^{β}, where it interfaces with the α and β contacts, respectively. $L = x^{\beta} - x^{\alpha}$ is the thickness of the absorber. The electron and hole partial current densities (J_n and J_p) describe the rates at which electrons and holes escape to the external circuit. The partial current densities must sum to a fixed current density

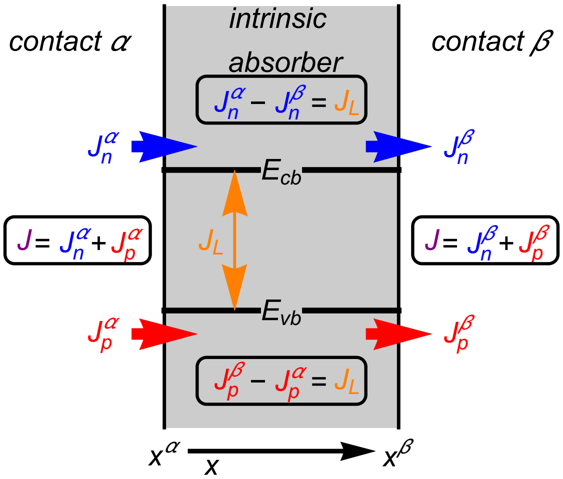

FIGURE 3. Diagram depicting the essential processes considered in our model. Electrons and holes are generated by photon absorption in the bulk of the absorber, and travel to the contacts, where they either recombine or escape the device and travel through an external circuit. J_L is determined by the rate of electron and hole generation. The equations highlighted are consequences of the continuity equation, our assumptions, and current conservation, as spelled out in the text. They constrain the partial currents so that we can calculate them as a function of the total current in the device.

throughout the device, including at the contacts as long as the device is in steady state, which will always be assumed. We will assume that current moving in the positive x direction (to the right) is positive.

The generation of electrons and holes due to photon absorption is assumed to be uniform, and determines the relation between the partial currents for each individual carrier, as we will see later. We use the electrochemical potential, $\bar{\mu} = \mu + zq\phi$, where μ is the chemical potential, z is $+1$ for holes and -1 for electrons, and ϕ is the electrostatic potential. We make the following critical assumptions:

1. Electrons and holes in the absorber are thermalized to the conduction and valence bands respectively, so that they can be described by the electrochemical potentials $\bar{\mu}_n$ and $\bar{\mu}_p$. These are equivalent to the electron and hole quasi-Fermi levels. This assumption is almost universally valid, as the relaxation times of

electrons that are given more energy than the bandgap energy are much shorter than the time needed to extract them from the absorber.[69–75]

2. There are no transport limitations in the absorber so that slopes in the quasi-Fermi levels are negligibly small (i.e. $\frac{d\bar{\mu}_n}{dx} \approx \frac{d\bar{\mu}_p}{dx} \approx 0$)

3. Bulk recombination is neglected. [1]

4. The boundary conditions for each of the four partial currents at the contacts can be written as follows:

$$J_n(x^\alpha) = J_n^\alpha = J_{0n}^\alpha \left(\frac{n(x^\alpha)}{n_0(x^\alpha)} - 1 \right) \tag{3.1a}$$

$$J_p(x^\alpha) = J_p^\alpha = -J_{0p}^\alpha \left(\frac{p(x^\alpha)}{p_0(x^\alpha)} - 1 \right) \tag{3.1b}$$

$$J_n(x^\beta) = J_n^\beta = -J_{0n}^\beta \left(\frac{n(x^\beta)}{n_0(x^\beta)} - 1 \right) \tag{3.1c}$$

$$J_p(x^\beta) = J_p^\beta = J_{0p}^\beta \left(\frac{p(x^\beta)}{p_0(x^\beta)} - 1 \right) \tag{3.1d}$$

where the J_{0n} and J_{0p} are electron and hole equilibrium exchange current densities. The carrier densities and equilibrium carrier densities (i.e. n, p, n_0, and p_0) are evaluated in the semiconductor at both the α and β interfaces. The equilibrium densities are determined by contact properties.

5. The equilibrium carrier densities obey the law of mass action:

---

[1] Note that assumptions 2 and 3 are both implicitly assumed in both the Shockley model of the p-n junction (recombination is considered in the quasi neutral regions, but not in the depletion region) and the Schottky diode. The efficacy of these assumptions is tested in the Simulations chapter.

$$n_0(x)p_0(x) = n_i^2 \tag{3.2}$$

where n_i is the intrinsic carrier density, given by

$$n_i = \sqrt{N_c N_v} e^{-\frac{E_g}{2qV_t}}. \tag{3.3}$$

6. The electric field in both contacts is zero, and their chemical potentials, μ^α and μ^β, are voltage independent.

Equation 3.1 is the set of boundary conditions relating the carrier densities at the interfaces to the relevant partial currents. In essence, they state that the partial currents are proportional to a voltage independent constant times the excess carrier density at a contact. The excess carrier density is referenced to the equilibrium density, which is usually determined by the contact Fermi-level, be it a semiconductor or a metal. These boundary conditions are appropriate for a metal-semiconductor contact, but can also be appropriate for Schottky contacts with an insulator used to reduce the escape of minority carriers (i.e. a passivating layer), and for doped semiconductor contacts. The extent to which these more complicated device architectures can still be modeled by eq. 3.1 will be discussed in the Simulations chapter.

Electrons and holes are always generated at equal rates in the bulk of our solar cell absorber, as any photon with enough energy to promote an electron from the valence band to the conduction band by definition leaves behind a hole. We assume, for the sake of simplicity, that the generation rate is uniform throughout the absorber, so it is easy to calculate the total rate of electrons and holes being generated by multiplying the generation rate by the thickness of the absorber. We define the light current (density) as the product of the elementary charge times this rate:

$$J_L = qG_L L, \tag{3.4}$$

where G_L is the generation rate of electrons and holes per unit volume.

In general, the 1-D continuity equation for electrons in a semiconductor states that

$$q\frac{dn}{dt} = \frac{dJ_n}{dx} + q(G_L - R), \tag{3.5}$$

i.e. the number of electrons in some region of the absorber only changes if there are more electrons flowing into the region than out (indicated by $\frac{dJ_n}{dx}$, the 1-D divergence of the electron current), if electrons are created from generation via photon absorption (G_L),[2] or if they recombine (R). Given a uniform generation rate[3] and assumption 3, the continuity equation at steady state (i.e. $\frac{dn}{dt} = 0$) simplifies to

$$qG_L = -\frac{dJ_n}{dx}, \tag{3.6}$$

which readily gives

$$J_n^\alpha - J_n^\beta = qG_L L = J_L, \tag{3.7}$$

---

[2] Note that we neglect thermal generation, as it is generally negligible compared to photon induced generation. Additionally, it would be disingenuous to include thermal generation while we ignore direct recombination, which is the reverse process.

[3] In reality, generation in a semiconductor is expected to follow Beer-Lambert law absorption, i.e. the generation rate exponentially decays into the absorber according to the absorption coefficient. However, given assumptions 2 and 3, we expect the generated carriers will readily distribute themselves throughout the absorber, and thus the generation profile should not affect the result. We will test this expectation in the Simulations chapter.

using the fundamental theorem of calculus and eq. 3.4. This is a simple algebraic expression relating the partial currents on either side of the absorber. Usually in semiconductor physics, this relation would be much more complicated, and requires a numerical solution to the continuity equation. We assumed that there was no bulk recombination for the purposes of deriving the limiting behavior as determined by contacts, but this assumption is also critical in allowing us to find an analytic, rather than numerical solution to the continuity equation. As we will see, the analytic solution is practical for developing an intuitive understanding of how the contact-determined solar cell behaves.

By definition, the partial currents for each carrier sum to the total current throughout the device. Therefore, at the contacts, we know that

$$J = J_n^{\alpha} + J_p^{\alpha} \tag{3.8a}$$

$$J = J_n^{\beta} + J_p^{\beta}. \tag{3.8b}$$

Thus, we now have three constraints for the four, in general unknown, partial currents (or equivalently carrier densities via eq. 3.1) at the contacts. One more is needed.

The final constraint comes from the assumption that the quasi-Fermi levels (i.e. electrochemical potentials) for each carrier are constant throughout the absorber. Evaluating the electrochemical potential for each carrier at each contact using its definition gives

$$V_T \ln \frac{n(x^\alpha)}{n_i} - \phi^\alpha = V_T \ln \frac{n(x^\beta)}{n_i} - \phi^\beta \tag{3.9a}$$

$$V_T \ln \frac{p(x^\alpha)}{n_i} + \phi^\alpha = V_T \ln \frac{p(x^\beta)}{n_i} + \phi^\beta, \tag{3.9b}$$

where we have chosen to reference the electrochemical potentials to that for which $n = p = n_i$ and $\phi = 0$. Eliminating $\phi(x^\alpha) - \phi(x^\beta)$ from these equations yields

$$\frac{p(x^\beta)}{p(x^\alpha)} = \frac{n(x^\alpha)}{n(x^\beta)}, \tag{3.10}$$

or, equivalently,

$$n(x^\alpha)p(x^\alpha) = n(x^\beta)p(x^\beta). \tag{3.11}$$

Equation 3.11 is a constraint on the carriers at each contact, but can be written in terms of the partial currents via eq. 3.1. It can be thought of as a modified, or non-equilibrium, law of mass action applied at each contact; it simply takes into account that the quasi-Fermi-level splitting is in general non-zero (it is only zero at equilibrium).

Equations 3.7, 3.8a, 3.8b, and 3.11 (written in terms of the partial currents via eq. 3.1) then, are four algebraic constraint equations for the four unknowns, J_n^α, J_p^α, J_n^β, J_p^β in terms of the four J_0's, J_L, the four equilibrium carrier densities at the contacts, and the total current, J. Unfortunately, eq. 3.11 is nonlinear, so we will have to do some algebraic gymnastics in order to solve them. One can readily use Mathematica to solve this system of equations (in fact this is how they were first solved), however, this does not necessarily put them in useful or intelligible forms. Detailed algebraic solutions are therefore provided in Chapter 4. I find the algebraic solutions enlightening and rather elegant (despite the complexity of the algebra involved), however the non-mathematically curious can skip Chapter 4.

There is one more thing to do before this though; the solutions to the partial currents at the contacts, or the equivalent carrier densities don't directly tell us about what we want to know: the performance of the solar cell. For this, we need to know how the voltage across the device relates to these quantities. By definition the voltage difference across the device is proportional to the electrochemical potential difference for electrons between the two contacts:

$$-qV = \bar{\mu}^{\alpha} - \bar{\mu}^{\beta}. \tag{3.12}$$

Note that $\bar{\mu}^{\alpha}$ and $\bar{\mu}^{\beta}$ are not equivalent to $\bar{\mu}(x^{\alpha})$ and $\bar{\mu}(x^{\beta})$, respectively. The first two refer to the electrochemical potentials in the contacts themselves, whereas the second two refer to the electrochemical potentials in the semiconductor at the interfaces to the contacts. Using the definition of $\bar{\mu}$ yields

$$-qV = \mu^{\alpha} - q\phi^{\alpha} - (\mu^{\beta} - q\phi^{\beta}). \tag{3.13}$$

At equilibrium, the electrochemical potentials of the contacts must be equal:

$$\mu_0^{\alpha} - q\phi_0^{\alpha} = \mu_0^{\beta} - q\phi_0^{\beta}. \tag{3.14}$$

Equations 3.13 and 3.14 can be combined with assumption 6 to the chemical potentials, yielding:

$$V = \phi^{\alpha} - \phi^{\beta} - (\phi_0^{\alpha} - \phi_0^{\beta}). \tag{3.15}$$

Writing the electrostatic potentials in terms of the chemical potentials via eq. 3.9 (evaluated at both a general applied bias and equilibrium) leads to

$$V = V_T \ln\left(\frac{n(x^{\alpha})n_0(x^{\beta})}{n_0(x^{\alpha})n(x^{\beta})}\right) = V_T \ln\left(\frac{p(x^{\beta})p_0(x^{\alpha})}{p_0(x^{\beta})p(x^{\alpha})}\right) \tag{3.16}$$

In addition to the voltage across the device, the quasi-Fermi-level splitting (ΔE_f) can be calculated for arbitrary currents/voltages:

$$\frac{\Delta E_f}{q} = \frac{\bar{\mu}_n - \bar{\mu}_p}{q} = V_T \ln\left(\frac{n(x^{\alpha})p(x^{\alpha})}{n_0(x^{\alpha})p_0(x^{\alpha})}\right) = V_T \ln\left(\frac{n(x^{\beta})p(x^{\beta})}{n_0(x^{\beta})p_0(x^{\beta})}\right) \tag{3.17}$$

The model that has been layed out above is the basis of the theory presented in both Roe et al. 2018 and Roe et al. 2019. In the next chapter, the current-voltage curve, as well as the open circuit voltage and quasi-Fermi-level splitting at V_{oc} will be derived algebraically, using the constraints arrived at here. All of the algebra derived in the next chapter, and all of the results discussed in the two subsequent chapters rely on the assumptions of our model, as presented above.

CHAPTER IV

PRIMARY DERIVATIONS

This chapter contains the necessary algebraic derivations leading to the theoretical results presented in Chapters 5 and 6. It is taken from the Supporting Information of both Roe et al. 2018 and Roe et al. 2019. A few semantic changes have been made for clarity and continuity purposes, however the math remains the same.

Voltage as a Function of Current

We solve the system of Eqs. 3.7, 3.8a 3.8b, and 3.11 for J_n^β as a function of J_L, the four J_0's, and J. The solution for J_n^β is easily used to obtain the other three partial currents, by substituting back into Eqs. 3.7, 3.8a and 3.8b.

We first rewrite the modified law of mass action (Eq. 3.11) in terms of the partial currents at the contacts using Eq. 3.1. Below are the necessary substitutions:

$$n^\beta = n_0^\beta \left(1 - \frac{J_n^\beta}{J_{0n}^\beta}\right) \tag{4.1a}$$

$$p^\beta = p_0^\beta \left(1 + \frac{J_p^\beta}{J_{0p}^\beta}\right) \tag{4.1b}$$

$$n^\alpha = n_0^\alpha \left(1 + \frac{J_n^\alpha}{J_{0n}^\alpha}\right) \tag{4.1c}$$

$$p^\alpha = p_0^\alpha \left(1 - \frac{J_p^\alpha}{J_{0p}^\alpha}\right). \tag{4.1d}$$

Thus, Eq. 3.11 reads:

$$n_0^\beta p_0^\beta \left(1 - \frac{J_n^\beta}{J_{0n}^\beta}\right)\left(1 + \frac{J_p^\beta}{J_{0p}^\beta}\right) = n_0^\alpha p_0^\alpha \left(1 + \frac{J_n^\alpha}{J_{0n}^\alpha}\right)\left(1 - \frac{J_p^\alpha}{J_{0p}^\alpha}\right). \tag{4.2}$$

Using the equilibrium law of mass action (Eq.3.3) and dividing by n_i^2, this simplifies to:

$$\left(1 - \frac{J_n^\beta}{J_{0n}^\beta}\right)\left(1 + \frac{J_p^\beta}{J_{0p}^\beta}\right) = \left(1 + \frac{J_n^\alpha}{J_{0n}^\alpha}\right)\left(1 - \frac{J_p^\alpha}{J_{0p}^\alpha}\right). \tag{4.3}$$

Next, the constraints $J_p^\alpha = J - J_n^\alpha$ and $J_p^\beta = J - J_n^\beta$ (Eqs. 3.8a and 3.8b) are used to eliminate J_p^α and J_p^β:

$$\left(1 - \frac{J_n^\beta}{J_{0n}^\beta}\right)\left(1 + \frac{J - J_n^\beta}{J_{0p}^\beta}\right) = \left(1 + \frac{J_n^\alpha}{J_{0n}^\alpha}\right)\left(1 - \frac{J - J_n^\alpha}{J_{0p}^\alpha}\right). \tag{4.4}$$

The final constraint is that $J_n^\alpha = J_L + J_n^\beta$ (Eq.3.7), giving:

$$\left(1 - \frac{J_n^\beta}{J_{0n}^\beta}\right)\left(1 + \frac{J - J_n^\beta}{J_{0p}^\beta}\right) = \left(1 + \frac{J_L + J_n^\beta}{J_{0n}^\alpha}\right)\left(1 - \frac{J - (J_L + J_n^\beta)}{J_{0p}^\alpha}\right). \tag{4.5}$$

All variables except J_n^β have been eliminated, next we manipulate the equation so that it is in quadratic form. First, we multiply both sides by $J_{0n}^\beta J_{0n}^\alpha J_{0p}^\beta J_{0p}^\alpha$:

$$\left(J_{0n}^\beta - J_n^\beta\right)\left(J_{0p}^\beta + J - J_n^\beta\right) J_{0n}^\alpha J_{0p}^\alpha = J_{0n}^\beta J_{0p}^\beta \left(J_{0n}^\alpha + J_L + J_n^\beta\right)\left(J_{0p}^\alpha - J + J_L + J_n^\beta\right). \tag{4.6}$$

Expanding and collecting terms, we have:

$$\begin{aligned}\left(J^{\alpha}_{0n}J^{\alpha}_{0p} - J^{\beta}_{0n}J^{\beta}_{0p}\right)(J^{\beta}_{n})^2& \\ + \left(J^{\alpha}_{0n}J^{\alpha}_{0p}(-J - J^{\beta}_{0p} - J^{\beta}_{0n}) + J^{\beta}_{0n}J^{\beta}_{0p}(J - 2J_L - J^{\alpha}_{0n} - J^{\alpha}_{0p})\right) J^{\beta}_{n}& \\ + \left(J^{\alpha}_{0n}J^{\alpha}_{0p}J^{\beta}_{0n}J + J^{\beta}_{0n}J^{\beta}_{0p}\left(J(J^{\alpha}_{0n} + J_L) - J_L(J_L + J^{\alpha}_{0n} + J^{\alpha}_{0p})\right)\right) &= 0. \end{aligned} \tag{4.7}$$

Dividing both sides by $J^{\beta}_{0n}J^{\beta}_{0p}$ and writing in terms of $\Lambda = \frac{J^{\alpha}_{0n}J^{\alpha}_{0p}}{J^{\beta}_{0n}J^{\beta}_{0p}}$, this is simplified to:

$$\begin{aligned}(\Lambda - 1)(J^{\beta}_{n})^2 + \left(\Lambda(-J - J^{\beta}_{0p} - J^{\beta}_{0n}) + (J - 2J_L - J^{\alpha}_{0n} - J^{\alpha}_{0p})\right) J^{\beta}_{n}& \\ + \left(\Lambda J^{\beta}_{0n}J + \left(J(J^{\alpha}_{0n} + J_L) - J_L(J_L + J^{\alpha}_{0n} + J^{\alpha}_{0p})\right)\right) &= 0. \end{aligned} \tag{4.8}$$

According to the quadratic formula then, the solution for J^{β}_{n} is:

$$\begin{aligned} J^{\beta}_{n} &= \tfrac{1}{2(\Lambda-1)} \\ &\Bigg(\Lambda\left(J + J^{\beta}_{0p} + J^{\beta}_{0n}\right) + \left(2J_L + J^{\alpha}_{0p} + J^{\alpha}_{0n} - J\right) \\ &- \sqrt{\begin{aligned}&\left(\Lambda\left(J + J^{\beta}_{0p} + J^{\beta}_{0n}\right) + \left(2J_L + J^{\alpha}_{0p} + J^{\alpha}_{0n} - J\right)\right)^2 \\ &+4(1-\Lambda)\left(\Lambda J^{\beta}_{0n}J + \left(J(J^{\alpha}_{0n} + J_L) - J_L(J_L + J^{\alpha}_{0n} + J^{\alpha}_{0p})\right)\right)\end{aligned}}\Bigg). \end{aligned} \tag{4.9}$$

Note that we have dropped the '+' solution; the '+' solution sometimes results in J^{β}_{n} values that are not between $-J_L$ and 0 for $J = 0$ (recall that J^{β}_{n} is negative in our convention) and thus it is non-physical. In order to find the expression for $J(V)$, we first re-write eq. 3.15 in terms of J^{β}_{n}, giving:

$$V = V_T \ln \left(\frac{1 + \frac{J_L + J_n^\beta}{J_{0n}^\alpha}}{1 - \frac{J_n^\beta}{J_{0n}^\beta}} \right) \tag{4.10}$$

Plugging in the solution to J_n^β,

$$V = -V_T \ln \left(\frac{1 - \frac{1}{2J_{0n}^\beta(\Lambda - 1)} \left(2J_L + J_{0p}^\alpha + J_{0n}^\alpha - J + \Lambda(J + J_{0n}^\beta + J_{0p}^\beta) - \sqrt{R} \right)}{1 + \frac{J_L}{J_{0n}^\alpha} + \frac{1}{2J_{0n}^\alpha(\Lambda - 1)} \left(2J_L + J_{0p}^\alpha + J_{0n}^\alpha - J + \Lambda(J + J_{0n}^\beta + J_{0p}^\beta) - \sqrt{R} \right)} \right). \tag{4.11}$$

For brevity, we have replaced the radicand in J_n^β from eq. 4.9 with the symbol R. The next step is to combine the denominator and numerator under a common denominator for each:

$$V = -V_T \ln \left(\frac{\frac{1}{2J_{0n}^\beta(\Lambda - 1)} \left(J - 2J_L - J_{0p}^\alpha - J_{0n}^\alpha + \Lambda(J_{0n}^\beta - J_{0p}^\beta - J) + \sqrt{R} \right)}{\frac{1}{2J_{0n}^\alpha(\Lambda - 1)} \left(J_{0p}^\alpha - J_{0n}^\alpha - J + \Lambda(2J_L + J + J_{0n}^\beta + J_{0p}^\beta + 2J_{0n}^\alpha) - \sqrt{R} \right)} \right). \tag{4.12}$$

Eliminating common factors in the numerator and denominator, writing out the Λ's, and multiplying both by $J_{0n}^\beta J_{0p}^\beta$ leads to:

$$\begin{aligned} V = & -V_T \ln \left(\frac{J_{0n}^\alpha}{J_{0n}^\beta} \right) - \\ & V_T \ln \left(\frac{J_{0n}^\beta J_{0p}^\beta (J - 2J_L - J_{0p}^\alpha - J_{0n}^\alpha) + J_{0n}^\alpha J_{0p}^\alpha (J_{0n}^\beta - J_{0p}^\beta - J) + J_{0n}^\beta J_{0p}^\beta \sqrt{R}}{J_{0n}^\beta J_{0p}^\beta (J_{0p}^\alpha - J_{0n}^\alpha - J) + J_{0n}^\alpha J_{0p}^\alpha (2J_L + J + J_{0n}^\beta + J_{0p}^\beta + 2J_{0n}^\alpha) - J_{0n}^\beta J_{0p}^\beta \sqrt{R}} \right). \end{aligned} \tag{4.13}$$

Next, we multiply top and bottom by the conjugate of the denominator to get rid of the square root in the denominator. After factoring, the numerator is now equal to:

$$\begin{aligned}
&\left(\tfrac{2J_{0n}^{\alpha}}{J_{0n}^{\beta}}\right)(J_L + J_{0n}^{\beta} + J_{0n}^{\alpha}) \\
&(J_{0n}^{\beta}J_{0p}^{\beta} - J_{0n}^{\alpha}J_{0p}^{\alpha})\times \\
&\left(J_{0n}^{\alpha}J_{0p}^{\beta}J_{0p}^{\alpha} + J(J_{0n}^{\beta}J_{0p}^{\beta} + J_{0n}^{\alpha}J_{0p}^{\alpha}) + J_{0n}^{\beta}(J_{0n}^{\alpha}(J_{0p}^{\beta} - J_{0p}^{\alpha}) - J_{0p}^{\beta}(J_{0p}^{\alpha} + \sqrt{R}))\right).
\end{aligned} \tag{4.14}$$

The new denominator, below, has some common factors with the numerator:

$$4J_{0n}^{\alpha}J_{0p}^{\alpha}(J_L + J_{0n}^{\beta} + J_{0n}^{\alpha})(J + J_L + J_{0n}^{\alpha} + J_{0p}^{\beta})(J_{0n}^{\alpha}J_{0p}^{\alpha} - J_{0n}^{\beta}J_{0p}^{\beta}). \tag{4.15}$$

After canceling the common factors, the expression for $V(J)$ is:

$$\begin{aligned}
&V = -V_T \ln\Bigg(- J_{0n}^{\alpha}J_{0p}^{\beta}J_{0p}^{\alpha} - J(J_{0n}^{\beta}J_{0p}^{\beta} + J_{0n}^{\alpha}J_{0p}^{\alpha}) \\
&-J_{0n}^{\beta}(J_{0n}^{\alpha}(J_{0p}^{\beta} - J_{0p}^{\alpha}) - J_{0p}^{\beta}(J_{0p}^{\alpha} + \sqrt{R}))\Bigg) - V_T \ln\left(2J_{0n}^{\beta}J_{0p}^{\alpha}(J + J_L + J_{0n}^{\alpha} + J_{0p}^{\beta})\right)
\end{aligned} \tag{4.16}$$

After redistributing terms in a more sensible way in the numerator and in the radicand, we now have a well-simplified $V(J)$:

$$
\begin{aligned}
&V(J) = -V_T \ln \Bigg(\tfrac{1}{2J^{\beta}_{0n} J^{\alpha}_{0p} (J + J_L + J^{\alpha}_{0n} + J^{\beta}_{0p})} \\
&\Bigg(-J^{\alpha}_{0n} J^{\alpha}_{0p} \left(J - J^{\beta}_{0n} + J^{\beta}_{0p} \right) - J^{\beta}_{0n} J^{\beta}_{0p} \left(J + J^{\alpha}_{0n} - J^{\alpha}_{0p} \right) \\
&+ \sqrt{\begin{array}{l} \left(J^{\alpha}_{0n} J^{\alpha}_{0p} \left(J + 2J_L + J^{\beta}_{0n} + 2J^{\alpha}_{0n} + J^{\beta}_{0p} \right) - J^{\beta}_{0n} J^{\beta}_{0p} \left(J + J^{\alpha}_{0n} - J^{\alpha}_{0p} \right) \right)^2 \\ +4J^{\alpha}_{0n} J^{\alpha}_{0p} \left(J^{\beta}_{0n} J^{\beta}_{0p} - J^{\alpha}_{0n} J^{\alpha}_{0p} \right) \left(J_L + J^{\beta}_{0n} + J^{\alpha}_{0n} \right) \left(J + J_L + J^{\alpha}_{0n} + J^{\beta}_{0p} \right) \end{array}} \Bigg) \Bigg).
\end{aligned}
\tag{4.17}
$$

Current as a Function of Voltage

We could end this here, but it turns out the inverted expression for $J(V)$ is simpler and more revealing. Thus, we proceed to derive $J(V)$. The first steps are to divide by $-V_T$, exponentiate both sides, and then multiply by the denominator of the Log argument:

$$
\begin{aligned}
&e^{-V/V_T} \left(2J^{\beta}_{0n} J^{\alpha}_{0p} (J + J_L + J^{\alpha}_{0n} + J^{\beta}_{0p}) \right) = \\
&-J^{\alpha}_{0n} J^{\alpha}_{0p} \left(J - J^{\beta}_{0n} + J^{\beta}_{0p} \right) - J^{\beta}_{0n} J^{\beta}_{0p} \left(J + J^{\alpha}_{0n} - J^{\alpha}_{0p} \right) \\
&+ \sqrt{\begin{array}{l} \left(J^{\alpha}_{0n} J^{\alpha}_{0p} \left(J + 2J_L + J^{\beta}_{0n} + 2J^{\alpha}_{0n} + J^{\beta}_{0p} \right) - J^{\beta}_{0n} J^{\beta}_{0p} \left(J + J^{\alpha}_{0n} - J^{\alpha}_{0p} \right) \right)^2 \\ +4J^{\alpha}_{0n} J^{\alpha}_{0p} \left(J^{\beta}_{0n} J^{\beta}_{0p} - J^{\alpha}_{0n} J^{\alpha}_{0p} \right) \left(J_L + J^{\beta}_{0n} + J^{\alpha}_{0n} \right) \left(J + J_L + J^{\alpha}_{0n} + J^{\beta}_{0p} \right) \end{array}}
\end{aligned}
\tag{4.18}
$$

Next, the square root term is isolated, we divide by $J^{\beta}_{0n} J^{\beta}_{0p}$, and re-substitute $\Lambda = \frac{J^{\alpha}_{0n} J^{\alpha}_{0p}}{J^{\beta}_{0n} J^{\beta}_{0p}}$ where appropriate:

$$
\begin{aligned}
&2e^{-V/V_T \frac{J_{0p}^{\alpha}}{J_{0p}^{\beta}}}(J + J_L + J_{0n}^{\alpha} + J_{0p}^{\beta}) \\
&+\Lambda \left(J - J_{0n}^{\beta} + J_{0p}^{\beta}\right) + \left(J + J_{0n}^{\alpha} - J_{0p}^{\alpha}\right) \\
&= \sqrt{\begin{aligned}&\left(\Lambda \left(J + 2J_L + J_{0n}^{\beta} + 2J_{0n}^{\alpha} + J_{0p}^{\beta}\right) - \left(J + J_{0n}^{\alpha} - J_{0p}^{\alpha}\right)\right)^2 \\ &+4\Lambda\left(1-\Lambda\right)\left(J_L + J_{0n}^{\beta} + J_{0n}^{\alpha}\right)\left(J + J_L + J_{0n}^{\alpha} + J_{0p}^{\beta}\right)\end{aligned}}.
\end{aligned}
\tag{4.19}
$$

Since we need to solve for J in the end, it is advantageous to write the left hand side in descending order of J:

$$
\begin{aligned}
&J\left(2e^{-V/V_T \frac{J_{0p}^{\alpha}}{J_{0p}^{\beta}}} + 1 + \Lambda\right) \\
&+\left(2e^{-V/V_T \frac{J_{0p}^{\alpha}}{J_{0p}^{\beta}}}(J_{0n}^{\alpha} + J_{0p}^{\beta} + J_L) + \Lambda(J_{0p}^{\beta} - J_{0n}^{\beta}) + J_{0n}^{\alpha} - J_{0p}^{\alpha}\right) \\
&= \sqrt{\begin{aligned}&\left(\Lambda \left(J + 2J_L + J_{0n}^{\beta} + 2J_{0n}^{\alpha} + J_{0p}^{\beta}\right) - \left(J + J_{0n}^{\alpha} - J_{0p}^{\alpha}\right)\right)^2 \\ &+4\Lambda\left(1-\Lambda\right)\left(J_L + J_{0n}^{\beta} + J_{0n}^{\alpha}\right)\left(J + J_L + J_{0n}^{\alpha} + J_{0p}^{\beta}\right)\end{aligned}}.
\end{aligned}
\tag{4.20}
$$

From this point, it is advantageous to use some variable substitutions in order to simplify things:

$$c_1 = J_L + J_{0p}^{\beta} + J_{0n}^{\alpha} \tag{4.21a}$$

$$c_2 = J_L + J_{0n}^{\beta} + J_{0n}^{\alpha} \tag{4.21b}$$

$$c_3 = J_{0n}^{\alpha} - J_{0p}^{\alpha} \tag{4.21c}$$

$$c_4 = 2e^{-V/V_T}\frac{J_{0p}^{\alpha}}{J_{0p}^{\beta}}. \tag{4.21d}$$

Thus, our equation becomes:

$$J\left(c_4+1+\Lambda\right)+\left(c_4c_1+\Lambda(c_1-c_2)+c_3\right)$$
$$=\sqrt{\left(\Lambda\left(J+c_1+c_2\right)-\left(J+c_3\right)\right)^2+4\Lambda\left(1-\Lambda\right)c_2\left(J+c_1\right)\qquad}. \tag{4.22}$$

Square both sides to get rid of the radical:

$$J^2\left(c_4+1+\Lambda\right)^2+2J\left(c_4+1+\Lambda\right)\left(c_4c_1+\Lambda(c_1-c_2)+c_3\right)+\left(c_4c_1+\Lambda(c_1-c_2)+c_3\right)^2$$
$$=\left(\Lambda\left(J+c_1+c_2\right)-\left(J+c_3\right)\right)^2+4\Lambda\left(1-\Lambda\right)c_2\left(J+c_1\right)\ . \tag{4.23}$$

Collecting terms and writing in quadratic form gives:

$$\begin{aligned}J^2&\left(c_4^2+2c_4+2\Lambda c_4+4\Lambda\right)\\&+J\left(2c_4^2c_1+2c_4c_1+4\Lambda c_4c_1+2c_3c_4+4\Lambda c_3+4\Lambda c_1-4\Lambda c_2-2\Lambda c_4c_2\right)\\&+\left(c_4^2c_1^2+2c_4c_1c_3+2\Lambda c_1^2c_4+4\Lambda c_1c_3-2\Lambda c_2c_4c_1-4\Lambda c_1c_2\right)=0.\end{aligned} \tag{4.24}$$

This can be factored. First, look for the quadratic coefficient in the linear coefficient and factor a c_1 out of the zeroth order term:

$$\begin{aligned}J^2&\left(c_4^2+2c_4+2\Lambda c_4+4\Lambda\right)\\&+J\left(c_1(c_4^2+2c_4+2\Lambda c_4+4\Lambda)+c_4^2c_1+2c_4c_3+2\Lambda c_1c_4+4\Lambda c_3-2\Lambda c_2c_4-4\Lambda c_2\right)\\&+c_1\left(c_4^2c_1+2c_4c_3+2\Lambda c_1c_4+4\Lambda c_3-2\Lambda c_2c_4-4\Lambda c_2\right)=0.\end{aligned} \tag{4.25}$$

Now divide through by the quadratic term coefficient:

$$J^2 + J\left(c_1 + \frac{c_4^2 c_1 + 2c_4 c_3 + 2\Lambda c_1 c_4 + 4\Lambda c_3 - 2\Lambda c_2 c_4 - 4\Lambda c_2}{c_4^2 + 2c_4 + 2\Lambda c_4 + 4\Lambda}\right) + c_1 \frac{c_4^2 c_1 + 2c_4 c_3 + 2\Lambda c_1 c_4 + 4\Lambda c_3 - 2\Lambda c_2 c_4 - 4\Lambda c_2}{c_4^2 + 2c_4 + 2\Lambda c_4 + 4\Lambda} = 0. \quad (4.26)$$

Thus it is clear that the solutions for J are:

$$J = -c_1 \quad (4.27a)$$

$$J = -\frac{c_4^2 c_1 + 2c_4 c_3 + 2\Lambda c_1 c_4 + 4\Lambda c_3 - 2\Lambda c_2 c_4 - 4\Lambda c_2}{c_4^2 + 2c_4 + 2\Lambda c_4 + 4\Lambda}. \quad (4.27b)$$

Plugging in the definition of c_1 for the first solution, we have

$$J = -J_L - J_{0n}^{\alpha} - J_{0p}^{\beta}. \quad (4.28)$$

This solution is non-physical because in the dark, J_L is zero, yet the current is non-zero. Thus, we settle for the second solution. Before writing J explicitly in terms of V, it is worth simplifying the expression as much as possible. First, we long divide the solution:

$$J = \frac{-c_1(c_4^2 + 2c_4 + 2\Lambda c_4 + 4\Lambda) + 2c_4c_1 + 4\Lambda c_1 + 4\Lambda c_2 + 2\Lambda c_4 c_2 - 2c_3c_4 - 4\Lambda c_3}{c_4^2 + 2c_4 + 2\Lambda c_4 + 4\Lambda} \tag{4.29}$$

$$= -c_1 + \frac{2c_4c_1 + 4\Lambda c_1 + 4\Lambda c_2 + 2\Lambda c_4 c_2 - 2c_3c_4 - 4\Lambda c_3}{c_4^2 + 2c_4 + 2\Lambda c_4 + 4\Lambda} \tag{4.30}$$

$$= -c_1 + \chi. \tag{4.31}$$

The remainder, χ, can be simplified via partial fractions (note that the denominator is easily factored):

$$\chi = \frac{2c_4c_1 + 4\Lambda c_1 + 4\Lambda c_2 + 2\Lambda c_4 c_2 - 2c_3c_4 - 4\Lambda c_3}{(c_4 + 2)(c_4 + 2\Lambda)} = \frac{\zeta}{c_4 + 2} + \frac{\iota}{c_4 + 2\Lambda}. \tag{4.32}$$

Multiplying both sides by $(c_4 + 2)(c_4 + 2\Lambda)$ gives:

$$2c_1(c_4 + 2\Lambda) + 2\Lambda c_2(c_4 + 2) - 2c_3(c_4 + 2\Lambda) = (c_4 + 2\Lambda)\zeta + (c_4 + 2)\iota. \tag{4.33}$$

This equation must hold for all values of c_4. Choosing convenient values for c_4 allows us to find ζ and ι. First, we choose $c_4 = -2$. This easily produces:

$$\zeta = 2(c_1 - c_3). \tag{4.34}$$

Next, we choose $c_4 = -2\Lambda$. This leads to:

$$\iota = 2\Lambda c_2. \tag{4.35}$$

Thus, the solution for J is:

$$J = -c_1 + \frac{2\Lambda c_2}{c_4 + 2\Lambda} + \frac{2(c_1 - c_3)}{c_4 + 2}. \tag{4.36}$$

Finally, we must write out the explicit V dependence by substituting for the c's and Λ:

$$J = -(J_L + J_{0n}^{\alpha} + J_{0p}^{\beta}) + \frac{2\frac{J_{0p}^{\alpha} J_{0n}^{\alpha}}{J_{0p}^{\beta} J_{0n}^{\beta}}(J_L + J_{0n}^{\alpha} + J_{0n}^{\beta})}{2e^{-V/V_T}\frac{J_{0p}^{\alpha}}{J_{0p}^{\beta}} + 2\frac{J_{0p}^{\alpha} J_{0n}^{\alpha}}{J_{0p}^{\beta} J_{0n}^{\beta}}} + \frac{2(J_L + J_{0p}^{\beta} + J_{0n}^{\alpha} - (J_{0n}^{\alpha} - J_{0p}^{\alpha}))}{2e^{-V/V_T}\frac{J_{0p}^{\alpha}}{J_{0p}^{\beta}} + 2}. \tag{4.37}$$

This is is easily simplified for the final expression for $J(V)$:

$$J = -(J_L + J_{0n}^{\alpha} + J_{0p}^{\beta}) + \frac{J_L + J_{0n}^{\alpha} + J_{0n}^{\beta}}{1 + e^{-V/V_T}\frac{J_{0n}^{\beta}}{J_{0n}^{\alpha}}} + \frac{J_L + J_{0p}^{\beta} + J_{0p}^{\alpha}}{1 + e^{-V/V_T}\frac{J_{0p}^{\alpha}}{J_{0p}^{\beta}}}. \tag{4.38}$$

V_{oc} and ΔE_f at V_{oc}

It is perfectly valid to solve for V_{oc} by setting $J = 0$ in eq. 4.38 and solving for V. However, if we instead set $J = 0$ in eq. 4.9, the resulting expression for J_n^{β} can be readily used to derive both V_{oc} and the associated quasi-Fermi-level splitting. Doing so, we have

$$
\begin{aligned}
J_n^\beta =& \frac{1}{2(1-\Lambda)} \\
&\Bigg(-\Lambda \left(J_{0p}^\beta + J_{0n}^\beta \right) - \left(2J_L + J_{0p}^\alpha + J_{0n}^\alpha \right) \\
&+ \sqrt{\left(\Lambda \left(J_{0p}^\beta + J_{0n}^\beta \right) + \left(2J_L + J_{0p}^\alpha + J_{0n}^\alpha \right) \right)^2 - 4(1-\Lambda) J_L (J_L + J_{0p}^\alpha + J_{0n}^\alpha)} \Bigg)
\end{aligned} \tag{4.39}
$$

Note that we have multiplied both numerator and denominator by -1. Next, we define f^β as

$$f^\beta = -\frac{J_n^\beta}{J_L}. \tag{4.40}$$

f^β is therefore

$$f^\beta = \frac{1 + \Lambda\Gamma^\beta + \Gamma^\alpha - \sqrt{(\Lambda\Gamma^\beta + \Gamma^\alpha)^2 + (\Lambda - 1)(1 + 2\Gamma^\alpha)}}{1 - \Lambda}. \tag{4.41}$$

As long as no net current is flowing in the device, f^β is always between 0 and 1. Expanding and combining terms in the square root and factoring, we arrive at

$$f^\beta = \frac{1}{1-\Lambda} \left[1 + \left(\Lambda\Gamma^\beta + \Gamma^\alpha \right) \left(1 - \sqrt{1 + Y} \right) \right], \tag{4.42}$$

where

$$Y = \frac{2\Lambda(\Gamma^\beta + \Gamma^\alpha + \frac{1}{2})}{(\Lambda\Gamma^\beta + \Gamma^\alpha)^2} \tag{4.43}$$

and

$$\Gamma^{\alpha} = \frac{J_{0n}^{\alpha} + J_{0p}^{\alpha}}{2J_L} \tag{4.44a}$$

$$\Gamma^{\beta} = \frac{J_{0n}^{\beta} + J_{0p}^{\beta}}{2J_L}. \tag{4.44b}$$

The calculation of V_{oc} and ΔE_F are straightforward from here. For V_{oc}, we write Eq. 4.10 in terms of f^{β}, giving

$$V_{oc} = V_T \ln\left(\frac{\left(1 - f^{\beta}\right)\frac{J_L}{J_{0n}^{\alpha}} + 1}{f^{\beta}\frac{J_L}{J_{0n}^{\beta}} + 1}\right). \tag{4.45}$$

Similarly, $\Delta E_F/q$ is evidently

$$\frac{\Delta E_F}{q} = V_T \ln\left[\left(1 + f^{\beta}\frac{J_L}{J_{0n}^{\beta}}\right)\left(1 + f^{\beta}\frac{J_L}{J_{0p}^{\beta}}\right)\right]. \tag{4.46}$$

With expressions derived for the entire $J(V)$ curve as well as the V_{oc} and ΔE_F at V_{oc}, we are now able to discuss the implications of these results in detail in the following two chapters.

CHAPTER V

THE $J(V)$ CURVE

We now proceed to discuss the nature of the $J(V)$ curve derived in Chapter 4. The chapter is almost entirely taken from the results section of Roe et al. 2019, with some detail added for clarity.

The contact-determined $J(V)$ curve of our solar cell, as derived in the previous chapter, is given by

$$J = -\left(J_L + J_{0n}^{\alpha} + J_{0p}^{\beta}\right) + \frac{J_L + J_{0n}^{\alpha} + J_{0n}^{\beta}}{1 + \frac{J_{on}^{\beta}}{J_{on}^{\alpha}} e^{-V/V_T}} + \frac{J_L + J_{0p}^{\alpha} + J_{0p}^{\beta}}{1 + \frac{J_{op}^{\alpha}}{J_{op}^{\beta}} e^{-V/V_T}}. \tag{5.1}$$

It is remarkably simple, given the complexity of the algebra required to derive it. With the voltage convention we have chosen, the power quadrant (if there is one) is either quadrant II or IV. Given our assumptions discussed in the Model chapter, this equation is exact (i.e. we need not specify limits on the J_0's or J_L). It is very quickly evident, though, that only certain combinations of J_L's and J_0's will produce a meaningful power quadrant, and therefore a $J(V)$ curve worth studying:

1. The light current density must be larger than at least two of the four J_0's
2. The larger of the two electron J_0's must be at the opposite contact as that for holes.

The first is intuitive if we consider that the smaller J_0's for each carrier can be thought of as 'leakage rates' for each carrier; a solar cell will not work if it leaks carriers through the contacts faster than it can generate them through photon absorption. The second condition is also obvious in hindsight; there must be some built in asymmetry so that electrons prefer one contact while holes prefer the other in order to generate a current (electrons and holes being collected at the same contact amounts to recombination). This highlights the fact that the solar cell is fundamentally a two carrier device, in that the behavior of both electrons and holes must be considered (this is not true for some other semiconductor devices, such as the Schottky diode, or even the transistor).

We restrict our consideration to a device that obeys the two conditions described above. Furthermore, we now assume that the α contact is better at collecting holes than electrons, and therefore dub it the 'hole' contact, replacing the α superscript with h. We assume the opposite for the β contact, which we now call the electron contact. It turns out that this assumption is not strictly necessary to create a functioning solar cell (we will consider an exception to this later), but most working devices are likely to fit into this category. To emphasize our assumptions about which J_0's are bigger than others, we use boldface font for the majority, or larger J_0's and lower case for the smaller (minority) J_0's such that

$$\mathbf{J^e_{0n}} \gg j^h_{0n} \tag{5.2a}$$

$$\mathbf{J^h_{0p}} \gg j^e_{0p}. \tag{5.2b}$$

Again, these assumptions are not necessary, but are expected to apply for most functioning solar cells, and they aid us in developing an intuitive understanding of the $J(V)$ curve. Note that we have replaced the α and β superscripts with h and e, referring to the hole and electron contacts respectively. Bearing these assumptions in mind, the $J(V)$ curve becomes

$$J = -\left(J_L + j_{0n}^h + j_{0p}^e\right) + \frac{J_L + j_{0n}^h + \mathbf{J}_{\mathbf{0n}}^{\mathbf{e}}}{1 + \frac{\mathbf{J}_{\mathbf{0n}}^{\mathbf{e}}}{j_{on}^h} e^{-V/V_T}} + \frac{J_L + \mathbf{J}_{\mathbf{0p}}^{\mathbf{h}} + j_{0p}^e}{1 + \frac{\mathbf{J}_{\mathbf{0p}}^{\mathbf{h}}}{j_{op}^e} e^{-V/V_T}}. \tag{5.3}$$

It should be noticed right away that this function is different from the ideal solar cell equation (eq. 2.1) in that the light current is not simply subtracted off from the 'dark diode equation'; J_L appears in the voltage dependent parts of the function. This has obvious implications on the relation between light intensity and performance, and will be further discussed later on.

Perhaps the most interesting feature of this function is that it is readily divided into three terms, each of which has distinct features. The leftmost term is voltage independent, and is simply an offset equal to the light current plus the two minority J_0's or 'leakage rates'. Given assumption 1 above, we know that $J_L \gg j_{on}^h$ and $J_L \gg j_{op}^e$, so the first term is always approximately equal to J_L for any functional solar cell. Meanwhile, the other two terms are both voltage dependent. Critically, one only depends on electron J_0's and J_L, while the other only depends on hole J_0's and J_L. The shape of both functions is essentially a smeared out step-function; thus we dub one the 'electron step' and the other the 'hole step'. The $J(V)$ curve is, in general, a superposition of these three components.

Right away, one notices that the step-like nature of the curve is different from the ideal solar cell equation because the current eventually levels off at a fixed value in forward bias (positive V), instead of increasing exponentially. The 'height' (i.e. the difference between the current density at voltages above the step vs. below the step), is given by $J_L + \mathbf{J}_{\mathbf{0n}}^{\mathbf{e}} + j_{0n}^h \approx J_L + \mathbf{J}_{\mathbf{0n}}^{\mathbf{e}}$ for the electron step and $J_L + \mathbf{J}_{\mathbf{0p}}^{\mathbf{h}} + j_{0p}^e \approx J_L + \mathbf{J}_{\mathbf{0p}}^{\mathbf{h}}$ for the hole step.

The origin of the step-function nature of the $J(V)$ curve can be readily explained by the diode-like boundary conditions for the partial currents (eq. 3.1) linked by the continuity equation. Consider, for instance, the limits of the current in far reverse bias given by eq. 5.3. The current must be negative throughout the device given our convention, and minority carriers are being depleted at their contacts, while there is a small excess of majority carriers at their respective contacts. Given eq. 3.1, however, minority currents can only be as large in magnitude as j_0 when their carriers are being depleted, as the carrier densities cannot go below zero. Because the continuity equation restricts the difference between electron and hole partial currents separately, to J_L, the maximum possible current magnitude in reverse bias occurs when the electron density at contact α and the hole density at contact β are pulled down to zero, giving a total current of $-j_{0n}^{\alpha} - j_{op}^{\beta} - J_L$.

Meanwhile, in far forward bias, the opposite occurs; there is a large excess of minority carriers at their contacts, while the densities of majority carriers are being drawn down to zero. In principle, the current of minority carriers is unbounded when they are in excess at a contact. However, the majority carrier partial currents are bounded by the $\mathbf{J_0}$'s, for the exact same reason the minority partial currents are bounded in reverse bias. Given the continuity equation, this leads to a maximum current of $\mathbf{J_{0n}^{\beta}} + \mathbf{J_{0p}^{\alpha}} + J_L$. The steps themselves are caused by minority carriers being put into excess as the bias goes from reverse to forward. Initially, an excess of minority carriers at their respective contacts does not contribute significantly to the current because the associated j_0's are so small, however eventually, the minority carrier densities exceed their equilibrium values by enough orders of magnitude that they start to change the partial current at that contact. Because the associated majority current at the opposite contact is linked by the continuity equation, this eventually forces the corresponding majority carrier density to be drawn down below equilibrium. For a more detailed explanation, refer to Appendix E.

Note that in practice, the leveling off of the second step is unlikely to be observed for the majority of solar cells. This is because there is usually at least one contact in a solar cell that is really good at extracting its intended carrier, and thus the current at which the $J(V)$ curve levels off is unlikely to be measured. Furthermore, for real devices, bulk recombination will always kick in eventually in forward bias. This allows for the difference between partial currents across the device to be unbounded, allowing the current to go to infinity like a normal diode. This will occur in place of the rollover of the second step whenever the J_0 associated with bulk recombination processes is larger than the smallest j_0. Regardless, the physical origin of the second step is useful in understanding the relative importance of electron and hole processes in the operation of a solar cell.

The inflection point, or center (i.e. the voltage at which the current is exactly halfway between the upper and lower current values of the step) can be easily calculated. This 'step' voltage is

$$V_{s,n} = V_T \ln(\frac{\mathbf{J}^{\beta}_{\mathbf{0n}}}{j^{\alpha}_{0n}}) = V_T \ln(S_n) \tag{5.4a}$$

$$V_{s,p} = V_T \ln(\frac{\mathbf{J}^{\alpha}_{\mathbf{0p}}}{j^{\beta}_{0p}}) = V_T \ln(S_p) \tag{5.4b}$$

for electrons and holes respectively. Here, we have introduced the electron and hole *carrier* selectivities as

$$S_n = \frac{\mathbf{J^{e}_{0n}}}{j^{h}_{0n}} \tag{5.5a}$$

$$S_p = \frac{\mathbf{J^{h}_{0p}}}{j^{e}_{0p}} \tag{5.5b}$$

respectively. The S parameters characterize carrier selectivity because they describe the relative rates of the electron or holes extraction ability across the device. The greater S is, the greater the asymmetry in the rates of these processes. On a log scale, S is the difference between the two J_0 values.

Because the carrier selectivities necessarily contain J_0's from *both* contacts, they are distinct from the notion of *contact* selectivity, which can be defined as the ratio of the J_0's from a single contact. A critical result of the theory then, is that the position of the steps in the $J(V)$ curve depend on the *carrier* selectivities, and not the selectivities of an individual contact.

Equation 5.3 provides a unified treatment of non-ideal solar cell phenomena such as dark/light crossover (i.e. failure of current superposition)[76, 77] and S-shaped curves.[78] For instance, it is immediately evident from eq. 5.3, that the $J(V)$ curve cannot be written in general as $J_{dark}(V) + J_{light}$ where J_{light} is voltage independent. In fact, the voltage at which the current crossover occurs can easily be calculated by setting eq. 5.3 equal to itself with and without J_L and solving for V. The solution is given by

$$V_{cross} = V_T \ln \sqrt{\frac{J^{\beta}_{0n} J^{\alpha}_{0p}}{J^{\alpha}_{0n} J^{\beta}_{0p}}} = V_T \ln \sqrt{S_n S_p} \tag{5.6}$$

This equation predicts that there is *always* dark/light crossover in *every* contact-limited solar cell. However, if the product of the selectivities is large enough, one may not be able to measure it because the current is likely to become strongly affected by series resistance and/or bulk recombination far into forward bias. Not only does crossover always happen in principle, the $J(V)$ is always S-shaped, in principle. Both phenomena are natural consequences of including the limitations due to majority carrier extraction for both carriers in the model. However, they only become relevant to the power quadrant when J_L is larger than the $\mathbf{J_0}$'s. This is discussed in more detail below.

Figure 4 is an example $J(V)$ curve produced from eq. 5.3 demonstrating the key features of the function. In reverse bias ($V < 0$), the current is approximately J_L, given that the j_0's are much smaller than J_L. We can tell that the j_0's are small relative to J_L and the $\mathbf{J_0}$'s just by glancing at the curve; they must be small in order for there to be an appreciable photovoltaic effect. In this example, the two steps are well separated in voltage. The first step (i.e. the step that occurs at smaller forward bias, colored blue in Fig. 4) is associated entirely with electron J_0's in this case. We can immediately tell from where the electron step ends (at $+10\,\mathrm{mA\,cm^{-2}}$) that $\mathbf{J_{0n}^{\beta}} = 10\,\mathrm{mA\,cm^{-2}}$ because the height of the electron step is approximately equal to $J_L + \mathbf{J_{0n}^{\beta}}$. Since the two steps are well separated in voltage, we can use the location of the center of the electron step at $\sim 420\,\mathrm{mV}$ (labeled V_n in Fig. 4) to calculate the value of j_{0n}^{α} from eq. 5.4a. Given a temperature of 300 K for Fig. 4, and that $\mathbf{J_{0n}^{\beta}} = 10\,\mathrm{mA\,cm^{-2}}$ as discovered above, $j_{0n}^{\alpha} \approx 10^{-6}\,\mathrm{mA\,cm^{-2}}$. In this case, the value for j_{0n}^{α} could also be determined or confirmed from the saturation current of a dark $J(V)$ measurement, since j_{0p}^{β} is much smaller than j_{0n}^{α}. The hole step, colored red in

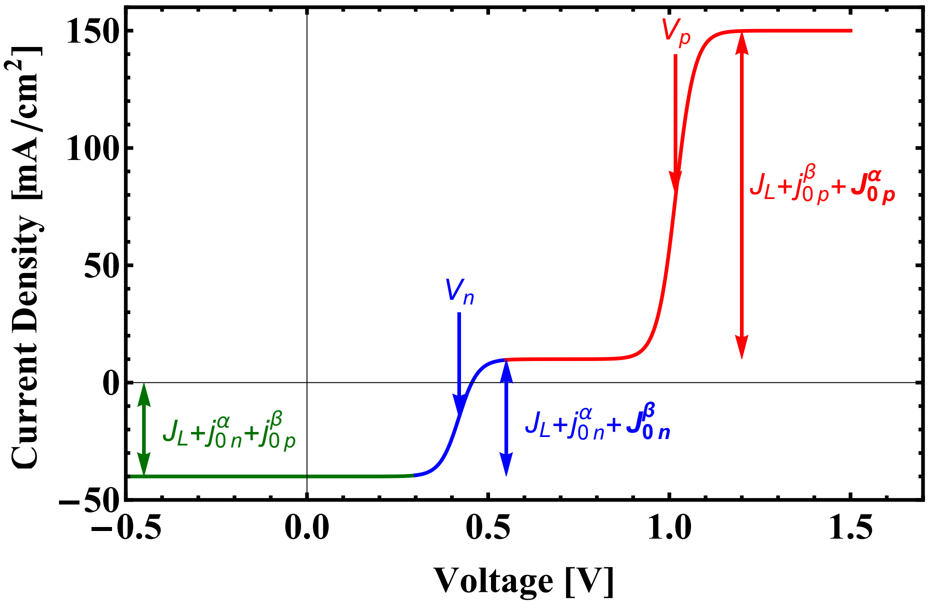

FIGURE 4. A sample $J(V)$ curve produced by eq. 5.3 using $J_L = 40$, $\mathbf{J}^{\beta}_{\mathbf{0n}} = 10$, $j^{\alpha}_{0n} = 10^{-6}$, $\mathbf{J}^{\alpha}_{\mathbf{0p}} = 100$, $j^{\beta}_{0p} = 10^{-15}$ mA cm^{-2}. In green, the current is fixed at approximately J_L. The blue section highlights the first step, whose location is determined, in this case, by electron J_0's. The red section highlights the second step, in this case entirely determined by hole J_0's.

Fig. 4, occurs entirely outside of the power quadrant, and therefore does not limit the efficiency of the device.

In the case of Fig. 4, the solar cell is limited by the 'electron selectivity'. Therefore, any increase in that ratio, either from decreasing j^{α}_{0n} or by increasing $\mathbf{J}^{\beta}_{\mathbf{0n}}$ will improve the efficiency of the device while changing the hole-associated J_0's will have no appreciable effect on the efficiency of the device. This knowledge is useful because it tells us that an appropriate improvement in *either* contact will increase device performance. Practically speaking, this means we might be able to improve the device efficiency with a thin insulating layer inserted at the α contact. Although this would likely decrease $\mathbf{J}^{\alpha}_{\mathbf{0p}}$, that does not affect the power quadrant, while reducing j^{α}_{0n} would improve the electron selectivity by reducing electron leakage.

Another consequence of the importance of carrier selectivity is that it is entirely possible to create a functional solar cell where both contacts are electron selective (or both are hole selective) as long as both carriers have at least *some* preference for opposite contacts. Here, by electron selective contact, we mean a contact whose electron J_0 is larger than its hole J_0 and visa-versa for a hole selective contact. Fig. 5 is an example of a $J(V)$ curve for a solar cell with two electron selective contacts, yet there is still an appreciable photovoltaic effect. Despite the fact that both contacts are electron selective, the holes still prefer the α compared to the β contact and visa versa for electrons because one contact is *much* more selective than the other. Note that while it is possible to create a functioning solar cell with two contacts of the same selectivity type or even if one of the two contacts is not selective, it is *not* possible to create a functioning solar cell if *neither* contact is selective. The requirement to achieve an appreciable photovoltaic effect in all cases is simply that the contacts encourage electrons to go to one contact and holes to the other contact. In other words, if the electrons prefer contact β due to it having a larger electron J_0 than contact α, the opposite must be true for holes.

In principle, all contact-determined $J(V)$ curves produced by eq. 5.3 are a simple superposition of the two steps centered at the step voltages for each carrier. However, because the current in reverse bias is approximately equal to J_L and because only the power quadrant determines device performance, it is important to consider the size of the steps relative to the light current. According to eq. 5.3, each step has a minimum height of J_L when the $\mathbf{J_0}$ associated with the step is small compared to J_L. Conversely, if the $\mathbf{J_0}$ associated with a step is much larger than J_L, the height of that step is approximately equal to that $\mathbf{J_0}$. These two limits naturally suggest two regimes that delineate distinct behavior for each carrier. A carrier is in high

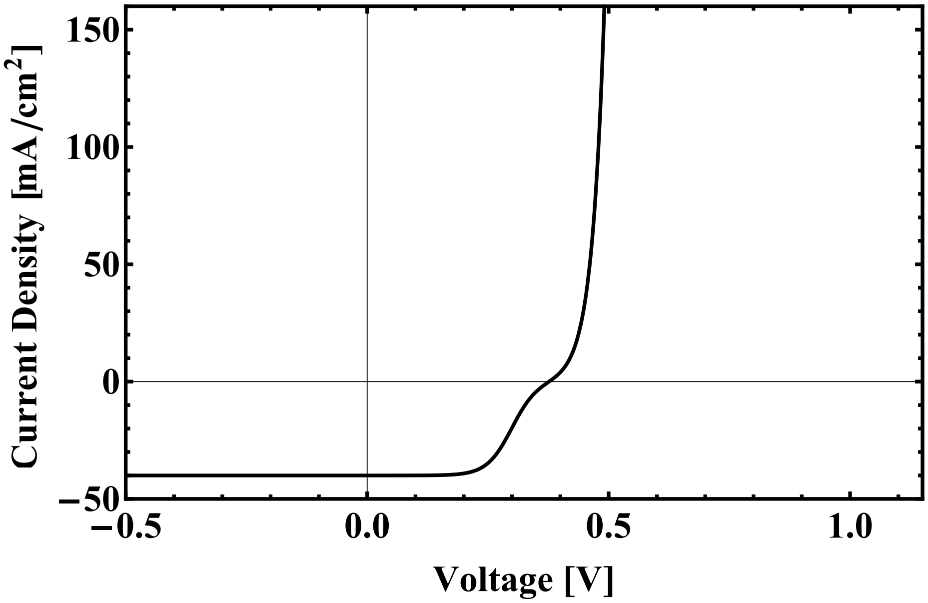

FIGURE 5. An example of a $J(V)$ curve produced by eq. 5.3 in which the electron J_0's of each contact are larger than the hole J_0's, meaning both contacts are electron selective. Parameters values are $J_L = 40$, $J_{0n}^{\beta} = 10^6$, $J_{0n}^{\alpha} = 10^{-6}$, $J_{0p}^{\alpha} = 10^{-8}$, $J_{0p}^{\beta} = 10^{-13}$ mA cm^{-2}. Note that we have not used the $\mathbf{J_0}$, $\jmath_0$ convention because the assumption that both contacts have the opposite selectivity is not valid in this case.

injection when the larger of the two J_0's of that carrier is much smaller than J_L, i.e. electrons are in high injection if $J_L \gg \mathbf{J_{0n}^{\beta}}$. The low injection limit applies to a carrier if the $\mathbf{J_0}$ of the carrier is much larger than J_L. These regimes correspond to different orders of recombination at the contacts; the high injection regime is associated with second order recombination while the low injection regime indicates the presence of quasi-first-order recombination. The nature of recombination as it is determined by high and low injection will be discussed in more detail in Chapter 6.

The motivation to separate these two regimes can be taken from eq. 3.1. The majority process is a significant limitation to device performance when a large excess of majority carriers is needed to provide a partial current on the order of J_L, which is necessary for any solar cell. In other words, the 'high injection' limit is that where the majority carrier density at a contact interface must be much larger than the equilibrium density as set by the contact in order to generate J_L of partial current. The 'low injection' limit meanwhile implies than only a very small excess of majority carriers at the contact is required to produce J_L. This naturally leads to the direct comparison of J_L to the $\mathbf{J_0}$ for each carrier. The difference between our definition of low and high injection and the usual definition is the density to which we compare the majority carrier density; in usual device physics, one compares to the dopant density, whereas here we compare to the equilibrium density as set by the contact. Note that we could easily define such a limit for the minority carriers as well, however, one cannot produce appreciable photovoltaic effect if $j_0 > J_L$, therefore, minority carriers are always in 'high injection' for all practical solar cells.

Figures 6 a and b display $J(V)$ curves where the first, or limiting step, is in low and high injection respectively. They reproduce the approximate performance parameters and shape from Figures 5a and 6a from Das et al.,[79] respectively, where various passivating amorphous silicon layers were used as selective contacts to either side of a crystalline silicon absorber. For the low-injection case, the $J(V)$ curve will always look qualitatively similar to Fig. 6a on the scale of J_L. That is, there will only be one visible step, and the current will not level off on the scale of J_L. The $J(V)$ curve is still S-shaped, but the S will not appear on the scale of J_L, meaning it will be irrelevant to the power quadrant, thus the superposition principle applies in the power quadrant. This is perhaps the simplest case, and it can be shown (see Appendix F) that the efficiency is solely dependent on the limiting j_0. The only way to improve such a device is to reduce the leakage rate of minority carriers, and because holes are the limiting carriers in this case, this means decreasing j_{0p}^{β}.

In contrast, the $J(V)$ curve can also look like Fig. 6b where the superposition principle clearly fails, producing an S-shaped curve in the power quadrant because

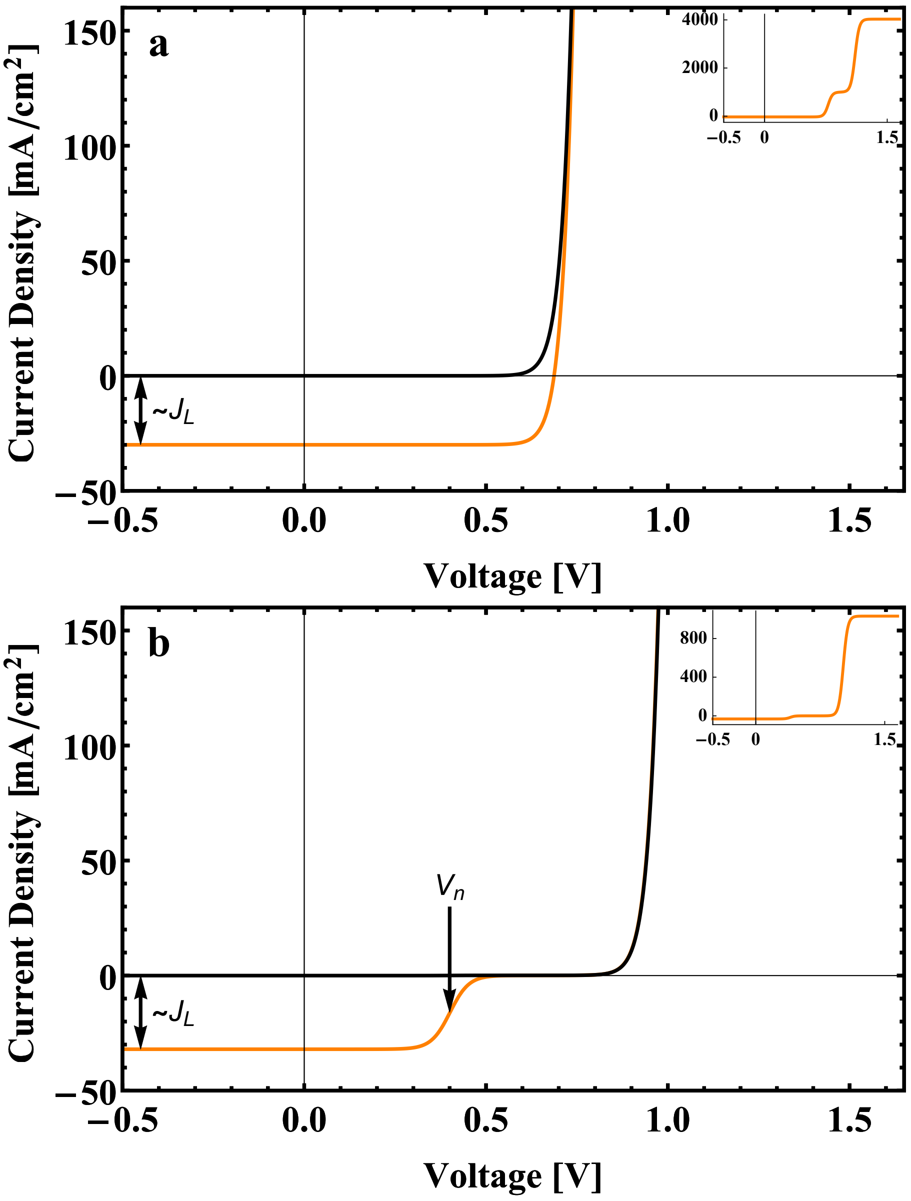

FIGURE 6. a) Dark (black) and light (orange) $J(V)$ curves produced from eq. 5.3 using $J_L = 30$, $\mathbf{J}^{\beta}_{\mathbf{0n}} = 3 \times 10^3$, $j^{\alpha}_{0n} = 10^{-15}$, $\mathbf{J}^{\alpha}_{\mathbf{0p}} = 10^3$, $j^{\beta}_{0p} = 10^{-10}$ $\mathrm{mA\,cm^{-2}}$. The inset shows the $J(V)$ light curve on a current scale sufficient to observe the biggest step. b) $J(V)$ curve produced using $J_L = 32$, $\mathbf{J}^{\beta}_{\mathbf{0n}} = 10^3$, $j^{\alpha}_{0n} = 10^{-14}$, $\mathbf{J}^{\alpha}_{\mathbf{0p}} = 10^{-1}$, $j^{\beta}_{0p} = 2 \times 10^{-8}$ $\mathrm{mA\,cm^{-2}}$. The inset again depicts the light $J(V)$ curve on a current scale sufficient to see both steps in their entirety.

the limiting carriers (holes in this case) are in high injection. The step for a carrier that is in high injection always ends at $J \approx 0$ (except when the steps occur at the same voltage), leading to a less-than-ideal fill factor. While electron J_0's can effect the V_{oc} in this case, they do not have a significant effect on the power quadrant and hence the efficiency as they are not the limiting carrier. As with Fig. 4, our model states that one could improve the device efficiency *both* by increasing the limiting $\mathbf{J_0}$ (in this case, $\mathbf{J_{0p}^{\alpha}}$), and by decreasing the limiting j_0 (in this case, j_{0p}^{β}). This might be useful, if for instance, it is not clear how to improve the hole *collection* of contact α. This is particularly insightful, because for instance, the thin-film/CdTe literature has frequently correlated current rollover to limited built-in potential, caused by an undesired barrier at the back contact.[50, 77, 80] Our explanation is consistent with this because the back barrier is what determines the J_0's for that contact, but we also show that improvements to the opposite contact would also be beneficial to performance. If instead, one *was* able to increase $\mathbf{J_{0p}^{\alpha}}$, an improvement of 2.5 orders of magnitude would be useful after which reducing j_{0p}^{β} would be the only way to improve efficiency.

It is important to be precise about what we mean by 'limiting step' (or equivalently 'limiting carrier'). One might assume that the carrier with the smallest step voltage (eq. 5.4) must be the limiting carrier, but this is only appropriate if both carriers are in high injection. If a carrier is in low injection, then the step voltage is not relevant to the power quadrant because the current at the step voltage will be well above zero (i.e. outside the power quadrant). In this case, it is the ratio of J_L (instead of $\mathbf{J_0}$) to j_0 that must be considered. We therefore define the critical voltages for each carrier as:

$$V_{c,n} = V_T \ln\left(\mathrm{Min}\left[\frac{\mathbf{J_{0n}^{\beta}}}{j_{0n}^{\alpha}}, \frac{J_L}{j_{0n}^{\alpha}}\right]\right) \tag{5.7a}$$

$$V_{c,p} = V_T \ln\left(\mathrm{Min}\left[\frac{\mathbf{J_{0p}^{\alpha}}}{j_{0p}^{\beta}}, \frac{J_L}{j_{0p}^{\beta}}\right]\right). \tag{5.7b}$$

The carrier with the smallest critical voltage is the limiting carrier. If the critical voltages are within a few kT/q of each other, both carriers will limit the device.

Note that if both contacts are ideal Schottky contacts, the carrier selectivities will be equal. However, the critical voltages of each carrier may not be equal in that case, depending on the work functions of the metals. Since many semiconductor-metal interfaces do not behave as ideal Schottky contacts, and since many solar cells use interfacial layers and/or doped semiconductors (as opposed to just a metal) as contacts to the absorber, one would expect that in practice, the carrier selectivities of electrons and holes will not generally be identical.

While knowledge of the shape of the $J(V)$ curve is useful, it is also essential to understand how the critical performance parameters such as V_{oc}, J_{sc}, and, ultimately, η depend on the J_0's. This discussion will be held in Chapter 6.

CHAPTER VI

PERFORMANCE PARAMETERS

This chapter derives and discusses the critical photovoltaic performance parameters that can be calculated with our model (either from the $J(V)$ curve or the constraints on the partial currents used to derive it). It contains material taken from both Roe et al. 2018 and Roe et al. 2019, and the supplementary material of the latter.

Short-circuit Current

The easiest parameter to derive from eq. 5.3 is the short circuit current. This is easily done by setting the voltage to zero, though some further simplification is useful, and will be presented here. We will make the same assumption as last chapter, namely that the β contact is electron selective, and the α contact is hole selective, and we will use the same $\mathbf{J_0}/j_0$ convention. Again, this assumption is useful for understanding, but it is not a necessary condition for an appreciable short circuit current. Setting the current to zero in eq. 5.3, we have:

$$J_{sc} = -(J_L + j_{0n}^h + j_{0p}^e) + \frac{J_L + j_{0n}^h + \mathbf{J_{0n}^e}}{1 + \frac{\mathbf{J_{0n}^e}}{j_{0n}^h}} + \frac{J_L + j_{0p}^e + \mathbf{J_{0p}^h}}{1 + \frac{\mathbf{J_{0p}^h}}{j_{0p}^e}}. \tag{6.1}$$

To further simplify, we re-write with a common denominator:

$$J_{sc} = \frac{-\left(J_L + j_{0n}^{h} + \mathbf{J_{0n}^{e}}\right)\left(1 + \frac{\mathbf{J_{0n}^{e}}}{j_{0n}^{h}}\right)\left(1 + \frac{\mathbf{J_{0p}^{h}}}{j_{0p}^{e}}\right)}{\left(1 + \frac{\mathbf{J_{0n}^{e}}}{j_{0n}^{h}}\right)\left(1 + \frac{\mathbf{J_{0p}^{h}}}{j_{0p}^{e}}\right)} + \\ \frac{\left(J_L + j_{0n}^{h} + \mathbf{J_{0n}^{e}}\right)\left(1 + \frac{\mathbf{J_{0p}^{h}}}{j_{0p}^{e}}\right)}{\left(1 + \frac{\mathbf{J_{0n}^{e}}}{j_{0n}^{h}}\right)\left(1 + \frac{\mathbf{J_{0p}^{h}}}{j_{0p}^{e}}\right)} + \frac{\left(J_L + j_{0p}^{e} + \mathbf{J_{0p}^{h}}\right)\left(1 + \frac{\mathbf{J_{0n}^{e}}}{j_{0n}^{h}}\right)}{\left(1 + \frac{\mathbf{J_{0n}^{e}}}{j_{0n}^{h}}\right)\left(1 + \frac{\mathbf{J_{0p}^{h}}}{j_{0p}^{e}}\right)} \tag{6.2}$$

The terms in the denominator are distributed and canceled:

$$J_{sc} = \frac{J_L\left(1 - \frac{\mathbf{J_{0n}^{e}}\mathbf{J_{0p}^{h}}}{j_{0n}^{h} j_{0p}^{e}}\right) + j_{0n}^{h}\left(-\frac{\mathbf{J_{0n}^{e}}}{j_{0n}^{h}} - \frac{\mathbf{J_{0n}^{e}}\mathbf{J_{0p}^{h}}}{j_{0n}^{h} j_{0p}^{e}}\right)}{\left(1 + \frac{\mathbf{J_{0n}^{e}}}{j_{0n}^{h}}\right)\left(1 + \frac{\mathbf{J_{0p}^{h}}}{j_{0p}^{e}}\right)} \\ + \frac{\mathbf{J_{0n}^{e}}\left(1 + \frac{\mathbf{J_{0p}^{h}}}{j_{0p}^{e}}\right) + j_{0p}^{e}\left(-\frac{\mathbf{J_{0p}^{h}}}{j_{0p}^{e}} - \frac{\mathbf{J_{0n}^{e}}\mathbf{J_{0p}^{h}}}{j_{0n}^{h} j_{0p}^{e}}\right) + \mathbf{J_{0p}^{h}}\left(1 + \frac{\mathbf{J_{0n}^{e}}}{j_{0n}^{h}}\right)}{\left(1 + \frac{\mathbf{J_{0n}^{e}}}{j_{0n}^{h}}\right)\left(1 + \frac{\mathbf{J_{0p}^{h}}}{j_{0p}^{e}}\right)} \tag{6.3}$$

Everything except the J_L terms in the denominator cancel:

$$J_{sc} = \frac{J_L\left(1 - \frac{\mathbf{J_{0n}^{e}}\mathbf{J_{0p}^{h}}}{j_{0n}^{h} j_{0p}^{e}}\right)}{\left(1 + \frac{\mathbf{J_{0n}^{e}}}{j_{0n}^{h}}\right)\left(1 + \frac{\mathbf{J_{0p}^{h}}}{j_{0p}^{e}}\right)}. \tag{6.4}$$

We get rid of the fractions in the denominator and numerators by multiplying by $\frac{j_{0n}^{h} j_{0p}^{e}}{j_{0n}^{h} j_{0p}^{e}}$:

$$J_{sc} = \frac{J_L\left(j^h_{0n} j^e_{0p} - \mathbf{J^e_{0n} J^h_{0p}}\right)}{\left(j^h_{0n} + \mathbf{J^e_{0n}}\right)\left(j^e_{0p} + \mathbf{J^h_{0p}}\right)} \tag{6.5a}$$

$$= \frac{J_L\left(j^h_{0n} j^e_{0p} + j^e_{0p}\mathbf{J^e_{0n}} - j^e_{0p}\mathbf{J^e_{0n}} - \mathbf{J^e_{0n} J^h_{0p}}\right)}{\left(j^h_{0n} + \mathbf{J^e_{0n}}\right)\left(j^e_{0p} + \mathbf{J^h_{0p}}\right)} \tag{S41b}$$

$$= J_L\left(\frac{j^e_{0p}\left(j^h_{0n} + \mathbf{J^e_{0n}}\right)}{\left(j^h_{0n} + \mathbf{J^e_{0n}}\right)\left(j^e_{0p} + \mathbf{J^h_{0p}}\right)} - \frac{\mathbf{J^e_{0n}}\left(j^e_{0p} + \mathbf{J^h_{0p}}\right)}{\left(j^h_{0n} + \mathbf{J^e_{0n}}\right)\left(j^e_{0p} + \mathbf{J^h_{0p}}\right)}\right) \tag{S41c}$$

$$= J_L\left(\frac{j^e_{0p}}{j^e_{0p} + \mathbf{J^h_{0p}}} - \frac{\mathbf{J^e_{0n}}}{j^h_{0n} + \mathbf{J^e_{0n}}}\right). \tag{S41d}$$

This is easily written in terms of the carrier selectivities (given in eq. 5.5):

$$J_{sc} = J_L\left(\frac{1}{1+S_p} - \frac{1}{1+S_n^{-1}}\right). \tag{6.6}$$

Immediately, we notice that J_{sc} is directly proportional to J_L. This is significant because it means that it doesn't matter whether or not the solar cell is in high or low injection; the J_{sc} is always affected by the light intensity in a linear fashion. The maximum value (magnitude) of J_{sc} is reached when the either of the two terms in the parentheses goes to zero, while the other goes to 1. This occurs as both selectivities go to 0 or infinity (recall that a selectivity of 1 refers to a completely non-selective contact). As we have assumed that electrons are prefered at the β contact, and visa versa for holes, both selectivities are larger than one.

The biggest takeaway from eq. 6.6 is that the selectivities do not need to be all that large in order to maximize J_{sc}; as long as both carrier selectivities are larger than 100, the J_{sc} will be greater than or equal to 98% of J_L. This should always be the case for solar cells that demonstrate an appreciable photovoltaic effect.

Open-circuit Voltage and Quasi-Fermi-level Splitting

We now proceed to discuss the properties of the cell when no current is flowing through it. The most natural thing to do would be to set the current equal to zero in eq. 5.3 and solve for the voltage to calculate V_{oc}. This is perfectly legitimate, however in chapter 4, we chose to set the partial current across the device to zero and solve for both the voltage across the device and the corresponding quasi-Fermi splitting, as comparison of these quantities is instructive.

When no net current flows across the device, the partial currents must mirror each other at each point in the device. This is illustrated in Fig. 7, with an example of partial current profiles that would be a valid solution to the continuity equation when no net current is flowing. Because the partial currents must sum to zero, and the difference between a given partial current at each contact is J_L, the magnitudes of each partial current at the contact must be less than J_L.

For our understanding, it is also useful to know the relationship between the carrier densities at contacts and the V_{oc} and ΔE_f. Given our assumption that the quasi-Fermi levels are flat throughout the device, ΔE_f is single valued. The open-circuit voltage is, of course, single valued as well. Because the V_{oc} can be determined either by analyzing holes or electrons and the ΔE_f can be determined by the carrier densities at either contact, they are constrained in an elegant manner as shown in Fig. 8.

In general, the V_{oc} is not equal to ΔE_f, as should be obvious from eqs. 4.45 and 4.46. It is clear from Fig. 8 that the relative amount of excess holes at the hole collecting contact as well as the excess electrons at the electron contact must be small in order for V_{oc} to approach ΔE_f. This is in fact intuitive; it simply means that in order for the V_{oc} to be large enough to be dictated by recombination (which is always

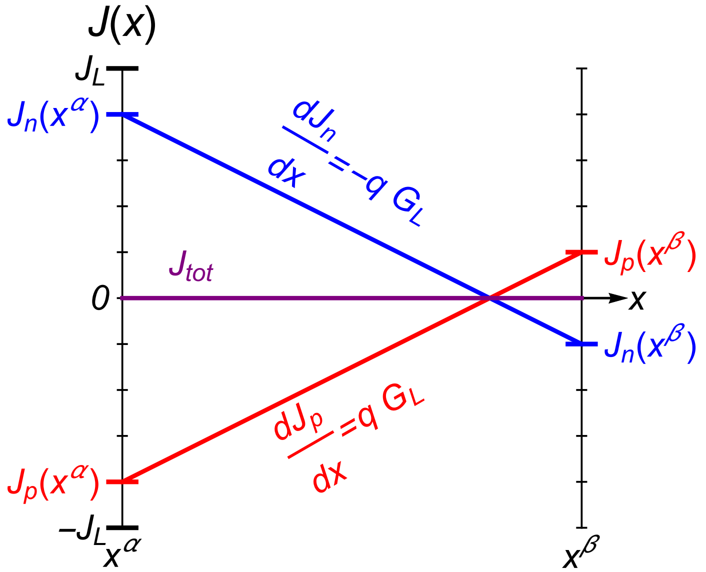

FIGURE 7. Example plot of electron (blue) and hole (red) partial currents as they are constrained at open-circuit. The magnitude of the slopes are determined by the generation rate, G_L. The partial currents must sum to zero at every point in the device.

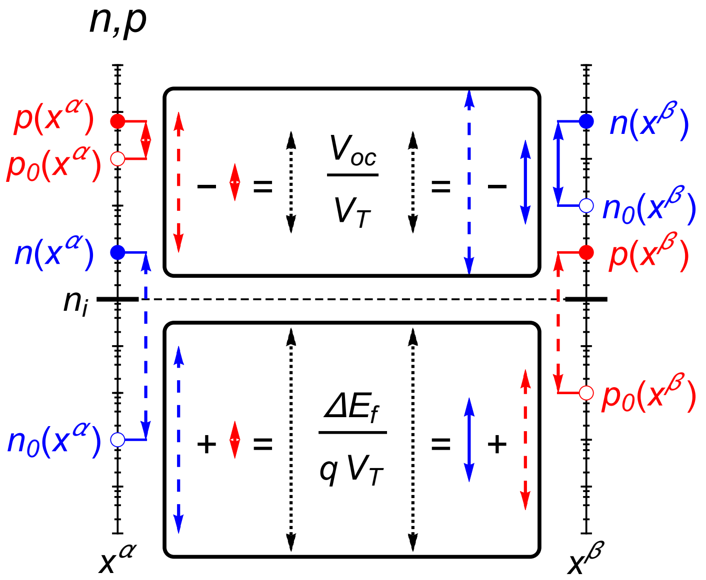

FIGURE 8. Schematic depicting the carrier densities at both interfaces on a log scale, and their relation to V_{oc} and ΔE_f. The length of the arrows corresponds to the log of the ratio of the carrier density over the equilibrium carrier density at the contact.

what limits ΔE_f in every solar cell), there must be no build up of majority carriers at their associated contacts. In other words, to maximize V_{oc}, the majority carriers must be able to provide a partial current as large as the light current without a large build up at the relevant contact. This, in fact, aligns precisely with our definition of high and low injection. If the majority J_0 of a carrier is much larger than J_L, then we don't require much excess carrier density in order to extract J_L of current out of that contact. If the opposite is true, we'll need to build up a lot of majority carriers at the corresponding contact to extract J_L. This means that there is not enough asymmetry in the device to support a voltage as large as the quasi-Fermi level splitting without help from an external power supply (which, of course would nullify the point of making such a solar cell).

The general expressions for both V_{oc} and ΔE_f, derived in chapter 4, are written in terms of $f^\beta = -\frac{J^\beta_{0n}}{J_L}$. They are reproduced here:

$$V_{oc} = V_T \ln \left(\frac{\left(1 - f^\beta\right) \frac{J_L}{J^\alpha_{0n}} + 1}{f^\beta \frac{J_L}{J^\beta_{0n}} + 1} \right) \tag{6.7a}$$

$$\frac{\Delta E_F}{q} = V_T \ln \left[\left(1 + f^\beta \frac{J_L}{J^\beta_{0n}}\right) \left(1 + f^\beta \frac{J_L}{J^\beta_{0p}}\right) \right]. \tag{6.7b}$$

where

$$f^\beta = \frac{1}{1-\Lambda} \left[1 + \left(\Lambda \Gamma^\beta + \Gamma^\alpha\right) \left(1 - \sqrt{1+Y}\right) \right]. \tag{6.8}$$

Given the definition of f^β, and the fact that no net current is flowing in the device, we know that f^β must be between 0 and 1 (negative f^β corresponds to electrons flowing into the absorber, and $f^{\beta} > 1$ corresponds to partial currents larger than J_L, both of which can't happen at V_{oc}).

Equations 6.7a and b work for any values of the J_0's and J_L, however they are complicated functions and do not readily lead to any intuitive understanding. Therefore, we will consider some limiting cases when the expressions can be simplified.

First though, we define a contact recombination parameter, R_m, that depends on the nature of the recombination. We consider quasi-first-order recombination ($m = 1$) to effectively depend only on the minority process at the contact, and define an associated first-order recombination parameter, R_1, as:

$$R_1 \equiv j_0 \tag{6.9}$$

Second-order recombination ($m = 2$) depends on both minority and majority processes, and we define a second-order recombination parameter R_2 as:

$$R_2 \equiv \sqrt{\mathbf{J_0} j_0} \tag{6.10}$$

The parameter R_2 characterizes second-order recombination because it captures an average of sorts of the electron and hole rate processes at the interface. Specifically, R_2 is the average of $\mathbf{J_0}$ and j_0 on a log scale. Note that we have defined the recombination parameter as a property of a single *contact*, while the selectivity parameter considers J_0's for a single *carrier*. This should be intuitive, because recombination requires opposite carriers to combine at a single location in space, while selectivity can be thought of as the built in asymmetry that a given carrier sees across a solar cell.

The Two-J_0 Case

It is illustrative to consider a simplified case that reduces the four J_0 problem to only two J_0's. To do this, we assume the J_0 values at the two contacts to be asymmetrically related so that $J_{0n}^{\beta} = J_{0p}^{\alpha} = \mathbf{J_0}$ and $J_{0p}^{\beta} = J_{0n}^{\alpha} = j_0$. Therefore, $R_m^{\alpha} = R_m^{\beta} = R_m$ and $S_n = S_p = S$. By symmetry, $f^{\beta} = 1/2$, and eqs. 6.7 a and b become:

$$\frac{\Delta E_F}{q} = V_T \ln\left[\left(\frac{J_L}{2\mathbf{J_0}} + 1\right)\left(\frac{J_L}{2j_0} + 1\right)\right] \tag{6.11}$$

$$V_{oc} = V_T \ln\left(\frac{\frac{J_L}{2j_0} + 1}{\frac{J_L}{2\mathbf{J_0}} + 1}\right). \tag{6.12}$$

Figure 9 shows contour plot representations of eqs. 6.11 and 6.12; $\Delta E_F/q$ and V_{oc} are plotted as a function of $\log(\mathbf{J_0}/J_L)$ and $\log(j_0/J_L)$. The contour plots are clipped at values of $\Delta E_F/q$ and V_{oc} greater than one so that the minimum and maximum values of the color scheme run consistently from 0 to 1. This can be seen as artificially imposing a maximum value of $\Delta E_F/q$ and V_{oc} due to radiative recombination (V_{oc}^{max}), and plotting $\Delta E_F/qV_{oc}^{max}$ and V_{oc}/V_{oc}^{max}.

The contours of both Figs. 9a and 9b clearly show two distinct regimes of behavior, separated by the gray horizontal dashed line in both figures. This dashed line represents the boundary between the high- and low-injection regimes, i.e. when $\mathbf{J_0} = J_L$.

The gradient of ΔE_F is different in the two regimes. In high-injection, it runs perpendicular to the line $\log[\mathbf{J_0}] + \log[j_0] = \textit{constant}$ or equivalently with the product $J_0 j_0$, i.e. R_2. As ΔE_F depends on contact recombination, this reflects the second-order nature of recombination in high-injection. In low injection, the gradient is parallel to the j_0 axis; ΔE_F only depends on j_0, i.e. R_1, reflecting the quasi-first-

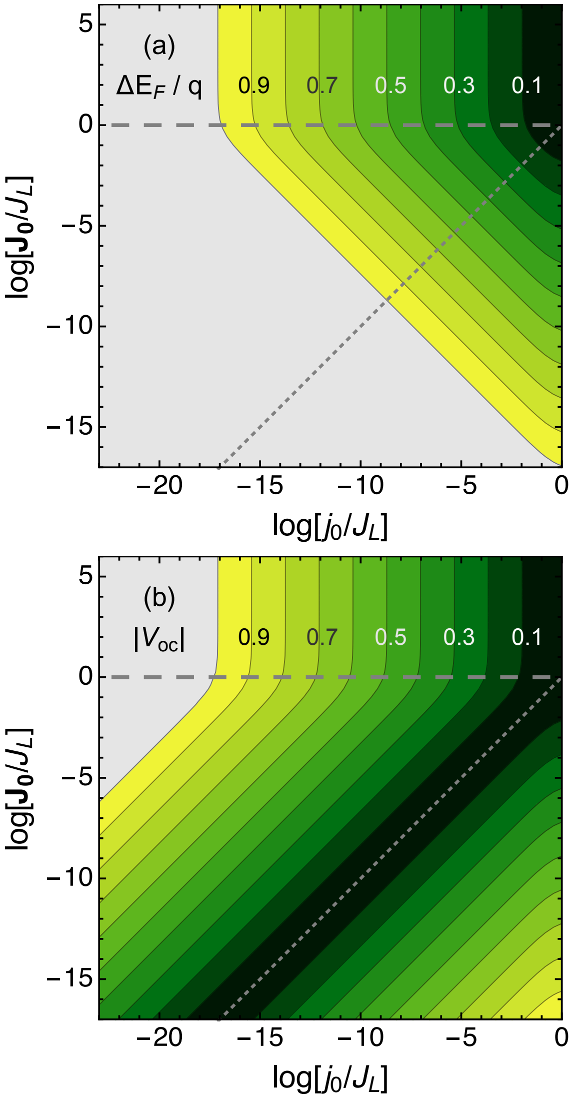

FIGURE 9. Contour plots of eqs. 6.11 and 6.12 showing: (a) $\Delta E_F/q$ and (b) $|V_{oc}|$ as a function of $\log(\mathbf{J_0}/J_L)$ and $\log(j_0/J_L)$. The value of the contours run from 0 V (dark green) to 1 V (yellow) with every other contour labeled in Volts. The plots are clipped with the gray regions representing values greater than 1 V. The dashed gray line at $\log(\mathbf{J_0}/J_L) = 0$ divides the low (above line) and high (below line) injection regimes. Note that the region above the dotted gray line marking $S = 0$ corresponds to $\mathbf{J_0} > j_0$, as considered in the text.

order nature of the recombination. The quantitative dependencies of ΔE_F on R_m can be readily seen by evaluating eq. 6.11 in either of the two limits $\mathbf{J_0} \gg J_L$ and $\mathbf{J_0} \ll J_L$ yielding:

$$\frac{\Delta E_F}{q} \approx m V_T \ln\left(\frac{J_L}{2R_m}\right) \tag{6.13}$$

with $m = 1$ for $\mathbf{J_0} \gg J_L$, and $m = 2$ for $\mathbf{J_0} \ll J_L$. The factor of two in the denominator of the log accounts for the two interfaces in the system.

The behavior of V_{oc} is also different in the two regimes. Comparison of Fig. 9a and 9b show that $V_{oc} = \Delta E_F$ in low injection. Indeed, evaluating eq. 6.12 in the limit $\mathbf{J_0} \gg J_L$ yields:

$$V_{oc} \approx V_T \ln\left(\frac{J_L}{2R_1}\right) = V_T \ln\left(\frac{J_L}{2j_0}\right), \tag{6.14}$$

which is identical to the low injection expression for ΔE_F. In low injection, the V_{oc} is recombination limited depending on the balance of generation and recombination via leakage of minority carriers. In contrast, the high-injection V_{oc} does not follow ΔE_F. Rather, the gradient of V_{oc} in high injection runs perpendicular to $\log \mathbf{J_0} - \log j_0 =$ *constant* lines. Thus, it depends on the ratio $\mathbf{J_0}/j_0$, i.e. S. Indeed, evaluating eq. 6.12 in the limit $\mathbf{J_0} \ll J_L$ yields:

$$V_{oc} \approx V_T \ln \frac{\mathbf{J_0}}{j_0} = V_T \ln S. \tag{6.15}$$

The V_{oc} is selectivity limited in high injection with V_{oc} always remaining smaller than ΔE_F; this is because the selectivity in high injection is never sufficient to support the full quasi-Fermi level splitting, which is always limited by recombination.

To summarize, V_{oc}, like ΔE_F, is determined solely by J_L/j_0 as long as the majority process is faster than J_L ($\mathbf{J_0} \gg J_L$). Selectivity *does not* limit the device, and the only way to improve a device in this regime is to decrease j_0. However, when $\mathbf{J_0} \ll J_L$, the device selectivity is not large enough to support the recombination-determined ΔE_F, and V_{oc} becomes both selectivity limited and illumination independent. In this regime, either an increase in the the contacts' ability to extract majority carriers, or a decrease in the leakage rate of minority carriers can improve the V_{oc}.

The General Case in High and Low injection

The case of the previous section clearly illustrates how selectivity and contact recombination combine to determine V_{oc}, but because of its symmetry, it conflates the asymmetry at a given contact with that seen by a given carrier across the device. Hence, we return to treating the four J_0's considering both electrodes either in low or high injection. Recombination at the two contacts no longer has to be balanced; f^β no longer has to be 1/2.

The value of f^β is largely determined by the relative recombination rates at the two contacts. To understand why, we simplify the general result, eq. 6.8, under the assumptions of low and high injection. In low injection, the term Y in eq. 6.8 is much less than one, and f^β can be reasonably approximated with a first-order expansion of the square root term. In high injection, f^β can be simplified with an additional constraint, namely that $\sqrt{Y} \gg 1$, which amounts to:

$$2\frac{\sqrt{j_{0n}^{\alpha} j_{0p}^{\beta}}}{j_{0n}^{\alpha} + j_{0p}^{\beta}} \sqrt{\frac{J_L}{\mathbf{J_{0n}^{\beta}}} \frac{J_L}{\mathbf{J_{0p}^{\alpha}}}} \gg 1. \tag{6.16}$$

This inequality is satisfied when j_{0n}^{α} and j_{0p}^{β} are not too different from one another as compared to the difference between J_L and the $\mathbf{J_0}$'s. With these approximations, the limiting form for f^{β} is:

$$f^{\beta} \approx \frac{1}{1 + R_m^{\alpha}/R_m^{\beta}}. \tag{6.17}$$

with $m = 1$ for $\mathbf{J_0} \gg J_L$, and $m = 2$ for $\mathbf{J_0} \ll J_L$. The partitioning of recombination between the two contacts is determined by their relative R_m values.

The ΔE_F is calculated by inserting eq. 6.17 into eq. 6.7b in the appropriate limit yielding:

$$\frac{\Delta E_f}{q} \approx m V_T \ln\left(\frac{J_L}{R_m^{\alpha} + R_m^{\beta}}\right), \tag{6.18}$$

with the appropriate value of m. This is analogous to eq. 6.13 of the two-J_0 case, but it allows for asymmetries in the R_m values. When there is a significant imbalance, the interface with the larger R_m dominates the recombination and ultimately limits $\Delta E_F/q$.

The V_{oc} in the low-injection case equals $\Delta E_F/q$:

$$V_{oc} \approx V_T \ln\left(\frac{J_L}{R_1^{\alpha} + R_1^{\beta}}\right) = V_T \ln\left(\frac{J_L}{j_{0n}^{\alpha} + j_{0p}^{\beta}}\right). \tag{6.19}$$

As in the two-J_0 case, the V_{oc} is limited by contact recombination, not selectivity, in low injection. The classic expression for V_{oc} relating the photocurrent to the minority recombination current ($j_{0p}^{\beta} + j_{0n}^{\alpha}$) is obtained. If there is a significant imbalance between j_{0n}^{α} and j_{0p}^{β}, ΔE_F and V_{oc} are determined by the interface with the larger j_0 value.

The high-injection result for V_{oc} is:

$$V_{oc} \approx V_T \ln \sqrt{\frac{\mathbf{J_{0p}^{\alpha} J_{0n}^{\beta}}}{j_{0p}^{\beta} j_{0n}^{\alpha}}}. \tag{6.20}$$

The V_{oc} in the high-injection case is less than $\Delta E_F/q$. It is limited by the selectivity as in the two-J_0 case, but there is an important distinction. The V_{oc} is determined by the system or device selectivity, S_D, as defined by:

$$S_D = \sqrt{\frac{\mathbf{J_{0p}^{\alpha} J_{0n}^{\beta}}}{j_{0p}^{\beta} j_{0n}^{\alpha}}} = \sqrt{S_n S_p}. \tag{6.21}$$

With this definition and assumption 6.16, the V_{oc} in eq. 6.20 is simply:

$$V_{oc} \approx V_T \ln S_D. \tag{6.22}$$

The S_D is the average in log space of S_n and S_p. We see that the selectivity-limited V_{oc} cannot be described by the selectivity of only one of the carriers; the asymmetry in the rate processes for the entire system must be considered. In this case, a factor of 10 change in any one of the four J_0's will result in an equal magnitude shift in the V_{oc}. Of course, given what we know about the step nature of the $J(V)$ curve, it is important to emphasize that it is likely that only one of the carrier's selectivities will have an effect on the location of the efficiency of the device, unless the two carrier selectivities are identical.

Efficiency

While knowledge of the functional form of the contact-determined open-circuit voltage and quasi-Fermi level splitting is revealing, the most important performance metric for any solar cell will always by its efficiency, as determined by its maximum power point. Unfortunately, no general analytic expression exists for the voltage at the maximum power point given the $J(V)$ curve given by 5.3; this must be solved numerically. However, the $J(V)$ curve is easily simplified in low and high injection, and under these assumptions, an analytic expression is readily available. The details of both simplifications in both limits are provided in Appendix F.

If both carriers are in low injection, one can approximate the $J(V)$ (near the power quadrant) as

$$J(V) \approx \left(j_{0n}^{\alpha} + j_{0p}^{\beta}\right) e^{V/V_T} - J_L. \tag{6.23}$$

Note that this approximation requires the reasonable further assumption that the ratio of the j_0's is not large compared to both $\mathbf{J_0}$ to J_L ratios (see Appendix F for details). This expression is remarkably simple; it is nearly identical to the $J(V)$ of the SQ limit and the ideal solar cell (eq.2.1). The difference is simply that instead of $j_{0n}^{\alpha} + j_{0p}^{\beta}$, the SQ limit contains a J_0 determined by radiative recombination. It is readily apparent from the form of eq. 6.23 that in this regime, the superposition principle will apply, and the $J(V)$ will not be S-shaped around the power quadrant. One might note that eq 6.23 does not strictly go to zero when $V = 0$ and $J_L = 0$, which is simply a consequence of assuming that the j_0's are negligibly small relative J_L.

Importantly, the power quadrant in low injection is essentially independent of both $\mathbf{J_0}$'s. The recombination is quasi first-order, and is dictated by the leakage of minority carriers at each contact. The voltage at the maximum power point, V_m, is solved for in the usual fashion by finding the maximum of the power density function $(|(J(V) \times V|)$. In the low injection limit,

$$V_m \approx V_T \left(W \left[\frac{J_L e}{j_{0n}^{\alpha} + j_{0p}^{\beta}} \right] - 1 \right). \tag{6.24}$$

The efficiency (given by $\eta = \frac{|J(V_m) \times V_m|}{P_{inc}}$ where P_{inc} is the incident power density) is solely determined by the ratio of J_L to $j_{0n}^{\alpha} + j_{0p}^{\beta}$ and the temperature. Again, eq. 6.24 is identical to that derived in the SQ limit except that the J_0's are determined by the contacts instead of being set by radiative recombination. The comparison of the radiative J_0's to the contact-determined J_0's has already been considered in the literature; Swanson recognized that leakage at the contacts is the primary issue preventing silicon solar cells from approaching their optimal efficiency (after taking into account Auger recombination, reflection, and other unpreventable losses).[29]

When both carriers are in high injection, the $J(V)$ curve in the power quadrant can be approximated as

$$J(V) \approx J_L \left(\frac{1}{1 + S_n e^{-V/V_T}} + \frac{1}{1 + S_p e^{-V/V_T}} - 1 \right) \tag{6.25}$$

where we have replaced the $\mathbf{J_0}/j_0$ ratios with the appropriate carrier selectivities. It is clear that J_L linearly scales the *entire* curve, and therefore the position of V_{oc} is independent of J_L. This clearly violates superposition; in fact the voltage at which the light and dark $J(V)$ curve will intersect is approximately V_{oc}.

In order to derive an analytic expression for the maximum power point in high injection, we must further assume that one carrier is limiting (i.e. we must assume that one carrier selectivity is much larger than the other). If we do so, the $J(V)$ behavior in the power quadrant is solely determined by said carrier, and the voltage at the maximum power point is equal to:

$$V_m \approx V_T \left(W \left[\frac{S}{e} \right] + 1 \right) \tag{6.26}$$

where S is the smaller (i.e. limiting) of the two carrier selectivities. As opposed to low injection, the V_m in high injection is independent of the light current and depends on both J_0's of the limiting carrier, similar to the V_{oc}. Unlike V_{oc} however, the maximum power point is determined by the limiting carrier only, as long as the selectivities are significantly different. This is intuitive given the nature of the $J(V)$ curve; the curve is nearly flat at V_{oc} in high injection, so the location of V_{oc} does not necessarily determine the efficiency because the fill factor can vary dramatically based on the location of the second step.

To demonstrate how the efficiency in the low injection limit fits in with existing limits on device performance, Fig. 10 compares the SQ efficiency as a function of bandgap to our low-injection, contact-determined limit with a fixed $j_0 = j_{0n}^{\alpha} + j_{0p}^{\beta}$. The black curve shows the single absorber SQ efficiency as a function of bandgap, where the bandgap is used to calculate J_L by integrating the AM1.5 spectrum from the bandgap energy to infinity. J_L is determined in the same way for the other curves. However, for the colored curves, the j_0 is fixed by the contacts (as opposed to varying according to detailed balance as it does in the SQ model). As the bandgap increases, the j_0 needed to match the SQ limit decreases, because in the SQ model, the radiative recombination decreases strongly with bandgap. The point at which the SQ curve uses the same j_0 as the contact-limited model is where each of the curves intersect. Therefore, if one is considering using an absorber with a bandgap of, for instance, 1.3 eV, it is clear that the contacts will need to provide equilibrium exchange current densities for minority carriers as low as $\sim 10^{-15}\,\mathrm{mA\,cm^{-2}}$ in order to approach the SQ limiting efficiency.

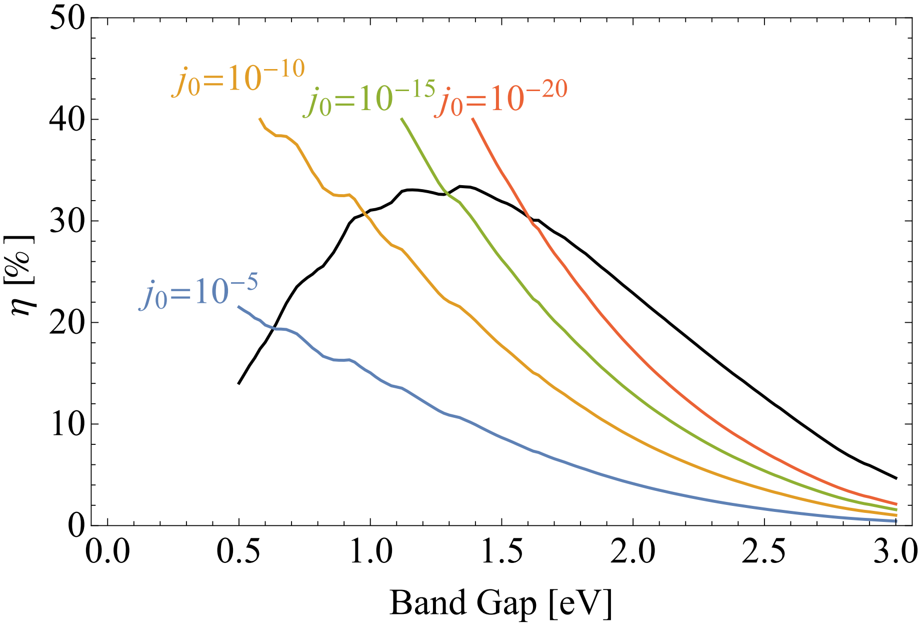

FIGURE 10. The SQ limiting efficiency as determined by radiative recombination (black) as a function of bandgap compared to the *low*-injection contact-determined efficiency (colors). In both cases, J_L is determined by integrating the AM1.5 spectrum from the bandgap energy to infinity. The j_0 for the black curve is a function of bandgap, as dictated by the SQ limit, whereas for the colored curves, j_0 is a fixed value determined by the contacts to the absorber, set to 10^{-5} (blue), 10^{-10} (orange), 10^{-15} (green) and 10^{-20} (red) $\mathrm{mA\,cm^{-2}}$.

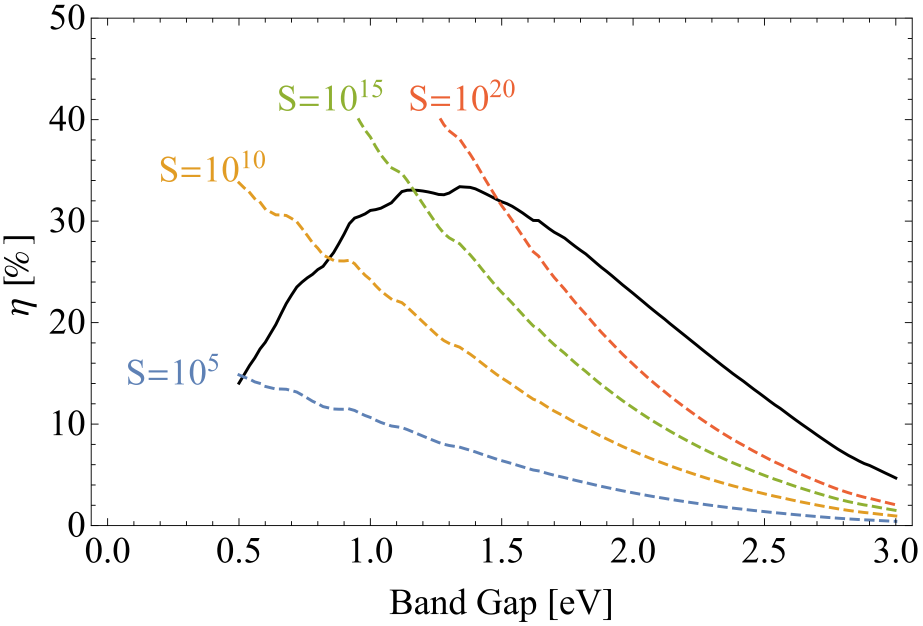

FIGURE 11. The SQ limiting efficiency as determined by radiative recombination (black) as a function of bandgap compared to the *high*-injection contact-determined efficiency. For all curves, J_L is again calculated by integrating the AM1.5 spectrum above the bandgap. The black curve uses j_0's determined via radiative recombination, while the colored curves have fixed carrier selectivities, S, set to 10^5 (blue), 10^{10} (orange), 10^{15} (green) and 10^{20} (red). Temperature is set to 300 K.

Figure 11 compares the efficiency calculated from the contact limited model with one limiting carrier in high injection, to the one-sun SQ limit. The limiting carrier selectivity is fixed to a different ratio for each of the colored curves, while the SQ limit, as a function of bandgap, is in black. As with low injection, the demands on the contacts become more and more stringent as the bandgap of the absorber increases. For a bandgap of $\sim 1.5\,\text{eV}$, the limiting carrier selectivity of a device must be on the order of 10^{20} in order to approach the SQ limit.

The primary results of the contact-determined theory have been presented in Chapters 5 and 6. These make testable predictions about the performance of solar cells. The easiest way to test these is to simulate the entire device physics (i.e. self consistent solutions to Poisson's equation, and the continuity equation and drift-diffusion equations) of various solar cell architectures. Chapter 7 will present simulations performed using the semiconductor module of COMSOL testing the current voltage curves, as well as the performance parameters derived from the $J(V)$ curve.

CHAPTER VII

SIMULATIONS

This chapter contains full device physics simulations performed by myself of various solar cell architectures in an attempt to assess the theoretical predictions of the previous two chapters. It is taken primarily from the Simulations section and Supplementary Matieral of Roe et al. 2019, with some re-organizing and re-writing for clarity.

Full device simulations were performed using the semiconductor module of COMSOL Multiphysics. By ‘full’, we mean simulations that include the physics that were neglected in the assumptions of the analytic model, i.e. bulk recombination and mobility limitations. In practice, this is achieved by numerically solving Poisson’s equation for the distribution of electric charge with the drift-diffusion equations for current plugged into the continuity equations for electrons and holes. COMSOL uses the finite-volume method to calculate the electric potential, electron density, and hole density as a function of position throughout the device. For detailed information about how it accomplishes this, refer to the COMSOL Multiphysics User’s Guide, and the Semiconductor Module User’s Guide. Below, the general features of the simulations will be described. Details specific to the device architecture under study will be layed out in the appropriate section.

All simulations performed herein are 1-dimensional, and all are done at room temperature, $T = 298\,\mathrm{K}$. We will consider multiple device structures, but we will always use an absorber which is undoped. In COMSOL, one can make a 1-D device out of an arbitrary number of semiconducting layers. Junctions between different semiconducting layers will be modeled with thermionic emission (as opposed to assuming continuous quasi-Fermi levels). Metals are used as contacts to an external circuit, and can either be modeled with a Schottky contact, or an ohmic contact to the adjoining semiconductor.

In order to solve for the electric potential and the electron and hole densities, boundary conditions must be specified. The boundary conditions for the electric potential are simply the voltages at both ends of the device; the difference between these is the applied voltage, or simply V, in the $J(V)$ curve. For each $J(V)$ curve simulated herein, a voltage step of $0.01\,\mathrm{V}$ is used.

Boundary conditions for the electron and hole densities at either end of the device depend on which type of metal contact we choose, Schottky or ohmic. For an ohmic contact, local thermodynamic equilibrium is assumed to apply at the contact so that the carrier densities are equal to the equilibrium densities, as defined by

$$n_{eq} = \frac{1}{2}\left(N_d^+ - N_a^-\right) + \frac{1}{2}\sqrt{\left(N_d^+ - N_a^-\right)^2 + 4n_i^2} \tag{7.1a}$$

$$p_{eq} = -\frac{1}{2}\left(N_d^+ - N_a^-\right) + \frac{1}{2}\sqrt{\left(N_d^+ - N_a^-\right)^2 + 4n_i^2} \tag{7.1b}$$

where N_d^+ and N_a^- are the donor and acceptor densities, respectively, at the interface to the absorber (while the absorber is intrinsic, we do consider a *p*-*i*-*n* architecture, so these are not always zero). Meanwhile, for Schottky metal contacts, the carrier densities are not necessarily at equilibrium, as defined by the Fermi level of the adjoining metal. The boundary conditions are given by

$$J_n(x^\alpha) = q\nu_n^\alpha(n(x^\alpha) - n_0) \tag{7.2a}$$

$$J_p(x^\alpha) = -q\nu_p^\alpha(p(x^\alpha) - p_0) \tag{7.2b}$$

$$J_n(x^\beta) = -q\nu_n^\alpha(n(x^\beta) - n_0) \tag{7.2c}$$

$$J_p(x^\beta) = q\nu_p^\alpha(p(x^\beta) - p_0). \tag{7.2d}$$

in conjunction with the constraint that $J_n(x^\alpha) + J_p(x^\alpha) = J = J_n(x^\beta) + J_p(x^\beta)$ at steady state. ν_n and ν_p are the charge transfer velocities for electrons and holes respectively, and the equilibrium carrier densities, n_0 and p_0, are set by the barrier height at the contacts via

$$n_0 = N_c \exp\left(-\frac{\phi_n}{k_B T}\right) \tag{7.3a}$$

$$p_0 = N_v \exp\left(-\frac{\phi_p}{k_B T}\right). \tag{7.3b}$$

where ϕ_n and ϕ_p are the electron and hole barrier heights, respectively, in eV. Note that eq. 7.2 is identical to eq. 3.1, except that the charge transfer velocity ν is used in place of J_0. They are related by

$$J_{0x}^y = q\nu_x^y x_0 \tag{7.4}$$

where x is either n or p for electrons or holes, and the superscript y is either α or β to denote the appropriate contact/interface. The J_0's for Schottky interfaces were calculated with various barrier heights and A^*'s, specific to each individual situation, according to

$$\mathbf{J_0} = A^* T^2 e^{-\frac{E_g/2 - \Delta\phi/2}{qV_T}} \tag{7.5a}$$

$$j_0 = A^* T^2 e^{-\frac{E_g/2 + \Delta\phi/2}{qV_T}}. \tag{7.5b}$$

The fact that there are only two J_0's is due to that fact that we assume the Richardson constant is equal for both interfaces.

Recombination was considered in all semiconducting layers, while generation was only considered in the absorber. Generation, denoted by $G(x)$, followed Beer-Lambert position dependence according to

$$G(x) = G_0 e^{-\alpha x} \tag{7.6}$$

where x is the depth into the absorber. The generation rate at the surface, G_0, is set by:

$$G_0 = \Phi_L \left(\frac{\alpha J_L}{q} \right) \tag{7.7}$$

where Φ_L is a unitless quantity indicating the number of suns, and J_L is the current density if 100% of the AM 1.5 spectrum above 1.5 eV were absorbed ($\sim 29\,\mathrm{mA/cm^2}$). Throughout, we will use electron and hole mobilities of 1000 $\mathrm{cm^2V^{-1}s^{-1}}$. This value is in line with what one can expect in both single crystal silicon and GaAs,[81–86] though it allows us to clearly demonstrate how mobility can limit the accuracy of the analytic model.

Double Schottky Contacts

One of the simplest possible tests for our model is a 1-D device consisting of an absorber with two Schottky metal contacts on either end. As Schottky contacts are well modeled by eq. 3.1 as long as thermionic emission is the rate-limiting process,[64] we expect that the simulations will only deviate from our theory because of limitations imposed by mobility and bulk recombination. In other words, if we were to simulate the $J(V)$ curve with unrealistically high mobility and low bulk recombination rates, we should recover the theory exactly.

We consider a generic thin film absorber, with a thickness, L, of one micron and a bandgap of 1.5 eV. The absorption coefficient, α, is chosen to be $3 \times 10^4\,\mathrm{cm}^{-1}$ (note that we are simplifying the absorption coefficient to a step function centered at the bandgap, i.e. 0 below the bandgap and α above it). Generation is spatially dependent, according to eq. 7.6. Direct recombination throughout the device is quantified by its coefficient, B, which is uniform throughout the absorber. Given the assumption of a step-function absorption coefficient, B can be approximated as

$$B = \frac{\alpha k_B T E_g^2 e^{-\frac{E_g}{k_B T}}}{\pi^2 \hbar^3 c^2 n_i^2} \tag{7.8}$$

where $\hbar$ is the reduced Planck's constant, c is the speed of light, and n_i is the intrinsic carrier density, equal to $2 \times 10^6\,\mathrm{cm}^{-3}$ for a bandgap of 1.5 eV with $N_c = N_v = 1 \times 10^{19}\,\mathrm{cm}^{-3}$. We will always assume these values for N_c and N_v unless otherwise stated. Given these, $B \approx 1.5 \times 10^{-11}\,\mathrm{cm}^3\mathrm{s}^{-1}$.

In COMSOL, a Schottky metal contact is distinguished by its work function, ϕ_m, and its Richardson coefficient, A^*. In principle, there are four different A^* values one could set in the simulation (one for both electrons and holes at both contacts). For

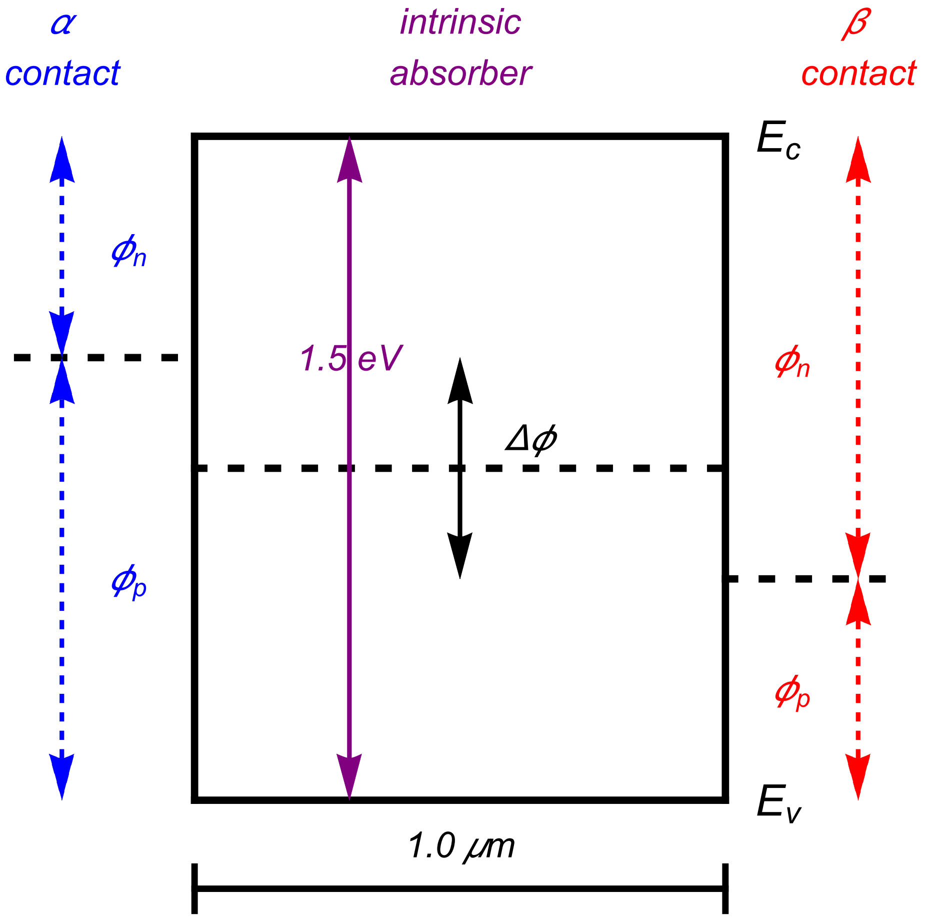

FIGURE 12. Schematic depicting the Fermi-level alignment in the double Schottky contact model. The Fermi-levels of the metals are set so that the barrier heights, ϕ, are equal for opposing carriers across the device. The difference in work functions between the contacts is quantified by $\Delta\phi$, which is varied in the simulations.

the sake of simplicity, we assume these are identical in each simulation. The work functions of the metal contacts are set so that the metal Fermi levels are symmetric about the intrinsic level of the absorber, as in Fig. 12. For instance, if $\Delta\phi = 0.2\,\mathrm{V}$, the work function of contact α is $0.1\,\mathrm{eV}$ below the intrinsic level and visa versa for the β contact. Given these assumptions, we are effectively replicating the 2 J_0 case from Chapter 6. For a complete list of all the parameters used to model the device in COMSOL, refer to Table 1.

TABLE 1. Schottky Device Parameters

Symbol	Description	Value	Unit
T	temperature	298	K
Φ_L	no. of suns	varied	1
absorber:			
L	absorber thickness	1	μm
E_g	bandgap	1.5	eV
ϵ_r	relative permittivity	10	1
N_C	effective conduction band DOS	1.0×10^{19}	cm^{-3}
N_V	effective valence band DOS	1.0×10^{19}	cm^{-3}
u_n	electron mobility	1000	$\mathrm{cm}^2\,\mathrm{V}^{-1}\,\mathrm{s}^{-1}$
u_p	hole mobility	1000	$\mathrm{cm}^2\,\mathrm{V}^{-1}\,\mathrm{s}^{-1}$
B	radiative recomb. coeff.	1.5×10^{-11}	$\mathrm{cm}^3\ \mathrm{s}^{-1}$
J_L	'perfect' one sun J_{sc}	29.01	$\mathrm{mA\,cm}^{-2}$
Contacts:			
$\Delta\phi$	contact work function difference	varied in simulation	eV
ϕ_{bn}^{α}	e^- Schottky barrier at contact α	$E_g/(2) + \Delta\phi/2$	eV
ϕ_{bp}^{α}	h^+ Schottky barrier at contact α	$E_g/(2) - \Delta\phi/2$	eV
ϕ_{bn}^{β}	e^- Schottky barrier at contact β	$E_g/(2) - \Delta\phi/2$	eV
ϕ_{bp}^{β}	h^+ Schottky barrier at contact β	$E_g/(2) + \Delta\phi/2$	eV
A_n^*	Richardson constant for electrons	varied	$\mathrm{A\ K}^{-2}\ \mathrm{cm}^{-2}$
A_p^*	Richardson constant for holes	varied	$\mathrm{A\ K}^{-2}\ \mathrm{cm}^{-2}$

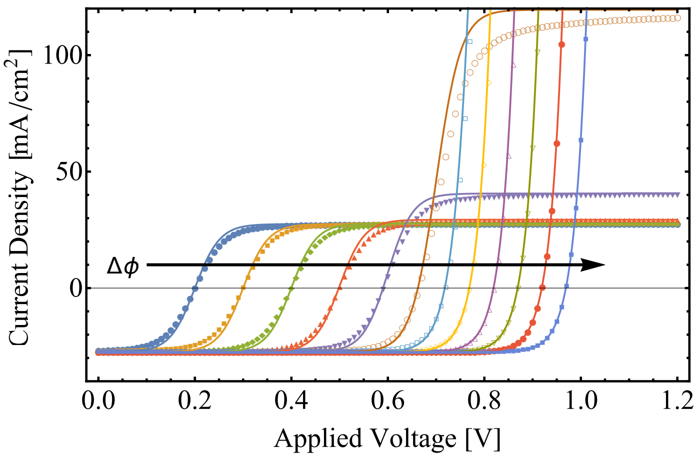

FIGURE 13. Plot of $J(V)$ comparing simulations (data points) to eq. 5.3 (solid lines) for a 1.5 eV bandgap intrinsic absorber with Schottky metal contacts with varying work functions as determined by $\Delta\phi$. The $\Delta\phi$ increases from 0.2 to 1.3 eV in steps of 0.1 and A^* is fixed at $\mathrm{A\,cm^{-2}\,K^{-2}}$. Note that because all A^*'s are the same, the electron and hole steps line up on top of each other, so that the size of the step is twice as large as a single step.

Figure 13 compares the simulated vs. theoretical $J(V)$ curves of the device described above. The A^* was set to $3\,\mathrm{A\,cm^{-2}\,K^{-2}}$, within the wide range of reported Richardson constants for thin-film semiconductors.[87–90] At low $\Delta\phi$, both electrons and holes are in high injection. Because the two j_0's are equal as well as the two $\mathbf{J_0}$'s, the electron and hole steps are on top of each other, thus we can only see one step. The size of the step is approximately $2J_L$ as long as the $\mathbf{J_0}$ is much smaller than J_L. As the $\mathbf{J_0}$ becomes comparable to J_L at $\Delta\phi = 0.6\,\mathrm{eV}$, the $J(V)$ curve transitions to low injection, and the step size becomes larger than $2J_L$.

The V_{oc}'s as predicted by theory are accurate for every $\Delta\phi$ value shown. However, for many of the $\Delta\phi$ values, the theoretical limit has a slightly larger fill factor than the simulated data. For the lower $\Delta\phi$ values, the fill factor is reduced in the simulated data because the mobility limits current collection when the carrier densities are low. At higher $\Delta\phi$, the higher carrier selectivities can support higher quasi-Fermi-level splitting and thus larger carrier densities in the bulk. The larger carrier densities in the bulk allow for higher conductivities, thus reducing the need for high mobility, and therefore the fill factor deficit is reduced. If direct recombination were to affect the simulated data, one would expect to see limitations around V_{oc} for the higher $\Delta\phi$ values, as the rate is proportional to the product of n and p. Here, we see no deviations at large $\Delta\phi$ indicating that the radiative recombination limit has not been approached. Indeed, one would not expect to see such limitations until the V_{oc} approaches 1.15 V for a bandgap of 1.5 eV and $B = 1.5 \times 10^{-11}\,\mathrm{cm}^3/\mathrm{s}$.

Figure 14 compares the theoretical efficiency (calculated numerically from eq. 5.3) of the device under discussion to the simulated efficiencies. The illumination intensity was varied exponentially from 10^{-3} to 10^{2} suns. The region where the lines converge denotes high injection, and each different light intensity curve moves off of the high injection curve at different values of $\Delta\phi$, as expected from our definitions of high and low injection. Whereas in high injection, the efficiency is independent of light intensity, in low injection, the efficiency becomes quasi-logarithmically dependent on light intensity as we expect. The simulated efficiencies in high injection are slightly below the theoretical limit due to finite mobility, as discussed above. Like Fig. 13, the simulated efficiencies are not yet being affected by bulk recombination as the voltages at the maximum power point are not approaching 1.15 V.

Our theoretical model works well, then, for a generic device with direct recombination and Schottky contacts as long as the mobility does not limit the rate at which carriers escape to the contacts. The model is expected to become less accurate as the mobility is decreased, or equivalently as the J_0's become larger with a fixed mobility (i.e. when bulk transport starts to limit the speed at which carriers can recombine at the contacts). This is indeed the case as can be seen in Fig. 15a where the Richardson constant is varied from $10^{-2}\,\mathrm{A\,cm^{-2}\,K^{-2}}$ to its ideal metal limit

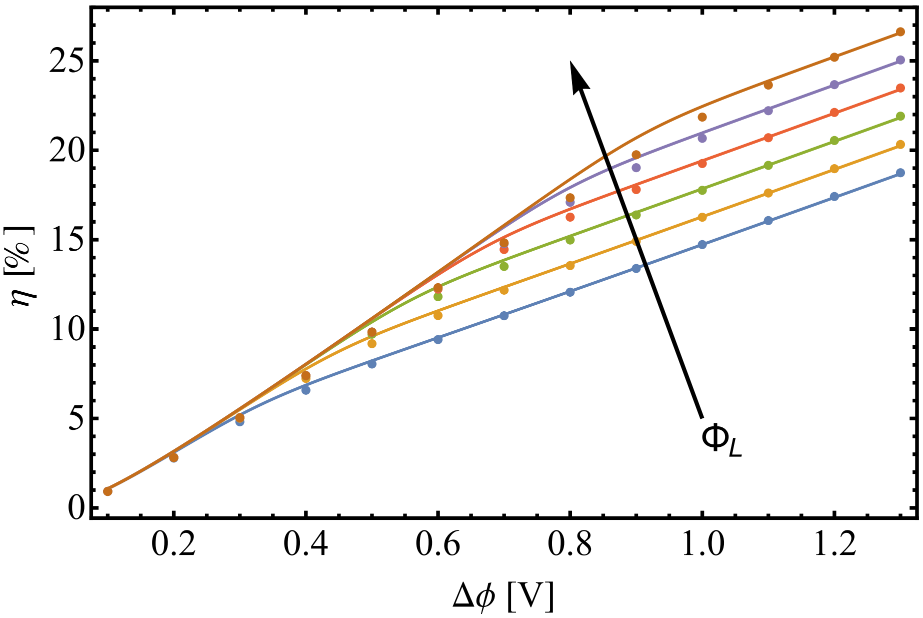

FIGURE 14. Simulated efficiency (data points) compared to that derived from eq. 5.3 (solid lines) for the same device as Fig. 13 with $A^* = 3\,\mathrm{A\,cm^{-2}\,K^{-2}}$ and $\Delta\phi$ increasing from 0.1 to 1.3 eV in steps of 0.1. The relative generation rate, Φ_L, was varied from 10^{-3} to 10^{2} suns by factors of 10.

($\sim 100\,\mathrm{A\,cm^{-2}\,K^{-2}}$), with a fixed $\Delta\phi = 1.0\,\mathrm{eV}$. The model becomes less accurate as A^* approaches $100\,\mathrm{A\,cm^{-2}\,K^{-2}}$. Specifically, the fill factor and J_{sc} are poor relative to theory, however, the V_{oc} is actually larger than theory predicts. This concept has been discussed extensively in the literature.[54, 91–94] Put simply, when the mobility is reduced to the point where carriers generated in the bulk cannot reach the contacts as fast as they recombine at the contacts, the actual contact recombination rate is smaller than that predicted by the J_0's, leading to a larger-than-predicted V_{oc}. However, the limited mobility also reduces the fill factor and J_{sc} as previously discussed.

Similar deviations from theory occur in Fig. 15b, where the A^* is varied over the same range, but the asymmetry is reduced ($\Delta\phi = 0.5\,\mathrm{eV}$). The deviation is much more evident outside of the power quadrant for the largest A^*, and is expected given that the limited asymmetry/selectivity prevents large quasi-Fermi-level splitting, limiting the carrier density and thus the conductivity in the bulk.

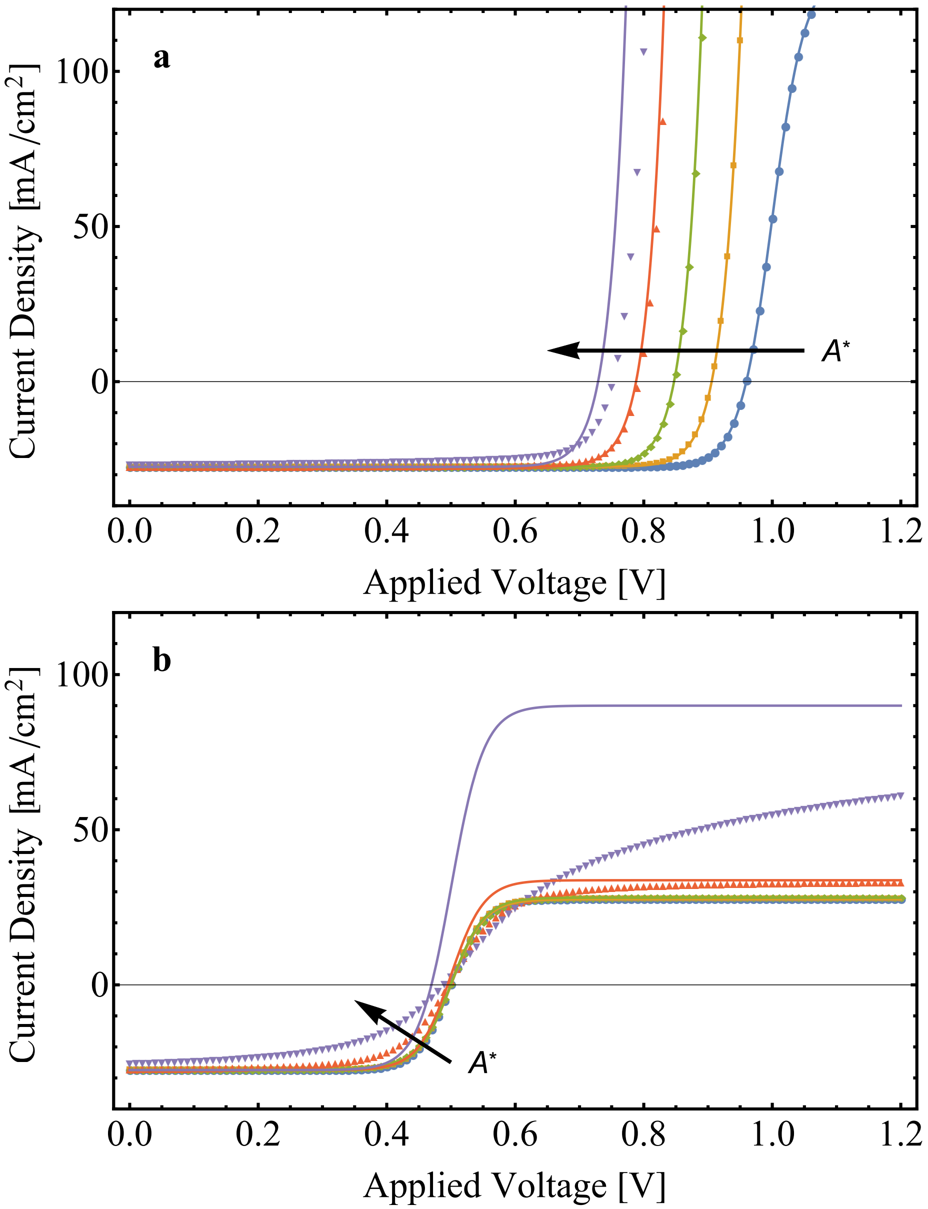

FIGURE 15. Simulated $J(V)$ (data points) compared with theory (lines) for a semiconductor ($E_g = 1.5\,\mathrm{eV}$) and Schottky metal contacts with metal work functions set b: (a) $\Delta\phi = 1.0$ eV and (b) 0.5 eV. In both cases, A^* was increased from 10^{-2} to $10^2\,\mathrm{A\,cm^{-2}\,K^{-2}}$ by factors of 10. Note that in b), the curves with lower A^* lie on top of each other, because in high injection, the $J(V)$ curve is only dependent on the selectivity, not the magnitudes of the J_0's.

For a more comprehensive survey of how mobility limitations affect all four performance parameters, J_{sc}, V_{oc}, FF, and η, consider the contour plots in Fig. 16. Here, we explore the parameter space of asymmetry and contact recombination by varying $\Delta\phi$ and A^*, respectively for Schottky contacts to the same $E_g = 1.5\,\mathrm{eV}$ absorber. The gray regions for all parameters indicate that the simulated performance parameter is within 2.5% of the theoretical value, given by using the A^*'s and $\Delta\phi$ to calculate the $\mathbf{J_0}$ and j_0's in eq. 5.3. Meanwhile, pink and green colors indicate that the simulated parameters are higher and lower than the theoretical values, respectively.

Straight away, we notice that for the entire parameter space, the V_{oc} is either equal to or larger than the theoretical limit, while the opposite is true for all the other parameters. For both J_{sc} and FF, the problematic region is where the A^*'s are large, and the $\Delta\phi$'s are low. The FF and J_{sc} are both dependent on carriers being able to be transported from the bulk of the absorber to contacts; this transport is dependent on the mobility and the carrier density. The carrier densities should be larger in the bulk of the device when the leakage rates of minority carriers are smaller, allowing for current to flow more easily. This will occur at smaller A^* values and higher $\Delta\phi$ values, consistent with the accurate theoretical values, indicated in Fig. 16. Meanwhile, the theoretical V_{oc} is only significantly inaccurate for the combination of large A^* and moderate $\Delta\phi$. One might imagine a situation in which the V_{oc} underestimate is large enough that the efficiency is also overestimated by our model (recall that $\eta = V_{oc}J_{sc}FF$), but this never occurs in this parameter space. Therefore, our model is an upper limit for efficiency, for this parameter range at least.

As direct recombination does not limit the devices we have so far considered, it is also worth simulating similar devices with larger values of B, the direct recombination coefficient. Figures 17a and b are reproductions of Figs. 13 and 14 from identical

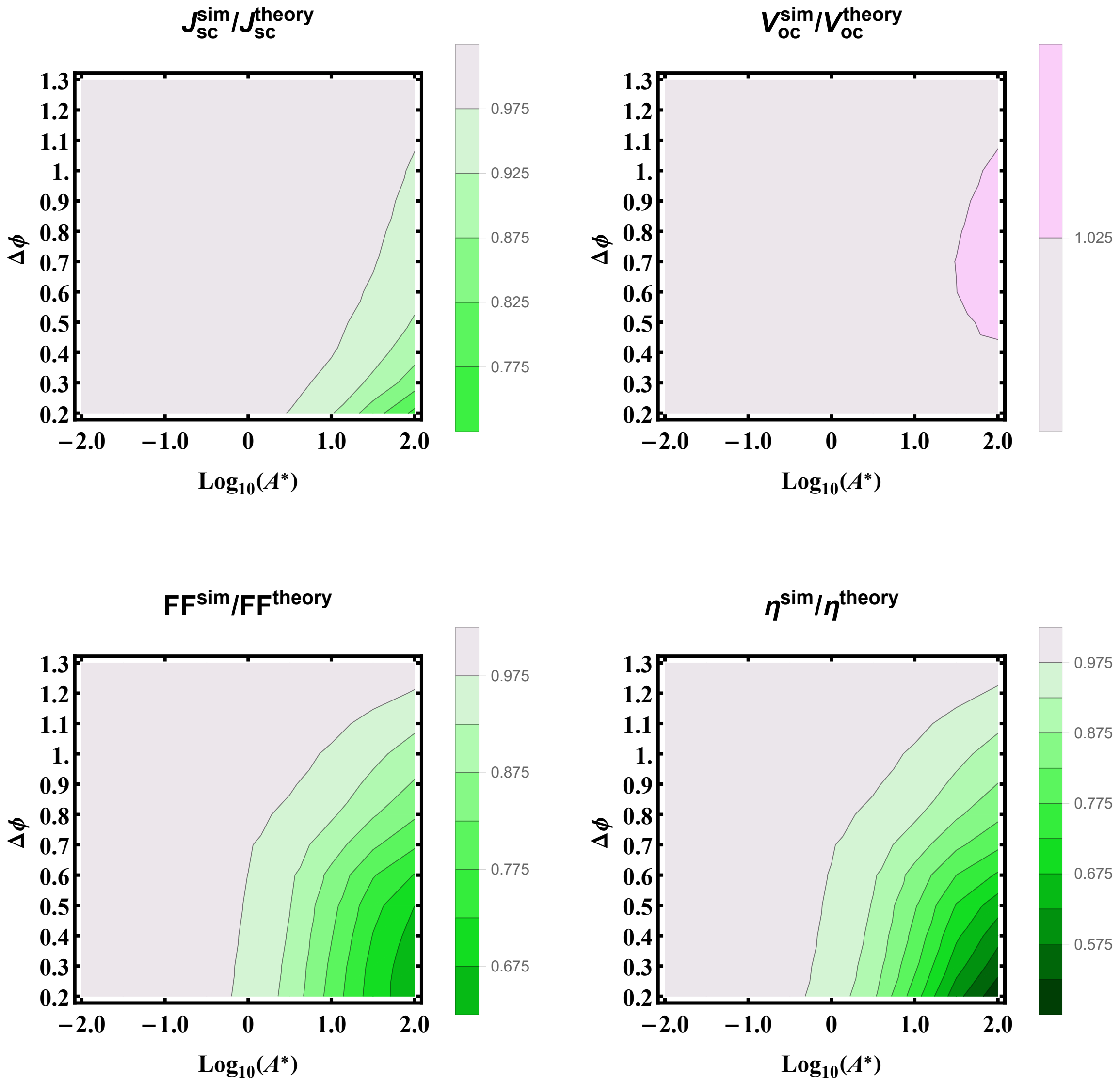

FIGURE 16. Ratios of simulated performance parameters, to those calculated from eq. 5.3 for an intrinsic, 1.5 eV bandgap absorber with radiative recombination and fixed mobility $\mu = 1000\,\mathrm{cm}^2\mathrm{V}^{-1}\mathrm{s}^{-1}$. The generation rate is fixed at 1 sun. The contact recombination is varied on the horizontal axis by varying the Richardson constant, A^*, equal for both carriers at both contacts. As with Fig. 13, the asymmetry is controlled by the parameter $\Delta\phi$, which determines how far each contact work function is from the intrinsic level. The asymmetry is restricted so that the work functions of the metal contacts are within 0.1 eV of the band edges. Pink indicates simulated values larger than theoretical values, and green indicates the opposite.

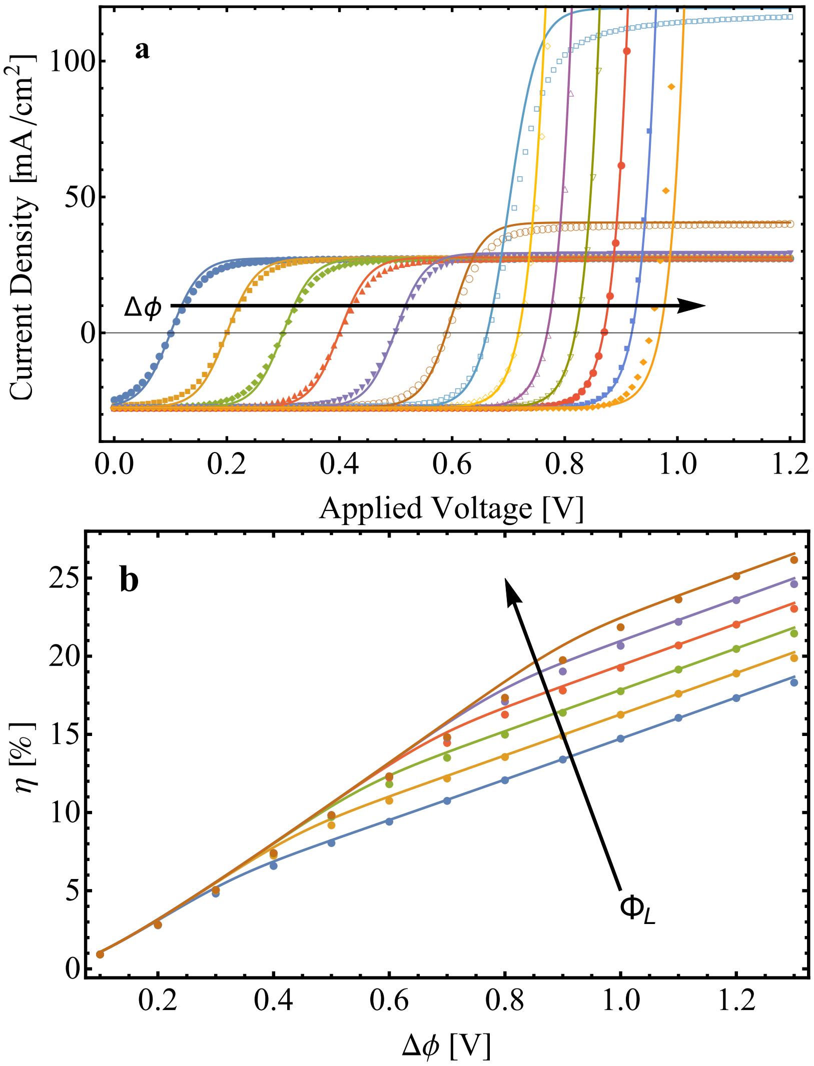

FIGURE 17. Comparison of simulated (data points) and theoretical (lines) $J(V)$ curves (a) and efficiencies (b). The theoretical curves were generated from eq. 5.3 using the same parameters as Fig. 13. The simulated data was generated from the same device parameters as Fig. 13 (see Table 1), except $B = 1.5 \times 10^{-8}\,\mathrm{cm}^3/\mathrm{s}$. The $\Delta\phi$ parameter was varied from 0.1 to 1.3 eV in steps of 0.1 Part a. This was also done in Part b, thought the different curves instead indicate the number of suns, Φ_L.

devices, except $B = 1.5 \times 10^{-8}\,\mathrm{cm}^3/\mathrm{s}$, 1000 times larger than the radiative limit of direct recombination. The simulated data in both figures are almost exactly identical, except for at the highest $\Delta\phi$ values. In Part a, the V_{oc} is indeed reduced somewhat from the theoretical limit, thought the rest of the curve appears unaffected. This deviation is also reflected in the calculations for efficiency for the largest value of $\Delta\phi$ in Part b.

p-*i*-*n* Heterostructure

For comparison, we have included simulations of a *p*-*i*-*n* structure with the absorber described above, where the contacts are instead wider bandgap, doped semiconductors. This structure bears resemblance to a large number of thin film technologies, where an intrinsic or lightly doped absorber is sandwiched by two thin, sometimes entirely different, semiconductors with opposite doping type. In the simulation, the absorber is sandwiched by equally doped n and p doped semiconductors with bandgaps 1.7 and 1.9 eV on either side (see Fig. 18). The absorber/contact interface is simulated with thermionic emission boundary conditions. The wide-bandgap contacts are in turn contacted by ohmic metal contacts. To vary the selectivity in a similar manner as before, the doping density of each contact is varied over a wide range of values. Note that there is no reason why the dopant densities have to be equal; this choice is made for the sake of simplicity. For a complete list of parameters used in the *p*-*i*-*n* simulations, refer to Table 2 below.

We calculate the effective J_0's for such a structure by using a barrier height for either contact as set by the energy difference between the Fermi level and the appropriate band edge (see Fig. 18). Thus, we are essentially treating the thin doped semiconductors as Schottky contacts. This is only expected to work as long as the Fermi levels of the contacts (as set by the dopant density) remain within the bandgap of the absorber. We also expect that for thicker doped contacts, diffusion, rather than thermionic emission will be the rate limiting process for the partial currents,

TABLE 2. *p*-*i*-*n* device parameters

Symbol	Description	Value	Unit
T	temperature	298	K
Φ_L	number of suns	varied	1
intrinsic absorber:			
L	absorber thickness	0.98	μm
E_g	bandgap	1.5	eV
ϵ_r	relative permittivity	10	1
N_C	effective conduction band DOS	1.0×10^{19}	cm^{-3}
N_V	effective valence band DOS	1.0×10^{19}	cm^{-3}
u_n	electron mobility	1000	$\mathrm{cm}^2\,\mathrm{V}^{-1}\,\mathrm{s}^{-1}$
u_p	hole mobility	1000	$\mathrm{cm}^2\,\mathrm{V}^{-1}\,\mathrm{s}^{-1}$
B	radiative recomb. coeff.	1.5×10^{-11}	$\mathrm{cm}^3\ \mathrm{s}^{-1}$
J_L	'perfect' one sun J_{sc}	29.01	$\mathrm{mA\,cm}^{-2}$
χ	electron affinity	1.0	eV
n-type contact:			
L	contact thickness	0.01	μm
E_g	bandgap	1.7	eV
ϵ_r	relative permittivity	10	1
N_C	effective conduction band DOS	1.0×10^{19}	cm^{-3}
N_V	effective valence band DOS	1.0×10^{19}	cm^{-3}
u_n	electron mobility	1000	$\mathrm{cm}^2\,\mathrm{V}^{-1}\,\mathrm{s}^{-1}$
u_p	hole mobility	1000	$\mathrm{cm}^2\,\mathrm{V}^{-1}\,\mathrm{s}^{-1}$
B	radiative recomb. coeff.	1.5×10^{-11}	$\mathrm{cm}^3\ \mathrm{s}^{-1}$
J_L	no generation assumed in contacts	0	$\mathrm{mA\,cm}^{-2}$
χ	electron affinity	0.9	eV
N_d	dopant density	varied	cm^{-3}
p-type contact:			
L	contact thickness	0.01	μm
E_g	bandgap	1.9	eV
ϵ_r	relative permittivity	10	1
N_C	effective conduction band DOS	1.0×10^{19}	cm^{-3}
N_V	effective valence band DOS	1.0×10^{19}	cm^{-3}
u_n	electron mobility	1000	$\mathrm{cm}^2\,\mathrm{V}^{-1}\,\mathrm{s}^{-1}$
u_p	hole mobility	1000	$\mathrm{cm}^2\,\mathrm{V}^{-1}\,\mathrm{s}^{-1}$
B	radiative recomb. coeff.	1.5×10^{-11}	$\mathrm{cm}^3\ \mathrm{s}^{-1}$
J_L	no generation assumed in contacts	0	$\mathrm{mA\,cm}^{-2}$
χ	electron affinity	0.8	eV
N_d	dopant density	varied	cm^{-3}

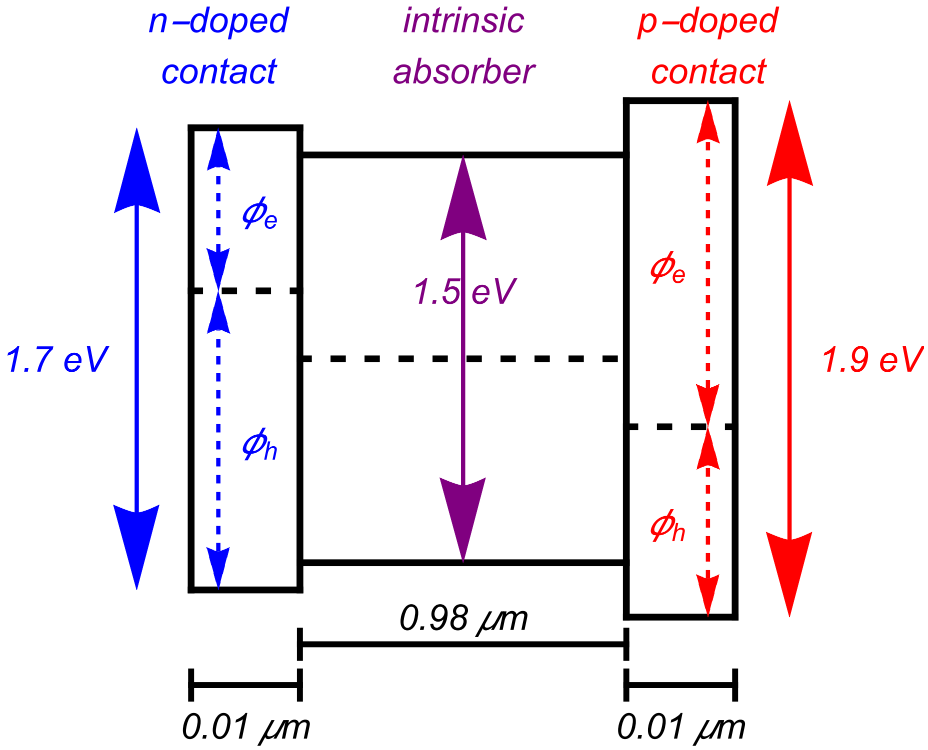

FIGURE 18. Schematic depicting the device structure (before equilibrating) used for the p-i-n simulations. Note that the x-axis is not to scale. Fermi levels for each layer are indicated by the dashed lines; the contact-Fermi levels are determined by the doping density, which is varied in the simulation. The electron affinity of each layer is set so that the intrinsic layers of each semiconductor are aligned and that the offsets of both bands at a given interface are equal. The effective barrier heights used to calculate each of the four J_0's are indicated by the dashed red and blue arrows. The Fermi level (dashed line) of the n contact is set by $E_c - E_f = k_B T \ln\left(\frac{N_c}{N_d}\right)$ while the $E_f - E_v = k_B T \ln\left(\frac{N_v}{N_d}\right)$ sets the Fermi level of the p contact.

and thus the J_0's for the contacts would be governed by the Shockley model. See Fig. 20 below for simulations detailing the transition between the two regimes.

The effective A^* is calculated according to

$$A^* = A_h^* = A_e^* = \frac{4\pi m^* k_B^2 q}{h^3} \tag{7.9}$$

where h is Planck's constant, and m^* is the carrier effective mass, given by

$$m^* = m_h^* = m_e^* = \frac{h^2}{2\pi k_B T}\left(\frac{N_c}{2}\right)^{2/3} \tag{7.10}$$

The effective masses and thus A^*'s are equal because we have assumed that $N_c = N_v$. Given a value of $1\times10^{19}\,\mathrm{cm^{-3}}$ for each of the effective densities of states, both effective A^*'s are equal to $65\,\mathrm{A\,cm^{-2}\,K^{-2}}$.

Figure 19a compares simulated $J(V)$ curves for the *p*-*i*-*n* heterostructure to those calculated with eq. 5.3 with A^*'s given by eq. 7.9 and barrier heights set by the blue and red ϕ_e's and ϕ_h's from Fig. 18. The dopant density of each contact, N_d, is varied in unison from 10^7 to $10^{15}\,\mathrm{cm^{-3}}$ to produce the different curves. Two steps are observed in most of the curves, because although the A^*'s on each side are identical, the effective barrier heights are not, leading to different selectivities for electrons and holes. The transition from low to high injection occurs around $N_d = 10^{11}\,\mathrm{cm^{-3}}$, meaning most practical devices of this type would operate in low injection under one sun. While the theory does not exactly match the simulation for voltages beyond V_{oc}, it is quite accurate inside of the power quadrant.

Finally, Fig. 19b compares the *p*-*i*-*n* heterojunction simulations with theory for a fixed $N_d = 10^{12}\,\mathrm{cm^{-3}}$ for both contacts while the generation rate is varied. Therefore, J_0's are fixed, while only J_L varies. The model is able to reproduce both steps, as well as the transition from low to high injection, which occurs around 10 suns in this case. The dopant density of the contacts is quite low here; for higher dopant densities, unrealistically high generation rates are required to push the device into high injection. With an absorber whose bandgap is 1.5 eV, it is clear that most practical dopant densities will result in the device working in low injection, at which point the device will be limited by recombination, as opposed to selectivity/asymmetry. This is not surprising; doped heterojunction and homojunction contacts are among the most effective contact technologies, as long as an ohmic contact can be made to the doped semiconductors.

Thermionic Emission or *SRH* Recombination?

The keen observer may have questioned whether it was appropriate to use thermionic emission to calculate the J_0's in the *p*-*i*-*n* heterostructure. The reason thermionic emission was used as opposed to the Shockley model was simply because the contact thickness was much smaller than the diffusion length implied by the direct recombination lifetime.

Here, we demonstrate that if we include *SRH* recombination in the smaller bandgap contact, the contact thickness can be varied over orders of magnitude so that the effective J_0 transitions from that determined by the effective barrier height (i.e. thermionic emission) to the Shockley junction J_0 (as determined by minority diffusion into the quasi neutral region of the contact):

$$J_0 = \frac{q p_{n0} D_p}{L_p} \tag{7.11}$$

where p_{n0} is the equilibrium hole density in the n doped layer, D_p is the hole diffusion constant, and $L_p = \sqrt{D_p \tau_p}$ is the hole diffusion length (τ_p is the hole SRH lifetime).

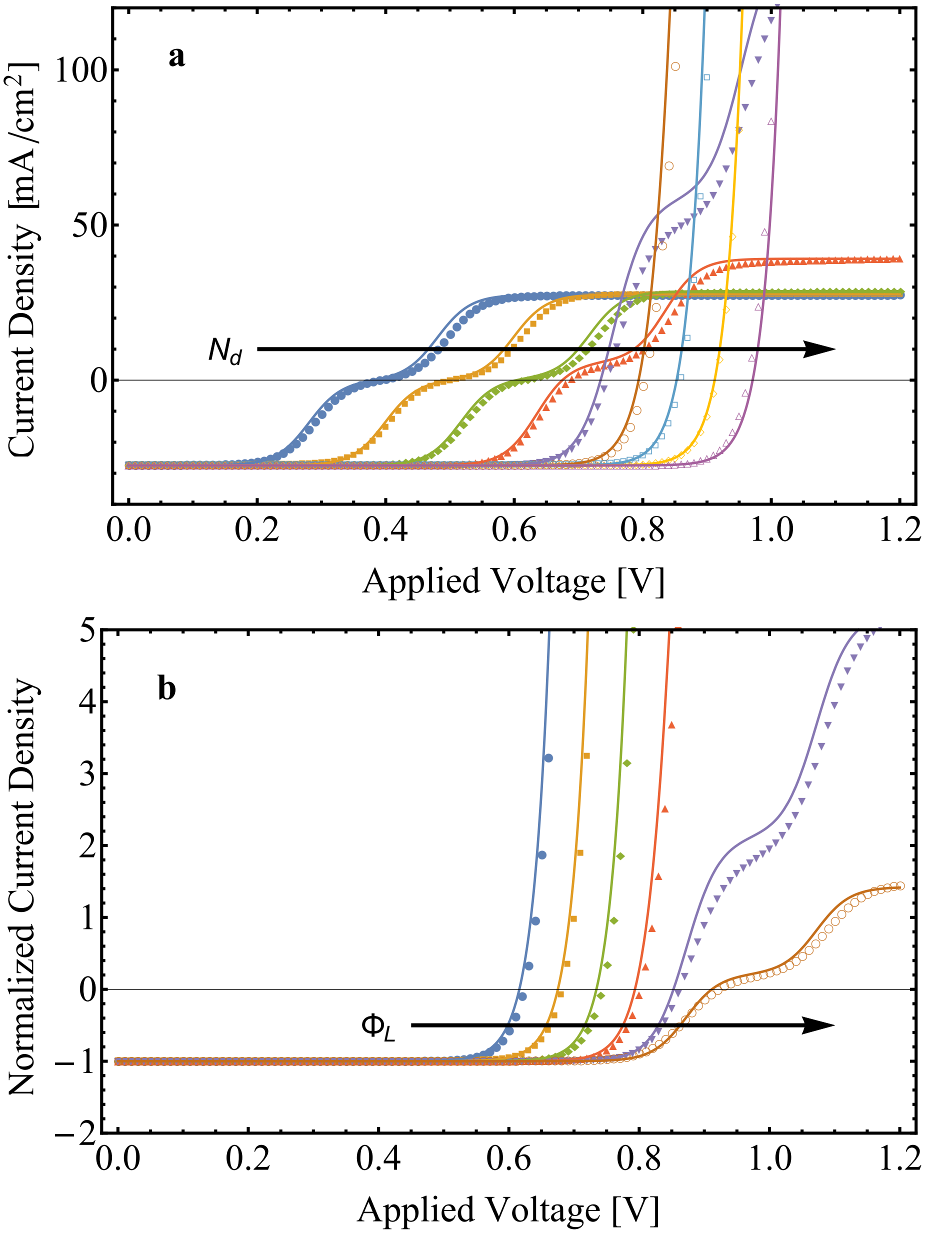

FIGURE 19. Simulated $J(V)$ curves (data points) compared with eq. 5.3 (lines) for the *p*-*i*-*n* heterostructure. In a), the dopant density N_d of both contacts is simultaneously stepped from 10^7 to $10^{15}\,\mathrm{cm}^{-3}$, by factors of 10. For b), the dopant densities of the contacts are fixed at $10^{12}\,\mathrm{cm}^{-3}$, the number of suns Φ_L is varied from 10^{-3} to 10^2 by factors of ten, and the current density is normalized by the short circuit current for each different light intensity.

Note that the smaller bandgap is chosen because it has the larger j_0 (calculated with the barrier heights as described in the text).

To demonstrate this, we used the same device structure from the previous section with a couple of changes:

- The thickness of the n-type contact was varied from 10 nm to 100 μm
- SRH recombination was added to the n-type contact with a lifetime of 100 ns
- The dopant density for each contact was fixed at $10^{14}\,\mathrm{cm}^{-3}$

The dopant density is chosen so that all of the curves are in low injection, thus the difference in V_{oc} can be attributed solely to the difference in the effective j_0's of the contacts. The $J(V)$ curve that results from the different contact thicknesses is shown in Fig. 20. As the thickness of the n-type contact is increased, the V_{oc} increases until it reaches a maximum when the contact thickness significantly exceeds the diffusion length (which is approximately 16 μm in this case). Thus, the simulation transitions from a regime in which the effective J_0 is determined by thermionic emission to one where it is determined by diffusion/recombination, as predicted. Note that the simulated curves with the largest V_{oc} start to have series resistance limitations due to the length of the contact, hence the sloping in the $J(V)$ curve around V_{oc}.

To summarize, then, it is clear that one can model the j_0's of a doped contact to an intrinsic absorber by considering the barrier heights as is done in the text, as long as the thickness of the contacts is much less than the diffusion length as determined by the SRH lifetime in the contact.

The following chapter will summarize the essential findings of this work, describing how results from each chapter have contributed to a better understanding of how contacts determined solar cell performance.

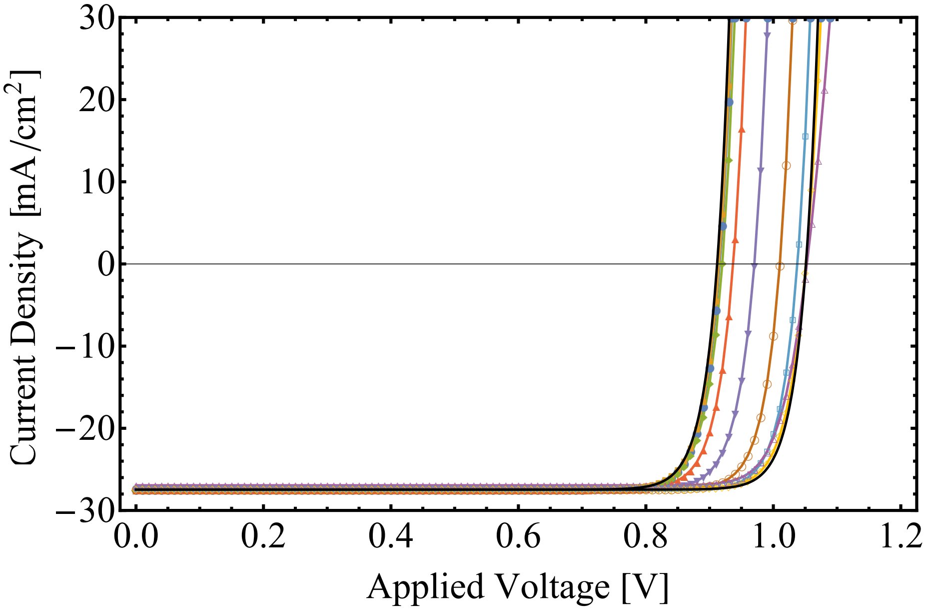

FIGURE 20. Simulated $J(V)$ curves of the p-i-n heterostructure device described above with the n-type (1.7 eV) contact thickness varied from 10 nm to 100 μm increasing from smaller to larger V_{oc} (i.e. increasing thickness from left to right). Note that the wider gap p-type contact and absorber thicknesses were fixed at 0.01 μm and 0.98 μm respectively. The left solid black curve is eq. 6.23 evaluated using j_0's calculated via 'thermionic emission' using the barriers from Fig. 18 in (smaller V_{oc}) and the right black curve was eq. 6.23 evaluated using Shockley j_0's (eq. 7.11).

CHAPTER VIII

CONCLUSION

In this work, I have presented theoretical and simulated results describing the limitations that contacts place on a solar cell's performance. The model requires knowledge of the four equilibrium exchange current densities (J_0's) that describe the rate of transfer of majority and minority carriers at both contacts to a semiconducting absorber. An analytic expression has been derived that quantitatively relates the $J(V)$ curve and performance parameters to the four J_0's and J_L, the total current due to generation from solar photons.

The analytic expression provides a unified explanation for both the S-shaped curve and current crossover/failure of superposition phenomena that are often signs of unoptimized contacts. In the ideal solar cell model/ideal diode models, there is no limit to the maximum possible current in forward bias. However, in our model, there is a such a maximum possible current, hence $J(V)$ curve always levels off, making an S-shaped curve. Because the maximum currents of such a curve in reverse and forward bias are asymptotically limited by minority and majority processes respectively, and because both values move in opposite directions due to changes in light current, the contact-limited solar cell will never obey the superposition principle. However, since the limitation of majority carrier injections can occur at very large current densities with a well-optimized contact, one will not always observe S-shaped behavior in the $J(V)$ curve around the power quadrant, which is typically all that is measured when characterizing a solar cell. In fact, comparing the majority J_0's ($\mathbf{J_0}$'s) to J_L will predict whether or not one will measure such non-ideal behaviors within sight of the power quadrant. This comparison delineates the high and low injection regimes.

In low injection, the contact recombination can be described as a first-order process, as it only depends on the leakage rate of minority carriers at the contacts. Here, V_{oc} and $\Delta E_F/q$ are equal, because the $\mathbf{J_0}$'s are large enough that no significant excess of majority carriers is required to provide J_L's worth of current. They are solely dependent on the balance of generation and recombination, quantified by ratio of the light current to the sum of the j_0's. The $J(V)$ curve will always look ideal in the vicinity of the power quadrant, in that the there will be no light/dark crossover and it will not be S-shaped. The only way to improve such a device is to reduce the leakage rate of minority carriers at the contacts.

Meanwhile, in high injection, majority carrier limitations become relevant because a large excess of majority carriers is required to generate J_L worth of current. The $\Delta E_F/q$ is still determined by the balance of recombination and generation, however the recombination is a second-order process, because it depends on both $\mathbf{J_0}$'s and j_0's. Meanwhile the V_{oc} no longer depends on this balance; it is limited by the asymmetry, or selectivity of the device. The majority carrier limitations typically lead to leveling off of the $J(V)$ curve at $J \approx 0$ leading to an S-shaped curve in the power quadrant and a less-than ideal fill factor. The efficiency of such a device would be improved by reducing the appropriate j_0, *or* by increasing the appropriate $\mathbf{J_0}$.

Critically, the two 'steps' that are always present in a contact-limited $J(V)$ curve are determined separately, by electron and hole J_0's. Improving a contact limited solar cell always amounts to moving these steps as far into forward bias as possible. Each step at a minimum brings J up to zero or larger current, so that it generates power at voltages more forward than the first step. Therefore, most of the time, only one of the two carrier's J_0's will limit the device. If a device is in low injection, then reducing the leakage of the limiting carrier at the contact that is intended to extract the other carrier is the only way to improve the device. However, if the limiting carrier is in high injection, one can move the ‘step’ further into forward bias both by reducing the leakage rate of the carrier at the contact intended to extract the other carrier, or by increasing the extraction of said carrier at its intended contact.

Simulations have been performed to test how bulk transport, bulk recombination, and more complicated device structures affect the validity of the theory. It is clear that bulk mobility plays a strong role in determining the theory’s accuracy. In general, the effect of limited mobility is to reduce the J_{sc} and FF from the theoretical limit, while the V_{oc} may actually be slightly improved over the theoretical value. These effects are most pronounced when the asymmetry of the contacts is limited, and in the case of Schottky diodes, when the Richardson constant approaches the ideal metal limit. Meanwhile, bulk recombination can reduce the V_{oc} from the theoretical limit, but this only occurs at larger asymmetries. I have also shown that the theory can be applied to a *p*-*i*-*n* heterostructure, where the J_0’s of the contacts are calculated assuming thermionic emission is the rate limiting process, as long as the contacts are much thinner than the diffusion length set by SRH recombination.

The model I have developed makes it clear how terms like contact recombination and carrier selectivity are related to solar cell performance. For most good solar cells, the $J(V)$ looks ideal, meaning the $J(V)$ is not S-shaped around the power quadrant. This means the device is in low injection, and therefore the term selectivity is only tangentially related to solar cell performance. One can increase the carrier selectivity of electrons or holes, but this does not necessarily decrease the leakage rate of said carrier because the selectivity involves a ratio of $\mathbf{J_0}$’s to j_0’s. It is correct, however, to say that reducing contact recombination will always improve such a device, as long as said contact’s recombination is the dominant recombination process in the device. In solar cells with yet-to-be optimized contacts, one is more likely to come across non-ideal $J(V)$ behaviors such as S-shaped curves in the power quadrant, indicating the device is in high injection. Here, it is correct to say that the device is limited by asymmetry or selectivity. One may still improve the device performance by reducing contact recombination, however any such change that leads to an increase in performance will also signify an increase in selectivity. In the end, it is best to simply refer to the set of four J_0's, as they fundamentally determine the $J(V)$ curve of the contact-limited solar cell.

APPENDIX A

THE DENSITY OF STATES IN A SEMICONDUCTOR

To derive the density of states (DOS) of electrons and holes in a semiconductor, we approximate the electrons as nearly free, Bloch electrons. The physics of Bloch electrons is a very rich topic, but for our purposes, it will suffice to know that our electrons and holes are essentially free (meaning that they feel no potential) but they have effective masses, m_e^* and m_h^* respectively, that differ from the mass of a truly free electron. The value of the effective mass depends on the curvature of the detailed band structure of the conduction and valence bands of the semiconductor and is a highly non-trivial calculation that cannot in general be performed in an exact manner and thus will not be covered here.

To calculate the energetic DOS, we first need to estimate the number of k states within the Fermi-sphere in $k-$space. The wavefunction of a free electron in a potential-less crystal is proportional to $\sin(k_x x)\sin(k_y y)\sin(k_z z)$, and it must be zero outside of the crystal. Thus, the allowed values for k_x are

$$k_x = \pm\frac{2\pi}{L_x}n \tag{A.1}$$

where n is an integer. Thus, there is one k_x in every $\frac{2\pi}{L_x}$ interval in k_x. As this is analogously true for k_y and k_z, the three dimensional DOS in k-space is

$$DOS_k = \frac{L_x L_y L_z}{(2\pi)^3} = \frac{V}{(2\pi)^3} \tag{A.2}$$

where V is the volume of the crystal. The number of possible $k-$states within a sphere of radius k is then easily calculated

$$N(k) = 2\frac{V}{(2\pi)^3}\frac{4\pi k^3}{3} = \frac{Vk^3}{3\pi^2} \tag{A.3}$$

where the extra factor of two accounts for electron spin degeneracy. Inverting the $E(k)$ relationship for Bloch electrons to solve for k,

$$k(E) = \sqrt{\frac{2m^* E_k}{\hbar^2}} \tag{A.4}$$

we can now write down the number states as a function of energy:

$$N(E_k) = \frac{V}{3\pi^2}\left(\frac{2m^* E_k}{\hbar^2}\right)^{\frac{3}{2}} \tag{A.5}$$

Dividing by volume and differentiating, we obtain the free electron density of states per unit volume in energy space

$$DOS_E = \frac{1}{2\pi^2}\left(\frac{2m^*}{\hbar^2}\right)^{\frac{3}{2}}\sqrt{E_k}. \tag{A.6}$$

The energy of electrons in the conduction band is

$$E = E_c + E_k = E_c + \frac{\hbar^2 k^2}{2m^*}. \tag{A.7}$$

And thus, the DOS for electrons in the conduction band is

$$g_c(E) = \frac{1}{2\pi^2}\left(\frac{2m_e^*}{\hbar^2}\right)^{\frac{3}{2}}\sqrt{E - E_c} \tag{A.8}$$

Analogously for the valence band,

$$g_v(E) = \frac{1}{2\pi^2}\left(\frac{2m_p^*}{\hbar^2}\right)^{\frac{3}{2}}\sqrt{E_v - E} \tag{A.9}$$

where the effective masses for conduction and valance bands are m_e^* and m_p^* respectively.

APPENDIX B

EQUILIBRIUM CARRIER CONCENTRATIONS

The concentration of free electrons (n) and holes (p) are important quantities in a semiconductor as one cannot calculate the current in a device without them. The electron concentration is given by

$$n = \int_{E_c}^{\infty} g_c(E) f(E) dE \tag{B.1}$$

In general, semiconductors are operated in the regime such that $E_c - E_f \gg k_B T$. Practically speaking, this means that the doping of the semiconductor must not bring the Fermi level within less than a few $k_B T$ of either band edge. As $k_B T$ is roughly 26 meV at room temperature, this is certainly the case for most solar cell absorbers under standard operating conditions. Thus, the Fermi-Dirac distribution can be approximated by the Boltzmann distribution,

$$f(E) \approx e^{\frac{-\left(E - E_f\right)}{k_B T}}. \tag{B.2}$$

We now proceed to carry out the integral,

$$\begin{aligned} n(E_f) &= \frac{1}{2\pi^2} \left(\frac{2m_e^*}{\hbar^2} \right)^{\frac{3}{2}} \int_{E_c}^{\infty} \sqrt{E - E_c}\, e^{-\frac{E - E_f}{k_B T}} dE \\ &= \frac{1}{2\pi^2} \left(\frac{2m_e^* k_B T}{\hbar^2} \right)^{\frac{3}{2}} e^{-\frac{E_c - E_f}{k_B T}} \int_0^{\infty} \sqrt{u}\, e^{-u} du \\ &= 2 \left(\frac{m_e^* k_B T}{2\pi\hbar^2} \right)^{\frac{3}{2}} e^{-\frac{E_c - E_f}{k_B T}} \\ &= N_c e^{-\frac{E_c - E_f}{k_B T}}, \end{aligned} \tag{B.3}$$

where we have used the substitution $u = \frac{E-E_c}{k_B T}$, and introduced the constant, N_c, called the effective conduction band density of states:

$$N_c = 2\left(\frac{m_e^* k_B T}{2\pi\hbar^2}\right)^{\frac{3}{2}} \tag{B.4}$$

Analogously for holes, we have

$$p(E_f) = N_v e^{\frac{E_v - E_f}{k_B T}} \tag{B.5}$$

where the effective valence band density of states, N_v, is defined as

$$N_v = 2\left(\frac{m_p^* k_B T}{2\pi\hbar^2}\right)^{\frac{3}{2}} \tag{B.6}$$

APPENDIX C

THE $J(V)$ CHARACTERISTICS OF THE $P - N$ JUNCTION

To derive the ideal $p - n$ junction $J(V)$ characteristics, we will follow the derivation of Sze, section 3.4.[95] We assume an abrupt depletion edge, that the electron and hole currents are uniform across the depletion region, and that the semiconductor is neutral outside of this region. The built in potential, V_{bi}, is defined as the difference in potential of either the conduction or valence bands between the two neutral regions. It can be shown that

$$V_{bi} = \frac{k_B T}{q} \ln \frac{N_A N_D}{n_i^2} \tag{C.1}$$

where n_i is the intrinsic carrier concentration. At equilibrium on the n side of the junction, $n_{n0} \approx N_D$ and on the p side of the junction, $p_{p0} \approx N_A$ where we use the subscript $n0$ to indicate the n side of the junction, at equilibrium. The law of mass action dictates that

$$\begin{aligned} n_i^2 &= p_{p0} n_{p0} \\ &= p_{n0} n_{n0} \end{aligned} \tag{C.2}$$

We can now write the carrier concentrations in terms of their respective values on the other side of the junction using C.1 and C.2

$$\begin{aligned} n_{n0} &= n_{p0} e^{\frac{qV_{bi}}{k_B T}} \\ p_{p0} &= p_{n0} e^{\frac{qV_{bi}}{k_B T}} \end{aligned} \tag{C.3}$$

We now assume that under an applied bias, we can relate the carrier densities across the junction with the following modification:

$$n_n = n_p e^{\frac{q(V_{bi}-V)}{k_B T}} \tag{C.4}$$

where we have dropped the 0 subscript because the applied bias, V, is driving us away from equilibrium. Note that we assume low injection conditions, i.e. that the injected minority carrier density is small so that the majority carrier density is unchanged. Using C.3, we find that

$$n_p = n_{p0} e^{\frac{qV}{k_B T}}. \tag{C.5}$$

for the electron concentration at the edge of the depletion region on the p side. We then subtract n_{p0} and write

$$n_p - n_{p0} = n_{p0}\left(e^{\frac{qV}{k_B T}} - 1\right). \tag{C.6}$$

Similarly for holes, we find that

$$p_n = p_{n0} e^{\frac{qV}{k_B T}}. \tag{C.7}$$

and

$$p_n - p_{n0} = p_{n0}\left(e^{\frac{qV}{k_B T}} - 1\right). \tag{C.8}$$

for the concentration at the edge of the depletion edge on the n side. We assume that there is no generation and recombination in the depletion region, and thus the current of each carrier is equal on each side of the depletion region. Since there is assumed to be no electric field in the neutral region, the continuity equation reduces to

$$\frac{d^2 p_n}{dx^2} - \frac{p_n - p_{n0}}{D_p \tau_p} = 0 \tag{C.9}$$

at steady state. This is a second order, homogeneous linear differential equation which can easily be solved for p_n. The particular solution to the full equation is just the constant p_{n0}. Thus the general solution is

$$p_n - p_{n0} = c_1 e^{\frac{x}{L_p}} + c_2 e^{-\frac{x}{L_p}} \tag{C.10}$$

where $L_p = \sqrt{D_p \tau_p}$, the hole diffusion length. At $x = \infty$, we know that p_n must be equal to the equilibrium concentration and thus $c_1 = 0$. At $x = x_n$, the edge of the depletion layer on the n side, we use C.7 as a boundary condition, and find that

$$c_2 = p_{n0} \left(1 - e^{\frac{qV}{k_B T}}\right) e^{\frac{x_n}{L_p}} \tag{C.11}$$

Putting it all together then, we find that

$$p_n(x) - p_{n0} = p_{n0} \left(1 - e^{\frac{qV}{k_B T}}\right) e^{-\frac{(x - x_n)}{L_p}}. \tag{C.12}$$

As we have already assumed that the field is zero at x_n, the current can be easily calculated,

$$J_p(x_n) = -q D_p \frac{dp_n}{dx}|_{x_n} = \frac{q D_p p_{n0}}{L_p} \left(e^{\frac{qV}{k_B T}} - 1\right). \tag{C.13}$$

The analogous calculation for the electron current on the p side of the junction gives

$$J_n(-x_p) = \frac{q D_n n_{p0}}{L_n} \left(e^{\frac{qV}{k_B T}} - 1\right). \tag{C.14}$$

Using our assumption that the current is constant across the depletion region, the total current throughout the device is equal to

$$J(V) = J_s \left(e^{\frac{qV}{k_B T}} - 1 \right) \tag{C.15}$$

where J_s is the saturation current density, defined as

$$J_s = \frac{qD_p p_{n0}}{L_p} + \frac{qD_n n_{p0}}{L_n} \tag{C.16}$$

APPENDIX D

THE SHOCKLEY-QUESSIER LIMIT

This derivation will highlight the essential quantities derived in Shockley and Queisser (SQ)'s seminal paper, titled 'Detailed Balance Limit of Efficiency of pn Junction Solar Cells.' [15] Everything in the original work was calculated assuming the sun's spectrum was a 6000 K blackbody. Here, we will first assume this in the initial derivation, then consider the additional information that we can glean from using the actual AM 1.5 spectrum.

SQ derive the $J(V)$ curve of a solar cell based on just a few parameters, namely the temperature of the cell (T_c), the bandgap of the absorber, (E_g), and the fraction of recombination that is direct recombination (f). To start off, consider all possible processes for free electrons and holes in the solar cell absorber:

1. F_s, the total rate (in carriers per second) at which electrons and holes in the device are generated via absorption of solar photons. This is independent of voltage because, for practical purposes, the conduction band will always be mostly empty of electrons and the valence band mostly empty of holes.
2. $F_c = F_{c0} \times \frac{np}{n_i^2} = F_{c0} \times e^{\frac{\Delta E_f}{k_B T}}$, the total rate of radiative recombination in the device. It is a function of voltage, as we will discuss.
3. non-radiative generation
4. non-radiative recombination
5. I/q, the rate of carriers taken away by the external circuit.

In order to calculate the steady-state current, one simply sums these processes, sets them equal to zero, and solves for I. In order to understand the voltage dependence, S-Q assumed that $\Delta E_f = V$, the applied voltage. For their purposes, this was sufficient. However, as is illustrated in Chapter 6, this is not always the case, as contacts can prevent efficient extraction of carriers.

Regardless, we are essentially trying to solve the macroscopic continuity equation for electrons and holes in the device (which is also what is done with different assumptions in the present work). To find the resulting efficiency (η), one calculates the maximum power of the $I(V)$ curve, then devides by the total solar power incident on the device (P_s). Therefore, we must first calculate F_s, F_{c0}, and P_s.

To do so, we consider a model in which our solar cell is a flat plate with area A_c on both sides, surrounded by 2π steradians of 300 K blackbody in both hemispheres (see Fig. 21). Both P_s and F_s involve a calculation of solar photons that are incident on the solar cell from above, while F_{c0} considers photons from a 300 K blackbody incident on the cell from all 4π steradians of both hemispheres.

To calculate the total rate of generation of electron and hole pairs from solar photons, we assume that any above gap photon incident on the solar cell will generate free carriers, while photons with energy $E_\gamma < E_g$ generate none. We treat the sun as a blackbody, with temperature T_s. It has a radius of r_s and is a distance d_s from the solar cell. The number of solar photons per unit energy per volume traveling towards the solid angle $d\Omega$ is given by:[96]

$$\frac{dn_\gamma}{dE} = \frac{1}{4\pi^3\hbar^3c^3}\frac{E^2 d\Omega}{e^{\frac{E}{k_B T_s}} - 1} \tag{D.1}$$

where E is the photon energy and n_γ is the number density of photons. To calculate the total rate of above gap photons hitting the solar cell, we need to know the flux

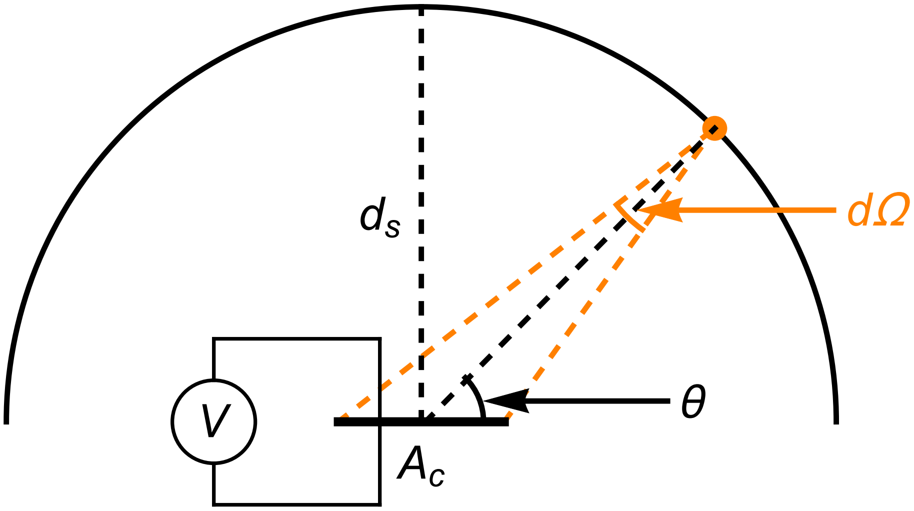

FIGURE 21. Schematic of the geometric considerations (not to scale) for a flat solar cell connected to a power sink (V), used to calculate F_s, F_{c0}, and P_s. The distance to the sun is d_s, $d\Omega$ is the solid angle subtended by the solar cell from the point of view of the sun, and A_c is the area of the flat side of the solar cell (meaning the total surface area is $2A_c$). The angle of incidence of solar radiation, θ, is measured from grazing incidence, so that $\theta = \pi/2$ for normal incidence.

heading that direction, and we sum over all energies above the bandgap. The flux is calculated by multiplying $\frac{dn_\gamma}{dE}$ by the projected area of the sun ($A_s = \pi r_s^2$) and the speed at which the photons are traveling (c):

$$F_s = \int_{E_g}^{\infty} \frac{dn_\gamma}{dE} dE \times A_s c \tag{D.2a}$$

$$= \frac{2\pi r_s^2 d\Omega}{h^3 c^2} \int_{E_g}^{\infty} \frac{E^2 dE}{e^{\frac{E}{k_B T_s}} - 1} \tag{D.2b}$$

Note the change from $\hbar$ to h. The solid angle of the solar cell from the point of view of the sun, $d\Omega$, is $\frac{A_c \sin\theta}{d_s^2}$. Substituting x for $\frac{E}{k_B T_s}$, we find

$$F_s = \frac{2A_c \sin(\theta)\, \Omega_s \left(k_B T_s\right)^3}{h^3 c^2} \int_{x_g}^{\infty} \frac{x^2 dx}{e^x - 1} \tag{D.3}$$

where we have used $\Omega_s = \frac{\pi r_s^2}{d_s^2}$ and $x_g = \frac{E_g}{k_B T_s}$. Next, we want to know the total power density incident on our solar cell, P_s, so that we may eventually calculate the efficiency. Luckily, this uses almost the exact math as F_s, but instead of considering the number distribution of photons ($\frac{dn_\gamma}{dE}$), we use the energy distribution instead:

$$\frac{dE_\gamma}{dE} = \frac{1}{4\pi^3 \hbar^3 c^3} \frac{E^3 d\Omega}{e^{\frac{E}{k_B T_s}} - 1} \tag{D.4}$$

Otherwise, the arguments are exactly the same, and we end up with

$$P_s = \frac{2A_c \sin(\theta)\, \Omega_s \,(k_B T_s)^4}{h^3 c^2} \int_{x_g}^{\infty} \frac{x^3 dx}{e^x - 1} \tag{D.5}$$

Finally, we need to calculate the total rate of above gap photons incident on the solar cell from the background 300 K environment. We assume that the temperature of the cell, T_c, is also 300 K. This calculation starts in the same place, with density of photons from the blackbody, but is slightly more complicated, as we must integrate over the hemisphere (given symmetry, we can do this once and multiply the end result by two). To get the total rate, we must integrate over the area of a fictional hemisphere surrounding the upper half of the solar cell. We can use any radius we like (it does not matter in the end). This integral is mandated by the fact that $d\Omega$ depends on which area of the sky we are looking at the solar cell from. Again, we also multiply by c to calculate the rate:

$$F_{c0} = 2 \int \int \frac{dn_\gamma}{dE} dE dA \times c \tag{D.6a}$$

$$= \frac{4A_c \,(k_B T_c)^3}{h^3 c^3 d_s^2} \int_{x_g}^{\infty} \frac{x^2}{e^x - 1} dx \int_0^{2\pi} \int_0^{\pi/2} \sin\theta \sin(\pi/2 - \theta)\, d_s^2 d\theta d\phi \tag{D.6b}$$

where we have again used $d\Omega = \frac{A_c \sin\theta}{d_s^2}$. Note that we neglect the small solid angle of the sky whose 300 K photons would be replaced by solar photons during the day, as this fraction of the sky is negligible. After simplification, this becomes

$$F_{c0} = \frac{4\pi A_c \left(k_B T_s\right)^3}{h^3 c^2} \int_{x_g}^{\infty} \frac{x^2}{e^x - 1} dx \tag{D.7}$$

We know that the rate of direct recombination at equilibrium (i.e. when the cell is surrounded by 4π steradians of 300 K blackbody) must be equal to F_{c0}. The same is true for indirect generation and recombination, which we denote as $R(0)$ and $R(V)$, respectively. In steady state, the sum of these four processes and the current extracted, I, must be zero (otherwise the carrier densities would change with time):

$$0 = F_s + F_{c0} - F(V) + R(0) - R(V) - I/q \tag{D.8}$$

where the sign of each term corresponds to whether that term adds or removes carriers from the absorber. For simplicity, we will now assume that $R(V) = R(0) = 0$ (i.e, $f = 1$). This assumption is often synonymous with the SQ limit, as direct recombination is the most fundamental process that can't be mitigated, no matter how perfect one's absorber is. [1]

Thus, the SQ current voltage curve is simply

$$I = qF_s + qF_{c0}(1 - e^{V/V_T}) \tag{D.9}$$

---

[1] Technically, Auger recombination is fundamental in a similar matter, but it has a more complicated voltage dependence, so we'll ignore it, as the more elegant presentation simply balances radiative recombination and generation.

Note that this equation uses the opposite current convention as the present work (i.e. the power quadrant is quadrant I, as opposed to quadrant IV). The short circuit current is obviously

$$I_{sc} = qF_s \tag{D.10}$$

while the open circuit voltage is easily determined by setting $I = 0$ and solving for V:

$$V_{oc} = V_T \ln \left(1 + \frac{F_s}{F_{c0}} \right) \tag{D.11}$$

As usual, the maximum power point occurs when $d(I \times V)/dV = 0$. The voltage at the maximum power point is

$$V_m = V_T W \left((e(1 + \frac{F_s}{F_{c0}}) \right) \tag{D.12}$$

where W is the Lambert W function.

What many refer to as the SQ limit is a plot of efficiency vs. bandgap, seen in Fig. 22 for both a 6000 K blackbody as the sun, and the AM1.5 spectrum. The basic rise and decline are readily explained by the need for a balance of maximizing the product of the current times the voltage; larger bandgaps lead to smaller currents, but larger voltages increase the energy/voltage per electron/hole extracted, so there is a moderate bandgap that will maximize this product. The details of exactly where this occurs depend, of course, on the incident spectrum. For the actual AM1.5 spectrum, there are two maxima that give similar efficiency values of 33-33.5 % at about 1.15 and 1.35 eV.

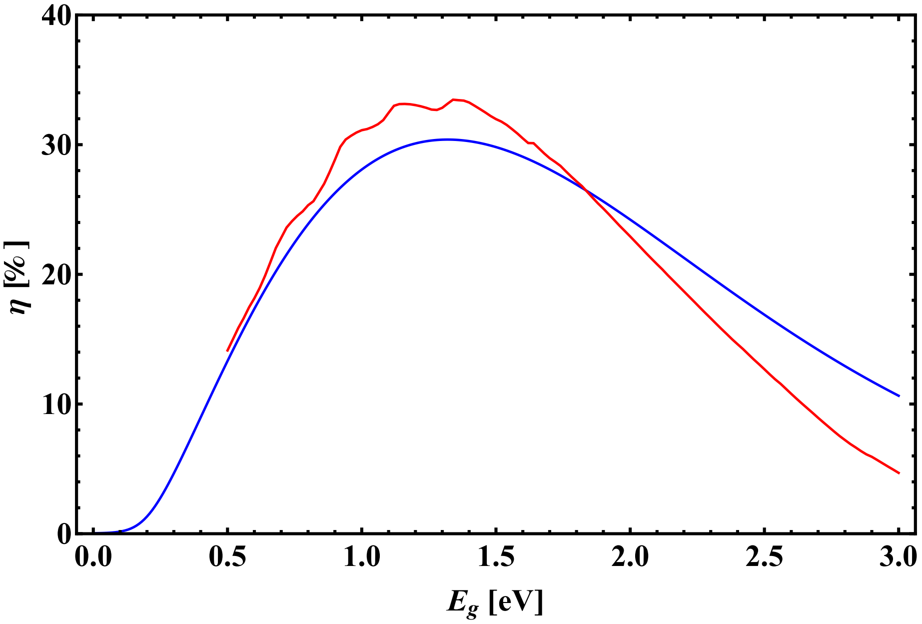

FIGURE 22. Plot of the SQ limiting efficiency as a function of bandgap for a single absorber solar cell, using a 6000 K blackbody as the sun (blue), and the AM1.5G spectrum (red).

APPENDIX E

PHYSICAL EXPLANATION OF CONTACT-LIMITED $J(V)$ BEHAVIOR

Here, we explain the physics determining the behavior of a sample $J(V)$ curve produced by eq. 5.3 by plotting the partial currents determined by eq. 3.1 at several critical points along the curve. Consider the sample curve, shown in Fig. 23a. The curve, as usual, features a constant negative current in reverse bias ($\sim -10\,\mathrm{mA/cm^2}$), two steps in forward bias, and finally a constant positive current far into forward bias ($\sim 50\,\mathrm{mA/cm^2}$).

The ratios of each carrier density at each contact to the corresponding equilibrium density are plotted in Fig. 23b as a function of voltage. They are calculated by using the appropriate equation from eq. 4.1 after solving for the corresponding partial current as described in Section 1 above. In reverse bias, the majority carriers (solid lines) are slightly in excess at their contacts, while there is a deficit of minority carriers (dashed lines) at both contacts. Far into forward bias, it is the minority carriers that are in excess (many orders of magnitude more than their equilibrium densities), while the majority carrier densities are drawn below equilibrium. The voltages at which the steps in current occur are consistent with the kinks in the carrier density plot. In general, the cause of the current step (with or without light) is that as the device is pushed further into forward bias, minority carriers start to form a large enough excess for current to be noticeable compared to the $\mathbf{J_0}$ of that carrier. Therefore, the voltage at the steps are determined by the ratios of the J_0's for a given carrier, i.e. the carrier selectivities. This plot is a useful guide in explaining the partial currents at four insightful voltages: 1) far into reverse bias, 2) at open circuit, 3) between the first and second steps in forward bias, 4) far in forward bias, after both steps have occurred. These are plotted in Fig. 24. Note that the partial currents are linear, which is dictated by the assumption of uniform generation. Non-uniform generation would change the shape of the partial current profiles, but only the difference between partial current values at the contacts matters for the explanation presented here.

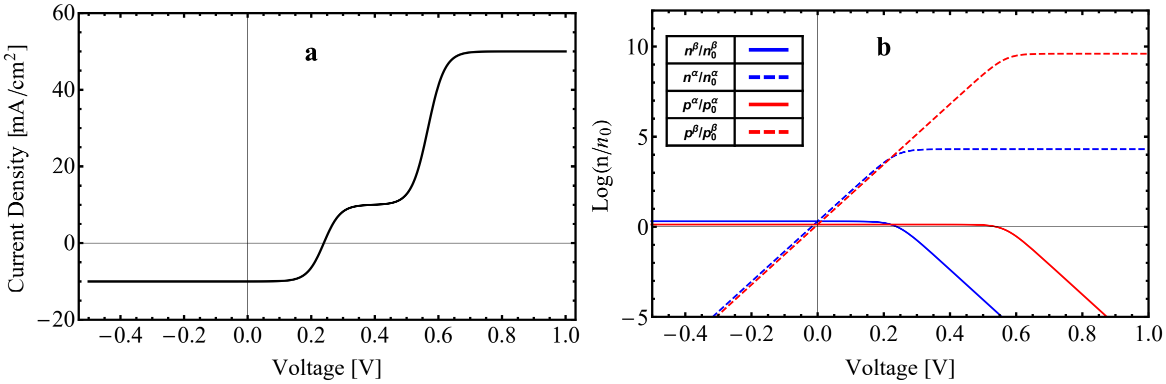

FIGURE 23. a) Sample $J(V)$ curve produced by eq. 5.3 using $J_L = 10$, $\mathbf{J}^{\beta}_{\mathbf{0n}} = 10$, $j^{\alpha}_{0n} = 10^{-3}$, $\mathbf{J}^{\alpha}_{\mathbf{0p}} = 30$, $j^{\beta}_{0p} = 10^{-8}$ $\mathrm{mA\,cm^{-2}}$. b) Log base 10 of the ratio of the carrier density to the corresponding equilibrium density for each carrier at each contact (i.e. the fraction terms in eq. 3.1) plotted vs. applied voltage.

First, consider the current in reverse bias (Fig. 24a), which is approximately equal to $-J_L$ (recall that we can always assume that the j_0's are much smaller than J_L if we have an appreciable photovoltaic effect). In reverse bias, the minority carrier densities are drawn down to zero. For electrons, this means that the electron partial current at the α contact is approximately zero. The continuity equation then dictates that the electron current at the β contact is $-J_L$, which requires a small excess of electrons at contact β. Similar logic applies for holes. Note that this is consistent with Fig. 23.

Meanwhile, at open-circuit(fig. 24b), the total current in the device must be zero. The current therefore increased significantly from $-J_L$ in reverse bias, and this is caused by whichever carrier has the smallest critical voltage (eq. 5.7), in this case, electrons. The partial current profile for holes is approximately the same as in

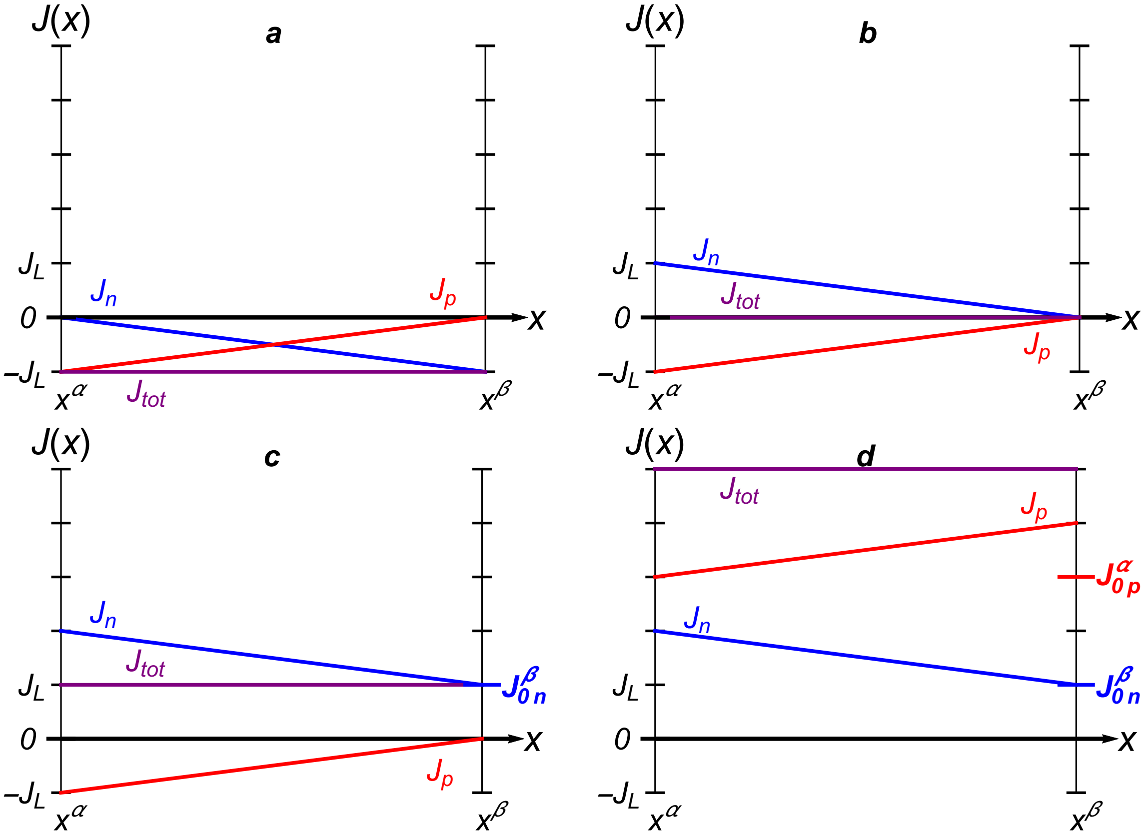

FIGURE 24. Plots of electron (blue) and hole (red) partial currents, as well as total current (purple) as a function of position from the α contact to the β contact for a) reverse bias, b) at V_{oc}, c) between the steps, and d) after the second step in forward bias. As has been our assumption throughout, the β contact is electron selective while the α contact is hole selective, and positive current flows from left to right.

reverse bias, as the hole step has yet to occur. Meanwhile, the electron density at the α contact is much higher than the equilibrium density (as seen in Fig. 23), so that the corresponding partial current is $+J_L$. The continuity equation then dictates that the electron current at the β contact must be zero, meaning the electron concentration at contact β is at equilibrium.

After the first step has occurred and before the second step (fig. 24c), the total current is approximately equal to $\mathbf{J}^{\beta}_{\mathbf{0n}}$ according to fig. 23a. This is again explained by the carrier densities in Fig. 23b; the hole step has yet to occur while the electron density at the β contact is being drawn to approximately zero, meaning the corresponding current is maximized at $\mathbf{J^\beta_{0n}}$. The continuity equation dictates that the electron current must be $J_L + \mathbf{J^\beta_{0n}}$ at the α contact, requiring a very large excess of electrons, given by the flat value after the kink in the dashed blue curve in Fig. 23.

Finally, the current levels off at $J_L + \mathbf{J^\beta_{on}} + \mathbf{J^\alpha_{0p}}$ after the hole step occurs in far forward bias (fig. 24d). Here, the hole density at the α contact is being drawn down to zero, providing the maximum possible partial current of $\mathbf{J^\alpha_{0p}}$. The hole density at the β contact dramatically exceeds its equilibrium value, in order to supply a partial current of $J_L + \mathbf{J^\alpha_{0p}}$.

APPENDIX F

DERIVATION OF LOW AND HIGH INJECTION LIMITS OF THE CONTACT-DETERMINED $J(V)$ CURVE

Low Injection

Our definition of low injection for both carriers is that $\mathbf{J}^{\beta}_{\mathbf{0n}} \gg J_L$ and $\mathbf{J}^{\alpha}_{\mathbf{0p}} \gg J_L$. Note that we will simplify the $J(V)$ curve assuming *both* carriers are in low injection. It is also fair to only consider one of the steps and completely neglect the other if one is only interested in the power quadrant as long as the limiting carrier selectivity is much smaller than the other. We will assume that the electron J_0 for contact β is the majority process and visa versa for the α contact, thus we will use the $\mathbf{J_0}$, j_0 convention as is done in the text. We will assume the both j_0's are small compared to both J_L and the $\mathbf{J_0}$'s. Neglecting these appropriately, we have

$$J(V) \approx -J_L + \frac{\mathbf{J}^{\beta}_{\mathbf{0n}}}{1 + \frac{\mathbf{J}^{\beta}_{\mathbf{0n}}}{j^{\alpha}_{0n}} e^{-V/V_T}} + \frac{\mathbf{J}^{\alpha}_{\mathbf{0p}}}{1 + \frac{\mathbf{J}^{\alpha}_{\mathbf{0p}}}{j^{\beta}_{0p}} e^{-V/V_T}}. \tag{F.1}$$

This can be re-written as:

$$J(V) \approx J_L + \frac{\mathbf{J}^{\beta}_{\mathbf{0n}} - J_L - J_L \frac{\mathbf{J}^{\beta}_{\mathbf{0n}}}{j^{\alpha}_{0n}} e^{-V/V_T}}{1 + \frac{\mathbf{J}^{\beta}_{\mathbf{0n}}}{j^{\alpha}_{0n}} e^{-V/V_T}} + \frac{\mathbf{J}^{\alpha}_{\mathbf{0p}} - J_L - J_L \frac{\mathbf{J}^{\alpha}_{\mathbf{0p}}}{j^{\beta}_{0p}} e^{-V/V_T}}{1 + \frac{\mathbf{J}^{\alpha}_{\mathbf{0p}}}{j^{\beta}_{0p}} e^{-V/V_T}}. \tag{F.2}$$

We can again neglect the $-J_L$'s in the numerator given the assumption of low injection:

$$J(V) \approx J_L + \frac{\mathbf{J}^{\beta}_{\mathbf{0n}}\left(1 - \frac{J_L}{j^{\alpha}_{0n}} e^{-V/V_T}\right)}{1 + \frac{\mathbf{J}^{\beta}_{\mathbf{0n}}}{j^{\alpha}_{0n}} e^{-V/V_T}} + \frac{\mathbf{J}^{\alpha}_{\mathbf{0p}}\left(1 - \frac{J_L}{j^{\beta}_{0p}} e^{-V/V_T}\right)}{1 + \frac{\mathbf{J}^{\alpha}_{\mathbf{0p}}}{j^{\beta}_{0p}} e^{-V/V_T}}. \tag{F.3}$$

Given that the V_{oc} in low injection is approximately $V_T \ln\left(\frac{J_L}{j^{\alpha}_{0n}+j^{\beta}_{0p}}\right)$, the exponential terms in the denominators will be much greater than one *within the power quadrant* as long as $\frac{\mathbf{J}^{\beta}_{\mathbf{0n}}}{J_L} \gg \frac{j^{\alpha}_{0n}+j^{\beta}_{0p}}{j^{\alpha}_{0n}}$ and $\frac{\mathbf{J}^{\alpha}_{\mathbf{0p}}}{J_L} \gg \frac{j^{\alpha}_{0n}+j^{\beta}_{0p}}{j^{\beta}_{0p}}$. In other words, we must further assume that the j_0's are not too different from one another as compared to the ratios of the $\mathbf{J_0}$'s to J_L. Note that if we cannot make this assumption, it will suffice to simply ignore the step of the non-limiting carrier completely, leading to an even simpler function. That derivation is not shown, but proceeds analogously to this one, ignoring the irrelevant step. If we do make this assumption, we have

$$J(V) \approx J_L + \frac{\mathbf{J}^{\beta}_{\mathbf{0n}}\left(1 - \frac{J_L}{j^{\alpha}_{0n}} e^{-V/V_T}\right)}{\frac{\mathbf{J}^{\beta}_{\mathbf{0n}}}{j^{\alpha}_{0n}} e^{-V/V_T}} + \frac{\mathbf{J}^{\alpha}_{\mathbf{0p}}\left(1 - \frac{J_L}{j^{\beta}_{0p}} e^{-V/V_T}\right)}{\frac{\mathbf{J}^{\alpha}_{\mathbf{0p}}}{j^{\beta}_{0p}} e^{-V/V_T}}. \tag{F.4}$$

which can easily simplified to

$$J(V) \approx \left(j^{\alpha}_{0n} + j^{\beta}_{0p}\right) e^{V/V_T} - J_L. \tag{F.5}$$

Note that this approximation is only guaranteed to be accurate for biases less than or equal to V_{oc} (i.e. in the power quadrant and in reverse bias).

High Injection

Recall that our definition for high injection for both carriers is that $\mathbf{J}^{\beta}_{\mathbf{0n}} \ll J_L$ and $\mathbf{J}^{\alpha}_{\mathbf{0p}} \ll J_L$. The approximation for $J(V)$ in high injection is very easily derived from eq. 5.3 by neglecting the J_0's much smaller than J_L in each of the three terms:

$$J(V) \approx -J_L + \frac{J_L}{1 + \frac{\mathbf{J_{0n}^{\beta}}}{j_{0n}^{\alpha}} e^{-V/V_T}} + \frac{J_L}{1 + \frac{\mathbf{J_{0p}^{\alpha}}}{j_{0p}^{\beta}} e^{-V/V_T}} = -J_L + \frac{J_L}{1 + S_n e^{-V/V_T}} + \frac{J_L}{1 + S_p e^{-V/V_T}}. \tag{F.6}$$

REFERENCES CITED

[1] E. T. Roe, K. E. Egelhofer, and M. C. Lonergan, “Exchange current density model for the contact-determined current-voltage behavior of solar cells,” *Journal of Applied Physics*, vol. 125, no. 22, p. 225302, 2019.

[2] E. T. Roe, K. E. Egelhofer, and M. C. Lonergan, “Limits of contact selectivity/recombination on the open-circuit voltage of a photovoltaic,” *ACS Appl. Energy Mater.*, vol. 1, no. 3, pp. 1037–1046, 2018.

[3] V. Masson-Delmotte, P. Zhai, H. Pörtner, D. Roberts, J. Skea, P. Shukla, A. Pirani, W. Moufouma-Okia, C. Péan, R. Pidcock, *et al.*, “Ipcc, 2018: Summary for policymakers,” *Global Warming of*, vol. 1, 2018.

[4] J. B. Pollack, O. B. Toon, and R. Boese, “Greenhouse models of venus’ high surface temperature, as constrained by pioneer venus measurements,” *Journal of Geophysical Research: Space Physics*, vol. 85, no. A13, pp. 8223–8231, 1980.

[5] A. T. Basilevsky and J. W. Head, “The surface of venus,” *Reports on Progress in Physics*, vol. 66, no. 10, p. 1699, 2003.

[6] L. P. Flynn, P. J. Mouginis-Mark, J. C. Gradie, and P. G. Lucey, “Radiative temperature measurements at kupaianaha lava lake, kilauea volcano, hawaii,” *Journal of Geophysical Research: Solid Earth*, vol. 98, no. B4, pp. 6461–6476, 1993.

[7] L. P. Flynn and P. J. Mouginis-Mark, “Temperature of an active lava channel from spectral measurements, kilauea volcano, hawaii,” *Bulletin of Volcanology*, vol. 56, no. 4, pp. 297–301, 1994.

[8] D. Lüthi, M. Le Floch, B. Bereiter, T. Blunier, J.-M. Barnola, U. Siegenthaler, D. Raynaud, J. Jouzel, H. Fischer, K. Kawamura, *et al.*, “High-resolution carbon dioxide concentration record 650,000–800,000 years before present,” *Nature*, vol. 453, no. 7193, p. 379, 2008.

[9] L. Rebecca, “Climate change: Atmospheric carbon dioxide,” *climate.gov*, 2018.

[10] A. K. Tripati, C. D. Roberts, and R. A. Eagle, “Coupling of co2 and ice sheet stability over major climate transitions of the last 20 million years,” *science*, vol. 326, no. 5958, pp. 1394–1397, 2009.

[11] J. H. Butler and S. A. Montzka, “The noaa annual greenhouse gas index (aggi),” *NOAA Earth System Research Laboratory*, 2016.

[12] G. Masson and I. Kaizuka, "Trends 2017 in photovoltaic applications," *Report IEA PVPS T1-32*, 2017.

[13] D. B. Needleman, J. R. Poindexter, R. C. Kurchin, I. M. Peters, G. Wilson, and T. Buonassisi, "Economically sustainable scaling of photovoltaics to meet climate targets," *Energy & Environmental Science*, vol. 9, no. 6, pp. 2122–2129, 2016.

[14] G. Wilson, "The multi-tw scale future for photovoltaics," in *AIP Conference Proceedings*, vol. 1924, p. 020003, AIP Publishing, 2018.

[15] W. Shockley and H. J. Queisser, "Detailed balance limit of efficiency of p-n junction solar cells," *J. Appl. Phys.*, vol. 32, no. 3, pp. 510–519, 1961.

[16] W. Ruppel and P. Würfel, "Upper limit for the conversion of solar energy," *IEEE Trans. Electron Devices*, vol. 27, pp. 877–882, Apr 1980.

[17] A. De Vos, "Detailed balance limit of the efficiency of tandem solar cells," *J. Phys. D: Appl. Phys*, vol. 13, no. 5, p. 839, 1980.

[18] H. Pauwels and A. D. Vos, "Determination of the maximum efficiency solar cell structure," *Solid-State Electron.*, vol. 24, no. 9, pp. 835 – 843, 1981.

[19] T. Tiedje, E. Yablonovitch, G. Cody, and B. Brooks, "Limiting efficiency of silicon solar cells," *IEEE Trans. Electron Devices*, vol. 31, pp. 711–716, May 1984.

[20] "Best Research Cell Efficiencies," 2019. Retrieved from https://www.nrel.gov/pv/assets/images/efficiency-chart.png.

[21] M. A. Green, "Radiative efficiency of state-of-the-art photovoltaic cells," *Progress in Photovoltaics: Research and Applications*, vol. 20, no. 4, pp. 472–476, 2012.

[22] O. D. Miller, E. Yablonovitch, and S. R. Kurtz, "Strong internal and external luminescence as solar cells approach the shockley–queisser limit," *IEEE Journal of Photovoltaics*, vol. 2, no. 3, pp. 303–311, 2012.

[23] S. Demtsu and J. Sites, "Effect of back-contact barrier on thin-film cdte solar cells," *Thin Solid Films*, vol. 510, no. 1-2, pp. 320–324, 2006.

[24] W. Jaegermann, A. Klein, and T. Mayer, "Interface engineering of inorganic thin-film solar cells–materials-science challenges for advanced physical concepts," *Advanced Materials*, vol. 21, no. 42, pp. 4196–4206, 2009.

[25] A. Moore, T. Song, and J. Sites, "Improved cdte solar-cell performance with an evaporated te layer before the back contact," *MRS Advances*, vol. 2, no. 53, pp. 3195–3201, 2017.

[26] T. Song, A. Moore, and J. R. Sites, "Te layer to reduce the cdte back-contact barrier," *IEEE Journal of Photovoltaics*, vol. 8, no. 1, pp. 293–298, 2018.

[27] P. T. Erslev, J. W. Lee, W. N. Shafarman, and J. D. Cohen, "The influence of na on metastable defect kinetics in cigs materials," *Thin Solid Films*, vol. 517, no. 7, pp. 2277–2281, 2009.

[28] A. Chirilă, P. Reinhard, F. Pianezzi, P. Bloesch, A. R. Uhl, C. Fella, L. Kranz, D. Keller, C. Gretener, H. Hagendorfer, *et al.*, "Potassium-induced surface modification of cu (in, ga) se 2 thin films for high-efficiency solar cells," *Nature materials*, vol. 12, no. 12, p. 1107, 2013.

[29] R. M. Swanson, "Approaching the 29% limit efficiency of silicon solar cells," in *Photovoltaic Specialists Conference, 2005. Conference Record of the Thirty-first IEEE*, pp. 889–894, 2005.

[30] B. Lim, T. Brendemühl, T. Dullweber, and R. Brendel, "Loss analysis of n-type passivated emitter rear totally diffused back-junction silicon solar cells with efficiencies up to 21.2%," *IEEE Journal of Photovoltaics*, vol. 6, no. 2, pp. 447–453, 2016.

[31] J. Schmidt, R. Peibst, and R. Brendel, "Surface passivation of crystalline silicon solar cells: Present and future," *Solar Energy Materials and Solar Cells*, vol. 187, pp. 39–54, 2018.

[32] F. Einsele, P. J. Rostan, M. B. Schubert, and U. Rau, "Recombination and resistive losses at zn o/ a-si: H/ c-si interfaces in heterojunction back contacts for si solar cells," *Journal of Applied Physics*, vol. 102, no. 9, p. 094507, 2007.

[33] K. Yoshikawa, W. Yoshida, T. Irie, H. Kawasaki, K. Konishi, H. Ishibashi, T. Asatani, D. Adachi, M. Kanematsu, H. Uzu, *et al.*, "Exceeding conversion efficiency of 26% by heterojunction interdigitated back contact solar cell with thin film si technology," *Solar Energy Materials and Solar Cells*, vol. 173, pp. 37–42, 2017.

[34] K. Yoshikawa, H. Kawasaki, W. Yoshida, T. Irie, K. Konishi, K. Nakano, T. Uto, D. Adachi, M. Kanematsu, H. Uzu, *et al.*, "Silicon heterojunction solar cell with interdigitated back contacts for a photoconversion efficiency over 26%," *Nature Energy*, vol. 2, no. 5, p. 17032, 2017.

[35] I. L. Braly, D. W. deQuilettes, L. M. Pazos-Outon, S. Burke, M. E. Ziffer, D. S. Ginger, and H. W. Hillhouse, "Hybrid perovskite films approaching the radiative limit with over 90% photoluminescence quantum efficiency," *Nature Photonics*, vol. 12, pp. 355–361, 2018.

[36] M. Abdi-Jalebi, Z. Andaji-Garmaroudi, S. Cacovich, C. Stavrakas, B. Philippe, J. M. Richter, M. Alsari, E. P. Booker, E. M. Hutter, A. J. Pearson, *et al.*, “Maximizing and stabilizing luminescence from halide perovskites with potassium passivation,” *Nature*, vol. 555, no. 7697, p. 497, 2018.

[37] Z. Liu, L. Kr´uckemeier, B. Krogmeier, B. Klingebiel, J. A. M´arquez, S. Levcenko, S. ´Oz, S. Mathur, U. Rau, T. Unold, *et al.*, “Open-circuit voltages exceeding 1.26 v in planar methylammonium lead iodide perovskite solar cells,” *ACS Energy Letters*, vol. 4, no. 1, pp. 110–117, 2018.

[38] N. Arora, M. I. Dar, A. Hinderhofer, N. Pellet, F. Schreiber, S. M. Zakeeruddin, and M. Grätzel, “Perovskite solar cells with cuscn hole extraction layers yield stabilized efficiencies greater than 20%,” *Science*, vol. 358, no. 6364, pp. 768–771, 2017.

[39] V. Sarritzu, N. Sestu, D. Marongiu, X. Chang, S. Masi, A. Rizzo, S. Colella, F. Quochi, M. Saba, A. Mura, *et al.*, “Optical determination of shockley-read-hall and interface recombination currents in hybrid perovskites,” *Scientific reports*, vol. 7, p. 44629, 2017.

[40] M. Stolterfoht, C. M. Wolff, J. A. Márquez, S. Zhang, C. J. Hages, D. Rothhardt, S. Albrecht, P. L. Burn, P. Meredith, T. Unold, *et al.*, “Visualization and suppression of interfacial recombination for high-efficiency large-area pin perovskite solar cells,” *Nature Energy*, vol. 3, no. 10, p. 847, 2018.

[41] E. L. Ratcliff, B. Zacher, and N. R. Armstrong, “Selective interlayers and contacts in organic photovoltaic cells,” *J. Phys. Chem. Lett.*, vol. 2, pp. 1337–1350, 2011.

[42] R. Po, C. Carbonera, A. Bernardi, and N. Camaioni, “The role of buffer layers in polymer solar cells,” *Energy Environ. Sci.*, vol. 4, pp. 285–310, 2011.

[43] F. Feldmann, M. Simon, M. Bivour, C. Reichel, M. Hermle, and S. W. Glunz, “Carrier-selective contacts for Si solar cells,” *App. Phys. Lett.*, vol. 104, p. 181105, May 2014.

[44] E. J. Juarez-Perez, M. Wuβler, F. Fabregat-Santiago, K. Lakus-Wollny, E. Mankel, T. Mayer, W. Jaegermann, and I. Mora-Sero, “Role of the selective contacts in the performance of lead halide perovskite solar cells,” *J. Phys. Chem. Lett.*, vol. 5, pp. 680–685, Feb 2014.

[45] S. Wheeler, F. Deledalle, N. Tokmoldin, T. Kirchartz, J. Nelson, and J. R. Durrant, “Influence of surface recombination on charge-carrier kinetics in organic bulk heterojunction solar cells with nickel oxide interlayers,” *Phys. Rev. Appl.*, vol. 4, p. 024020, August 2015.

[46] C. Battaglia, S. M. De Nicolas, S. De Wolf, X. Yin, M. Zheng, C. Ballif, and A. Javey, “Silicon heterojunction solar cell with passivated hole selective MoOx contact,” *Appl. Phys. Lett.*, vol. 104, no. 11, p. 113902, 2014.

[47] C. Reichel, U. Würfel, K. Winkler, H.-F. Schleiermacher, M. Kohlstädt, M. Unmüssig, C. A. Messmer, M. Hermle, and S. W. Glunz, “Electron-selective contacts via ultra-thin organic interface dipoles for silicon organic heterojunction solar cells,” *J. Appl. Phys.*, vol. 123, no. 2, p. 024505, 2018.

[48] H. Tan, A. Jain, O. Voznyy, X. Lan, F. P. G. De Arquer, J. Z. Fan, R. Quintero-Bermudez, M. Yuan, B. Zhang, Y. Zhao, *et al.*, “Efficient and stable solution-processed planar perovskite solar cells via contact passivation,” *Science*, vol. 355, no. 6326, pp. 722–726, 2017.

[49] X. Yang, E. Aydin, H. Xu, J. Kang, M. Hedhili, W. Liu, Y. Wan, J. Peng, C. Samundsett, A. Cuevas, and et al., “Tantalum nitride electron-selective contact for crystalline silicon solar cells,” *Adv. Energy Mater.*, vol. 8, p. 1800608, Apr 2018.

[50] A. Niemegeers and M. Burgelman, “Effects of the Au/CdTe back contact on IV and CV characteristics of Au/CdTe/CdS/TCO solar cells,” *J. Appl. Phys.*, vol. 81, no. 6, pp. 2881–2886, 1997.

[51] A. Wagenpfahl, D. Rauh, M. Binder, C. Deibel, and V. Dyakonov, “S-shaped current-voltage characteristics of organic solar devices,” *Phys. Rev. B*, vol. 82, p. 115306, Sep 2010.

[52] O. J. Sandberg, M. Nyman, and R. Österbacka, “Effect of contacts in organic bulk heterojunction solar cells,” *Phys. Rev. Applied*, vol. 1, p. 024003, Mar 2014.

[53] R. Brendel and R. Peibst, “Contact selectivity and efficiency in crystalline silicon photovoltaics,” *IEEE J. Photovolt.*, vol. 6, pp. 1413–1420, Nov 2016.

[54] O. J. Sandberg, A. Sundqvist, M. Nyman, and R. Österbacka, “Relating charge transport, contact properties, and recombination to open-circuit voltage in sandwich-type thin-film solar cells,” *Phys. Rev. Applied*, vol. 5, p. 044005, Apr 2016.

[55] S. Solak, A. G. Ricciardulli, T. Lenz, N. I. Crăciun, P. W. M. Blom, and G. A. H. Wetzelaer, “Open-circuit voltage loss in annealed P3HT:perylene diimide bulk heterojunction solar cells,” *Appl. Phys. Lett.*, vol. 110, no. 16, p. 163301, 2017.

[56] I. Mora-Sero and J. Bisquert, “Effect of reduced selectivity of contacts on the current-potential characteristics and conversion performance of solar cells,” *Sol. Energ. Mat. Sol. Cells*, vol. 85, pp. 51–62, Jun 2004.

[57] C. Crowell and S. Sze, “Current transport in metal-semiconductor barriers,” *Solid-State Electron.*, vol. 9, no. 11, pp. 1035 – 1048, 1966.

[58] R. E. Brandt, N. M. Mangan, J. V. Li, Y. S. Lee, and T. Buonassisi, “Determining interface properties limiting open-circuit voltage in heterojunction solar cells,” *J. Appl. Phys.*, vol. 121, no. 18, p. 185301, 2017.

[59] S. M. Sze and M. K. Lee, *Semiconductor Devices, Physics and Technology.* Hoboken, N.J.: Wiley, 3rd ed ed., 2012.

[60] W. Shockley, “The theory of p-n junctions in semiconductors and p-n junction transistors,” *Bell Syst. Tech. J*, vol. 28, pp. 435–489, 1949.

[61] E. Yablonovitch, T. Gmitter, R. M. Swanson, and Y. H. Kwark, “A 720 mv open circuit voltage SiOx:c-Si:SiOx double heterostructure solar cell,” *Appl. Phys. Lett.*, vol. 47, no. 11, pp. 1211–1213, 1985.

[62] T. Mikio, T. Akira, M. Eiji, and T. Makoto, “Obtaining a higher Voc in HIT cells,” *Prog Photovolt Res Appl.*, vol. 13, no. 6, pp. 481–488, 2005.

[63] R. M. Swanson, “Back side contact solar cell with doped polysilicon regions,” Dec. 23 2008. US Patent 7,468,485.

[64] E. H. Rhoderick and R. H. Williams, *Metal-Semiconductor Contacts.* Oxford [England]; New York: Clarendon Press ; Oxford University Press, 1988.

[65] M. X. Tan, P. E. Laibinis, S. T. Nguyen, J. M. Kesselman, C. E. Stanton, and N. S. Lewis, “Principles and applications of semiconductor photoelectrochemistry,” *Prog. Inorg. Chem.*, vol. 41, pp. 21–144, 1994.

[66] S. M. Sze, *Modern Semiconductor Device Physics.* New York: Wiley, 1998.

[67] F. E. Jones, C. Daniels-Hafer, B. P. Wood, R. G. Danner, and M. C. Lonergan, “Current transport at the p-InP—poly(pyrrole) interface,” *J. Appl. Phys.*, vol. 90, no. 2, pp. 1001–1010, 2001.

[68] C. Daniels-Hafer, M. Jang, S. W. Boettcher, R. G. Danner, and M. C. Lonergan, “Tuning charge transport at the interface between indium phosphide and a polypyrrole- phosphomolybdate hybrid through manipulation of electrochemical potential,” *J. Phys. Chem. B*, vol. 106, no. 7, pp. 1622–1636, 2002.

[69] Z. Vardeny and J. Tauc, “Hot-carrier thermalization in amorphous silicon,” *Physical Review Letters*, vol. 46, no. 18, p. 1223, 1981.

[70] R. Tommasi, P. Langot, and F. Vallée, “Femtosecond hole thermalization in bulk gaas,” *Applied physics letters*, vol. 66, no. 11, pp. 1361–1363, 1995.

[71] R. Tommasi, P. Langot, and F. Vallée, "Femtosecond hole thermalization in bulk gaas," *Applied physics letters*, vol. 66, no. 11, pp. 1361–1363, 1995.

[72] T. Elsaesser, J. Shah, L. Rota, and P. Lugli, "Initial thermalization of photoexcited carriers in gaas studied by femtosecond luminescence spectroscopy," *Physical review letters*, vol. 66, no. 13, p. 1757, 1991.

[73] X. Zhou, H. Van Driel, and G. Mak, "Femtosecond kinetics of photoexcited carriers in germanium," *Physical Review B*, vol. 50, no. 8, p. 5226, 1994.

[74] J. Shah, *Ultrafast spectroscopy of semiconductors and semiconductor nanostructures*, vol. 115. Springer Science & Business Media, 2013.

[75] J. M. Richter, F. Branchi, F. V. de Almeida Camargo, B. Zhao, R. H. Friend, G. Cerullo, and F. Deschler, "Ultrafast carrier thermalization in lead iodide perovskite probed with two-dimensional electronic spectroscopy," *Nature communications*, vol. 8, no. 1, p. 376, 2017.

[76] F. A. Lindholm, J. G. Fossum, and E. L. Burgess, "Application of the superposition principle to solar-cell analysis," *IEEE Trans. Electron Devices*, vol. 26, no. 3, pp. 165–171, 1979.

[77] J. E. Moore, S. Dongaonkar, R. V. K. Chavali, M. A. Alam, and M. S. Lundstrom, "Correlation of built-in potential and I–V crossover in thin-film solar cells," *IEEE J. Photovolt.*, vol. 4, no. 4, pp. 1138–1148, 2014.

[78] R. V. K. Chavali, J. R. Wilcox, B. Ray, J. L. Gray, and M. A. Alam, "Correlated nonideal effects of dark and light I–V characteristics in a-Si/c-Si heterojunction solar cells," *IEEE J. Photovolt.*, vol. 4, no. 3, pp. 763–771, 2014.

[79] U. Das, S. Hegedus, L. Zhang, J. Appel, J. Rand, and R. Birkmire, "Investigation of hetero-interface and junction properties in silicon heterojunction solar cells," in *Proc. 35th IEEE Photovoltaic Spec. Conf.*, pp. 001358–001362, IEEE, 2010.

[80] J. Pan, M. Gloeckler, and J. R. Sites, "Hole current impedance and electron current enhancement by back-contact barriers in CdTe thin film solar cells," *J. Appl. Phys.*, vol. 100, no. 12, p. 124505, 2006.

[81] G. Stillman, C. Wolfe, and J. Dimmock, "Hall coefficient factor for polar mode scattering in n-type gaas," *Journal of Physics and Chemistry of Solids*, vol. 31, no. 6, pp. 1199–1204, 1970.

[82] S. S. Li and W. R. Thurber, "The dopant density and temperature dependence of electron mobility and resistivity in n-type silicon," *Solid-State Electronics*, vol. 20, no. 7, pp. 609–616, 1977.

[83] N. D. Arora, J. R. Hauser, and D. J. Roulston, “Electron and hole mobilities in silicon as a function of concentration and temperature,” *IEEE Transactions on electron devices*, vol. 29, no. 2, pp. 292–295, 1982.

[84] J. Blakemore, “Semiconducting and other major properties of gallium arsenide,” *Journal of Applied Physics*, vol. 53, no. 10, pp. R123–R181, 1982.

[85] J. R. Lowney and H. S. Bennett, “Majority and minority electron and hole mobilities in heavily doped gaas,” *Journal of applied physics*, vol. 69, no. 10, pp. 7102–7110, 1991.

[86] D. Lancefield, “Electron mobility in gaas: overview,” *EMIS DATAREVIEWS SERIES*, vol. 16, pp. 41–45, 1996.

[87] A. Srivastava, B. Arora, and S. Guha, “Measurement of richardson constant of GaAs schottky barriers,” *Solid-State Electron.*, vol. 24, no. 2, pp. 185 – 191, 1981.

[88] M. Missous, E. H. Rhoderick, D. A. Woolf, and S. P. Wilkes, “On the richardson constant of intimate metal-GaAs schottky barriers,” *Semiconductor Science and Technology*, vol. 7, pp. 218–221, feb 1992.

[89] M. Pattabi, S. Krishnan, Ganesh, and X. Mathew, “Effect of temperature and electron irradiation on the I–V characteristics of Au/CdTe schottky diodes,” *Solar Energy*, vol. 81, no. 1, pp. 111 – 116, 2007.

[90] J. Ge, J. Chu, J. Jiang, Y. Yan, and P. Yang, “Characteristics of In-substituted CZTS thin film and bifacial solar cell,” *ACS Appl. Mater. Interfaces*, vol. 6, no. 23, pp. 21118–21130, 2014.

[91] C. Deibel, A. Wagenpfahl, and V. Dyakonov, “Influence of charge carrier mobility on the performance of organic solar cells,” *Phys. Status Solidi Rapid Res. Lett.*, vol. 2, pp. 175–177, Jun 2008.

[92] T. Kirchartz, B. E. Pieters, K. Taretto, and U. Rau, “Mobility dependent efficiencies of organic bulk heterojunction solar cells: Surface recombination and charge transfer state distribution,” *Phys. Rev. B*, vol. 80, p. 035334, Jul 2009.

[93] W. Tress, K. Leo, and M. Riede, “Optimum mobility, contact properties, and open-circuit voltage of organic solar cells: A drift-diffusion simulation study,” *Phys. Rev. B*, vol. 85, p. 155201, Apr 2012.

[94] A. Spies, M. List, T. Sarkar, and U. Würfel, “On the impact of contact selectivity and charge transport on the open-circuit voltage of organic solar cells,” *Adv. Energy Mater.*, vol. 7, no. 5, p. 1601750, 2017. 1601750.

[95] S. M. Sze, *Semiconductors devices, physics and technology.* New York, USA: Wiley, 2nd ed., 1985.

[96] P. Würfel, "Thermodynamic limitations to solar energy conversion," *Physica E*, vol. 14, pp. 18–26, Apr 2002.